

CMUG Phase 2 Deliverable

Reference: D3.1: Quality Assessment Report
Due date: June 2016
Submission date: July 2016
Version: 2.0c



Climate Modelling User Group

Phase 2 Deliverable 3.1 Quality Assessment Report

Version 2

Centres providing input: Met Office, MPI-M, ECMWF, MétéoFrance, SMHI, DLR, IPSL, LMU, BSC

Version nr.	Date	Status
2.0a	8 June 2016	First Draft
2.0b	4 July 2016	Contributions from all partners
2.0c	8 July 2016	Submission to ESA
2.0d	9 August 2016	Updated to address ESA comments



Max-Planck-Institut
für Meteorologie



Institut
Pierre
Simon
Laplace



CMUG Phase 2 Deliverable

Reference: D3.1: Quality Assessment Report
Due date: June 2016
Submission date: July 2016
Version: 2.0c



CMUG Phase 2 Deliverable 3.1

Quality Assessment Report

1.	Purpose and scope of this report	3
2.	CMUG methodology and approach for assessing quality in CCI products.....	3
3	Summary of CMUG assessment of Quality by WP	6
3.1	<i>Assessment of Marine ECVs in FOAM Ocean Model [WP 3.1].....</i>	<i>6</i>
3.2	<i>Integrated assessment of Marine ECVs in the ORA system [WP 03.1].....</i>	<i>12</i>
3.3	<i>Assimilation of several L2 ozone products in the ERA system [WP 3.2].....</i>	<i>17</i>
3.4	<i>Integrated assessment of the CCI Aerosols, GHG, and Ozone datasets [WP3.3].....</i>	<i>19</i>
3.5	<i>Integrated assessment of CCI terrestrial ECVs impact in the MPI-ESM [WP3.4]</i>	<i>30</i>
3.6	<i>Cross assessment of clouds, water vapour, aerosols, ozone, GHG, SST, radiation and soil moisture impact on global climate variability and trends [WP_03.4].....</i>	<i>34</i>
3.7	<i>Coupled climate model assessment [WP3.5].....</i>	<i>40</i>
3.8	<i>Improved process understanding from Arctic and Antarctic cross ECV assessment [WP3.6].....</i>	<i>46</i>
3.9	<i>Cross-Assessment of Aerosols, Cloud and Radiation CCI ECVs [WP3.7].....</i>	<i>52</i>
3.10	<i>Cross assessments of clouds, water vapour, radiation, soil moisture for regional climate models [WP3.8].....</i>	<i>54</i>
3.11	<i>Cross assessments of ESA CCI glacier, land cover and sea level data for hydrological modelling of the Arctic Ocean drainage basin [WP3.9].....</i>	<i>62</i>
3.12	<i>Cross-assessment of CCI-ECVs over the Mediterranean domain [WP3.10]</i>	<i>74</i>
3.13	<i>Assessment of sea ice concentration observational uncertainty from a data assimilation point of view [WPO3.11].....</i>	<i>79</i>
3.14	<i>Assessment of Antarctic ice sheet ECVs for modelling [WP3.12].....</i>	<i>85</i>
3.15	<i>Assessment of Greenland ice sheet ECVs for modelling [WP3.13].....</i>	<i>85</i>
4.	References.....	86

CMUG Phase 2 Deliverable

Reference: D3.1: Quality Assessment Report
Due date: June 2016
Submission date: July 2016
Version: 2.0c



1. Purpose and scope of this report

This document is a continuation from the 2015 version 1 which reported on CMUG CCI evaluations during the first 12-months of Phase 2. Its purpose is to assess the quality of the latest versions of CCI products and update feedback to ESA and the CCI teams. This assessment is being conducted by the climate modelling and reanalysis centres in the CMUG consortium using CCI Phase 2 data and includes a wide range of data and model interactions (assimilation, boundary conditions, optimisation, reanalysis, sensitivity studies etc). This second phase of evaluation continues to examine the following top level questions:

- Are the CCI data products of ‘climate quality’ i.e. is their quality adequate for use in climate modelling, reanalysis and for wider research applications?
- Are the error characteristics provided by CCI products adequate?
- Do the products meet the Global Climate Observing System (GCOS) quality requirements for satellite for Essential Climate Variables (ECV)?
- Is the quality of the products sufficient for climate service applications?

2. CMUG methodology and approach for assessing quality in CCI products

This report describes the results in the second 12 months of CMUG Phase 2 from CMUG Task 3 “Assessing consistency and quality of CCI products”. The work is spread across fifteen Work Packages¹ (WP) listed in Table 1, which includes the CCI product being assessed, the CMUG model being used to make the assessment, and the type of climate modeling experiment.

The CMUG results presented here provide information on the accuracy, consistency and usefulness of the latest CCI data sets. The analysis assesses the suitability of the CCI datasets for coupled climate model and reanalysis applications and evaluates the impact of the data products on model based studies, including quantification of the uncertainties associated with both the models and the observations (see Table 1). This information is aimed at the CCI teams producing the data but is also of use to other modelling centres which will use CCI data in the future.

The modeling experiments are described in the following sections of this report, and cover the following topics: assimilation of CCI data into climate models; cross assessments of CCI data (those which have physical links/interactions); applications for reanalysis; integrated

¹ Two new WPs have been included in the CMUG work plan since version 1 of this report in June 2015.

CMUG Phase 2 Deliverable

Reference: D3.1: Quality Assessment Report
Due date: June 2016
Submission date: July 2016
Version: 2.0c



assessment of CCI data in climate models; boundary condition forcing experiments; regional modeling; earth system process studies. The CMUG work reported here was conducted with the CCI data available at the time, which in most cases were from the final Phase 2 Climate Record Data Packages produced by the CCI projects. Where the results are not yet available, the section is marked “To be completed” Future versions of this report will include updates to these sections based on the latest Phase 2 CCI data.

CMUG Phase 2 Deliverable

Reference: D3.1: Quality Assessment Report

Due date: June 2016

Submission date: July 2016

Version: 2.0c



		CCI products													
		SST	SSH	Sea ice	OC	Cloud	Ozone	Aerosol	GHG	LC	SM	Fire	Ice sheets	Glacier	
CMUG Task 3: Assessing consistency and quality of CCI products															
WP	CMUG Model	Ocean				Atmosphere				Land				Experiment Type	
3.1	FOAM	X	X	X	X										Assimilation
O3.1	NEMOVAR, ORA	X	X	X	X										Assimilation and Detection
3.2	ERA-Clim						X								Assimilation
3.3	MACC-II						X	X	X						Assimilation
3.4	JSBACH, TM3								X	X	X	X			Assimilation
O3.4	EC-Earth/CMIP5	X				X	X	X	X		X				Assessment, evaluation
3.5	LMDz, ORCHIDEE								X	X	X	X			Boundary Condition
3.6	MPI-OM, MPI-ESM	X		X	X	X									Assimilation (Polar Regions)
3.7	EMAC-MADE					X		X							Comparison
3.8	RCA HARMONIE	X				X					X				Comparison/Eval (CORDEX Africa)
3.9	Arctic HYPE		X							X				X	Assessment
3.10	CNRM-RCM	X	X			X		X			X				Comparison (Med CORDEX)
O3.11	EC-Earth3	X	X	X	X										Cross-assessment
3.12	BISICLES / FETISH	X											X		Assessment, evaluation
3.13	GISM-VUB												X		Assessment, evaluation

Table 1: Summary of the CMUG Work Packages, CMUG models, CCI products, and CMUG experiments for assessing quality of the CCI products, as given in this report.



3 Summary of CMUG assessment of Quality by WP

3.1 Assessment of Marine ECVs in FOAM Ocean Model [WP 3.1]

Aim

The aim of this research is to make an integrated assessment of marine ECVs to assess their consistency within a global and shelf seas regional data assimilation environment, and to provide an assessment of the uncertainty. It will address the following scientific questions:

- Are the individual marine CCI CDRs good enough for assimilation purposes?
- What are the changes made to the analyses by assimilating the CCI data?
- Are the uncertainties provided useful to assign observation errors to the measurements?
- Are the four marine ECVs mutually consistent from an ocean assimilation point of view?
- What should be recommended to EUMETSAT for Sentinel-3 processing to operational centres?

Key Outcomes of CMUG Research

- Assimilating ocean colour data improves surface and sub-surface model chlorophyll, with some evidence of improvement in nutrients and carbon variables.
- Information gained by assimilating ocean colour data can be beneficial for model development.
- OC-CCI products are of at least equal quality to predecessor products, with some improvements due to increased spatial coverage and stability.
- OC-CCI V2 products are of at least equal scientific quality, and improved technical quality, to OC-CCI V1 products.
- Reanalyses assimilating ocean colour products produce realistic variability in response to climatic events, allowing their use as a tool for climate studies.
- An integrated multivariate assessment of marine ECVs is ongoing, with assessment to be completed during the remainder of Phase 2.

Summary of Results

Initial work has focused on assessment of the ocean colour CCI (OC-CCI) data for assimilation purposes. This is now being extended to an integrated assessment of all four marine ECVs. Both these pieces of work are summarised below, as well as a comparison between OC-CCI V1 and V2 products.

CMUG Phase 2 Deliverable

Reference: D3.1: Quality Assessment Report
Due date: June 2016
Submission date: July 2016
Version: 2.0c



At the end of Phase 1, a global ocean reanalysis was produced by assimilating OC-CCI V1 chlorophyll products into the FOAM-HadOCC coupled physical-biogeochemical ocean model (Storkey et al., 2010; Palmer and Totterdell, 2001; Hemmings et al., 2008; Ford et al., 2012), covering the period from September 1997 to July 2012. For comparison, a reanalysis was also produced assimilating the predecessor GlobColour products, as well as a control run with no data assimilation. A thorough assessment of the results has been performed during Phase 2, and a paper on the work will be submitted for publication in the forthcoming CCI special issue of Remote Sensing of Environment.

The OC-CCI V1 products were found to be of sufficient quality for data assimilation purposes, and of at least equal quality to the GlobColour products (more detail on the comparison with GlobColour is included in the “Quality relevant outcomes” sub-section below). Assimilating OC-CCI chlorophyll data improved the model’s representation of sea surface chlorophyll compared with both satellite data sets, and also a range of independent *in situ* observations. An example of this is shown in Figure 1, which plots a time series of sea surface chlorophyll from all three model runs at the Hawaii Ocean Time Series (HOT) site in the North Pacific, along with *in situ* observations. The assimilation results in a much better match for both the magnitude and seasonality of the observations. It is also able to produce a reanalysis which is stable with time whilst displaying inter-annual variability.

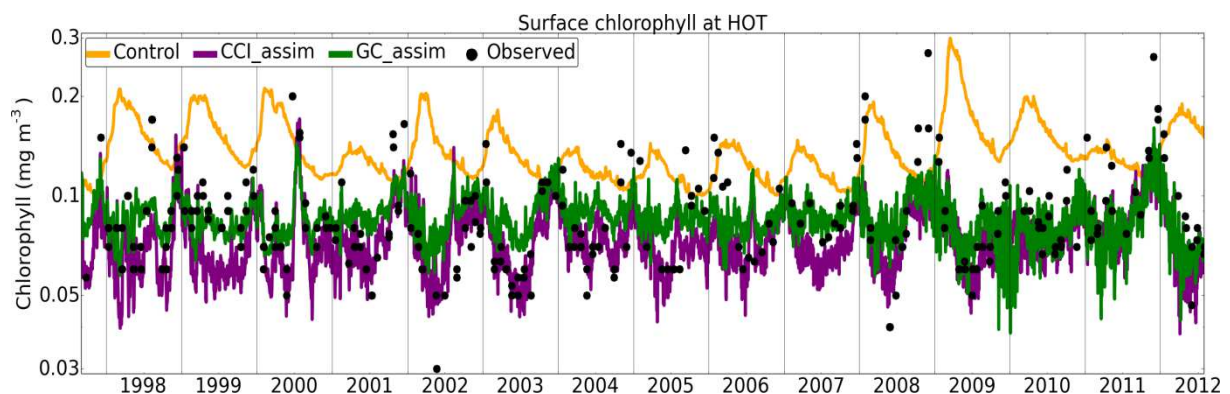


Figure 1: Time series of modelled and observed chlorophyll concentration in the surface 10 m at the HOT site. Observations have been obtained from <http://hahana.soest.hawaii.edu/hot>.

The largest impact of the assimilation was on sea surface chlorophyll, but an improved representation of chlorophyll was also found throughout the water column, including an improved representation of deep chlorophyll maxima. Corresponding changes were found in phytoplankton and zooplankton biomass, although limited observational data are available for validation. Changes to nutrient concentrations were small, with some evidence of improvement compared with *in situ* observations. This is an important result, as some studies have found a degradation of nutrients due to chlorophyll assimilation.



Validation has also focused on the impact of the assimilation on the model carbon cycle, as this is of particular relevance for climate studies. Validation has been performed against surface fugacity of carbon dioxide ($f\text{CO}_2$) observations from the SOCAT V2 database (Bakker et al., 2014). Overall, the effect of the chlorophyll assimilation was small compared with the magnitude of model biases. In part, this is because there are large physical controls on the carbon cycle. The impact on these of additionally assimilating physical ECVs is being assessed as part of ongoing Phase 2 activities. In regions of strong biological activity, the chlorophyll assimilation was found to have a beneficial impact on carbon variables, an example of which is shown in Figure 2. In some areas, the assimilation was found to improve representation of the biological component of the carbon cycle, but overall degrade $f\text{CO}_2$ compared with observations due to compensating errors in the physical component of the carbon cycle. This provides important information on model biases which can be fed back into model development activities. Again, the impact in these cases of combined assimilation of all marine ECVs will be assessed during Phase 2.

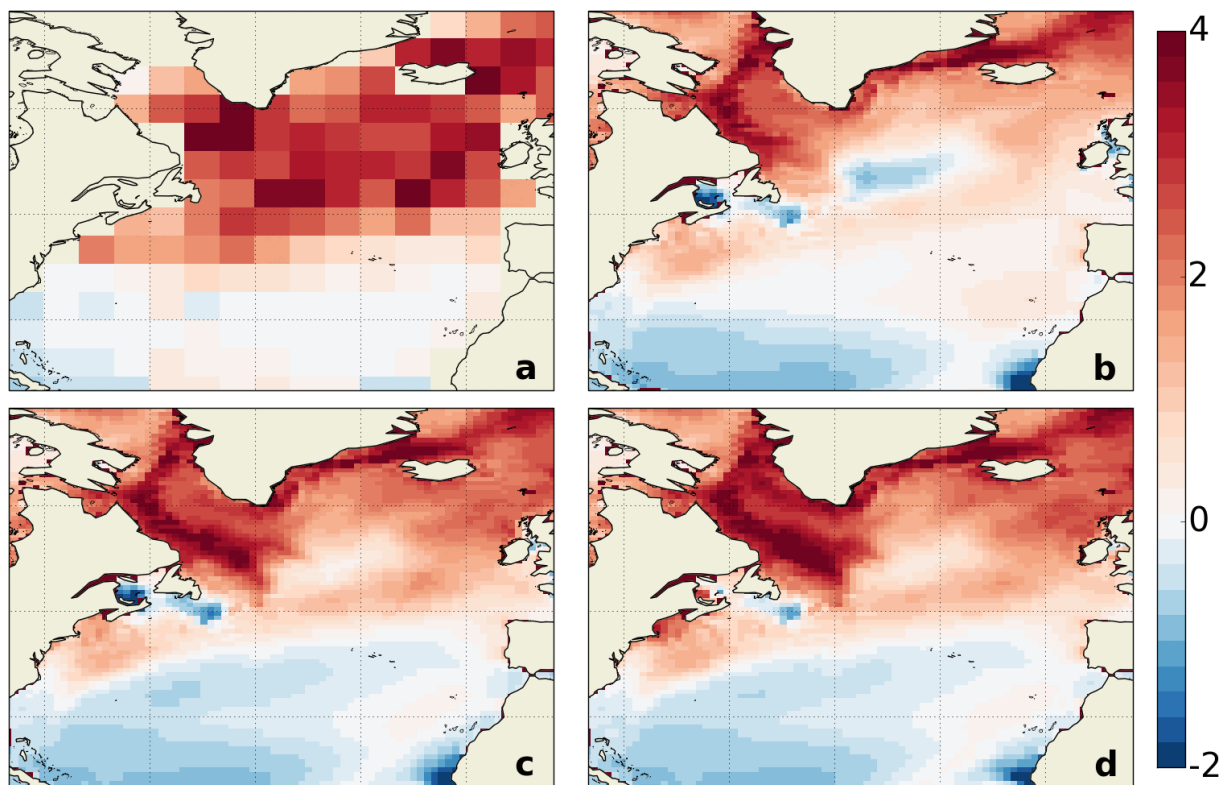


Figure 2: June mean air-sea CO_2 flux ($\text{mol C m}^{-2} \text{ yr}^{-1}$) in the North Atlantic from a) climatology of Takahashi et al. (2009), b) FOAM-HadOCC control, c) reanalysis assimilating GlobColour data, d) reanalysis assimilating OC-CCI data. Positive values represent a flux into the ocean. The reduction in spurious outgassing in the centre of the domain in c) and d) compared with b) is due to the assimilation reducing the chlorophyll bias in this area. An alternative version of this figure, not including OC-CCI data but mentioning the CCI project, has been published in Gehlen et al. (2015).

CMUG Phase 2 Deliverable

Reference: D3.1: Quality Assessment Report
Due date: June 2016
Submission date: July 2016
Version: 2.0c



Technical issues with the OC-CCI V1 products have already been reported on during Phase 1. OC-CCI V2 products have since been released, and CMUG have tested these in comparison with V1. The Product User Guide has been expanded on and improved, particularly regarding use of the uncertainty estimates, which is beneficial for users. The V2 products were not quite “plug-and-play” with the V1 products, since the variable names for the chlorophyll uncertainty have been changed in the NetCDF files. Whilst consistency between releases is generally preferred, in this case the change of variable name makes the contents of the variable clearer, so is a reasonable change to have made. Minor metadata errors which had been identified in the V1 products have been corrected, and no new errors identified. Short like-for-like assimilation runs have been performed using the V1 and V2 products, with similar results obtained, but small regional differences, indicating the V2 products to be of at least equal scientific quality to the V1 products, as well as of improved technical quality.

Experiments are now in progress to perform an integrated assessment of marine CCI products. These are using V2 OC, V1.1 SST, V1.1 SSH, and OSI SAF sea ice products, with a comparison to be made against the final Phase 2 releases towards the end of the project. Two sets of model runs are being performed with FOAM-HadOCC; long 1° resolution runs covering the overlapping period of the data sets (1998-2010), and higher resolution 0.25° resolution runs covering the final three years of this period. In each case, there is a non-assimilative control run, runs assimilating each CCI product individually, a run assimilating the four products in combination, and runs using other selected combinations of products. So far work has focused on setting up the model runs and processing the observation products for use with the assimilation.

The model runs are near completion, and assessment will be performed over the coming 12 months, with the aim of publishing the work in the peer-reviewed literature. The assessment will focus on how spatial features and temporal variability compare when using the products, the impact of each product on non-assimilated variables, and the impact of the assimilation on climate-relevant variables. Assessment will also be performed using the observation products and their uncertainty fields.

Quality relevant outcomes

A comparison between the OC-CCI V1 and GlobColour observation products has been performed to assess their stability and spatial coverage, building on that reported on at the end of Phase 1. GlobColour has greater spatial coverage prior to 2002, as it uses an older NASA SeaWiFS processing which discards fewer data points. Between 2002 and 2012, OC-CCI has greater coverage as more use is made of MERIS data. This is of particular benefit to the assimilation in certain regions, such as the Mauritanian upwelling region and the Arabian Sea during the Asian monsoon period, which were poorly covered by GlobColour. There is a lack of *in situ* observations with which to validate the results in these areas, but the model fields

CMUG Phase 2 Deliverable

Reference: D3.1: Quality Assessment Report
Due date: June 2016
Submission date: July 2016
Version: 2.0c



when assimilating OC-CCI data are in line with qualitative expectations. Furthermore, carbon cycle variables are improved in these regions when assimilating OC-CCI data, as a result of the improved coverage. The global mean and spatial standard deviation of the OC-CCI chlorophyll products are also more stable with time than for GlobColour. A reduction in variability is noted when MERIS is introduced in 2002, which could be due to differences in the properties of the sensors, or could simply be an artifact of the sudden increase in the number of data points. Such features are less clear in the reanalysis fields, as to some extent the model acts to smooth these out. Overall, very similar results are obtained whether OC-CCI or GlobColour products are assimilated, but where differences are found, there is evidence that results are improved due to the increased spatial coverage and improved stability of the OC-CCI data.

In the current line of work, the uncertainty estimates have been used to assign observation errors during the quality control stage, but not directly as part of the assimilation, which would require developments to the data assimilation scheme. As part of the quality control, the uncertainty estimates were found to be suitable for the purpose. The only issue found was that not every observation had a corresponding uncertainty, as reported during Phase 1, which led to these observations being automatically rejected. This is a known issue which the OC-CCI team is aware of. Some use has been made of the uncertainties in a validation context, and this will be explored more fully as part of the ongoing multivariate assessment.

Assessment of the seasonal and inter-annual variability of the reanalyses has also been performed, including the impact of the data assimilation on this variability, as an assessment of the applicability of the end product to climate monitoring activities. As mentioned above, the assimilation has a beneficial impact on the variability of model chlorophyll, and has also been found to impact phenological indicators, for instance the start dates of the North Atlantic spring bloom. The effect of the assimilation on the carbon cycle variability is more subtle, with it impacting the magnitude more than the variability of the air-sea CO₂ flux. Nonetheless, the model is able to capture observed variability relating to climate drivers such as the El Niño Southern Oscillation (ENSO), the North Atlantic Oscillation and the Atlantic Meridional Overturning Circulation. An example is shown in Figure 3, which plots time series of the Tropical Pacific mean air-sea CO₂ flux, along with the multivariate ENSO index. Anomalies are seen corresponding to El Niño and La Niña events, related to changes in upwelling. The impact of the different marine CCI products on such variability will be a key focus of the ongoing multivariate assessment.

CMUG Phase 2 Deliverable

Reference: D3.1: Quality Assessment Report

Due date: June 2016

Submission date: July 2016

Version: 2.0c

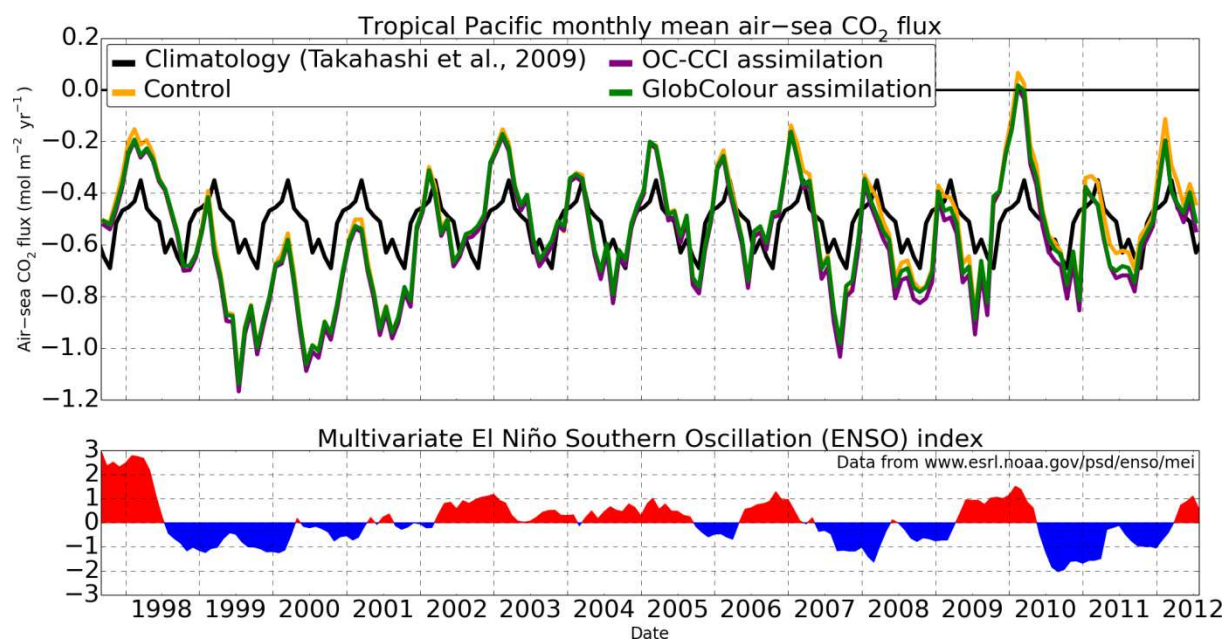


Figure 3: Top: Tropical Pacific mean air-sea CO₂ flux from the climatology of Takahashi et al. (2009) repeating in black, and each model run (coloured lines, as labeled). Bottom: multivariate ENSO index, as obtained from <http://www.esrl.noaa.gov/psd/enso/mei>.



3.2 Integrated assessment of Marine ECVs in the ORA system [WP O3.1]

Introduction

The aim of this WP is to perform an integrated assessment of CCI SST, SSH and SIC via assimilation using the ECMWF Ocean ReAnalysis (ORA) System. The focus is on multivariate detection of climate variability and change patterns in the set of CCI ECV in comparison with independent observational products.

The baseline ocean assimilation system ORAS5 used for this WP is closely related to the ORAP5 system described in Zuo et al. (2015) and Tietsche et al. (2015). It uses the ORCA1 global configuration of NEMO 3.4 forced by ERA-Interim (bulk formulas). Subsurface observations from EN4, SLA from Aviso V5, and SIC from OSI-SAF are assimilated using a 3DVar-FGAT algorithm with a 10 day assimilation window. SST is restored to observations from HadISST2 with a restoring strength of $200 \text{ Wm}^{-2}\text{K}^{-1}$.

The work on this WP has started in January 2016. Initial offline-inspection of the data has shown that the major climate modes of variability and change are very similar to pre-existing ECV data sets. However, for data assimilation, small differences in one variable can be amplified, or interact with how other variables are simulated. Therefore, a series of assimilation experiments has been started, where observational product in the baseline experiment are exchanged one by one with the CCI equivalent, as well as an experiment which uses all CCI-ECV considered here together (see Table 2). Depending on the outcome of these experiments, it is planned to perform additional experimentation to address specific questions regarding the inter-variable consistency of the CCI.

<i>Experiment</i>	<i>SST</i>	<i>SIC</i>	<i>SLA</i>	<i>Start</i>	<i>End</i>
ORA REF	HadISST2	OSI-SAF	Aviso	1975	2014
ORA CCI-SST	CCI v1.1	OSI-SAF	Aviso	1992	2010
ORA CCI-SIC	HadISST2	CCI SSMI v1.1	Aviso	1992	2008
ORA CCI-SLA	HadISST2	OSI-SAF	CCI v1.1	1993	2013
ORA CCI-ALL	CCI v1.1	CCI SSMI v1.1	CCI v1.1	1993	2008

Table 2: Overview of assimilation runs.

Preliminary results of ingesting CCI SST in the ORA system

Preliminary results from the assimilation experiment ORA CCI-SST that ingested SST from CCI v1.1 instead of HadISST2 are presented here. As shown in Figure 4, the variability and trend of global CCI SST in agrees well with the non-ECV data set HadISST2. However, CCI SST is warmer by a constant amount of 0.05K. Whether this is due to the different definitions

CMUG Phase 2 Deliverable

Reference: D3.1: Quality Assessment Report
Due date: June 2016
Submission date: July 2016
Version: 2.0c



of sea surface temperature regarding reference depth and diurnal cycle remains to be seen. Global SST in the two assimilation experiments ORA REF and ORA CCI-SST reproduce trend and variability of the two observational products very well, each being close to the observational product which was ingested into the system. The fact that the ORA CCI-SST experiment simulates SST which is often halfway between HadISST2 and CCI-SST suggests that subsurface ocean observations or atmospheric forcing tend to drive the model towards SST that are closer to HadISST2.

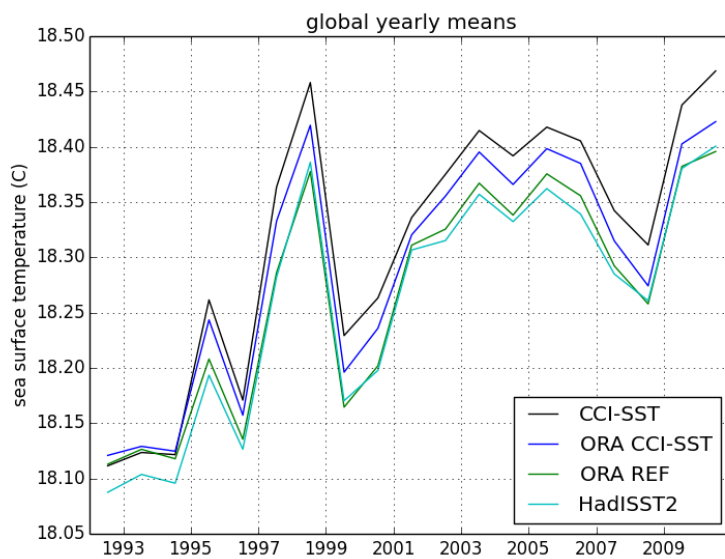


Figure 4: Global-mean SST in the observational data sets HadISST2 and CCI-SST, and the assimilation experiments ORA REF and ORA CCI-SST over 1992–2010.

To understand better the potential causes for differences between CCI-SST and HadISST2, maps of regional biases and trends are needed. As shown in Figure 5 (middle), there are systematic regional modulations to the global-mean warm offset. Averaged over the whole data set 1992-2010, the tropical oceans tend to be 0.1 to 0.3 K warmer in CCI-SST than in HadISST2. However, they are more than 0.2 K cooler in the North Pacific, and more than 0.5K cooler in the Sea of Okhotsk. The North Atlantic exhibits a complex pattern of cold and warm differences, which might be partially related to boundary currents and the presence of sea ice.

From the Figure 5 (left) it can be seen that the assimilation systems tends to dampen the differences between the two data sets: in ORA CCI-SST, the tropical oceans SST is slightly cooler than in CCI-SST, and slightly warmer in the North Pacific. Disagreements in the upwelling regions of the west coast of South America and Africa are apparent, which might

CMUG Phase 2 Deliverable

Reference: D3.1: Quality Assessment Report
Due date: June 2016
Submission date: July 2016
Version: 2.0c



be partly due to well-known model biases in these regions. In the Southern Ocean and the western boundary currents, the inability of the model to simulate mesoscale eddies leads to a strong and spatially variable bias pattern (Figure 5, left and right), which is not present when comparing the two observational data sets directly (Figure 5 middle).

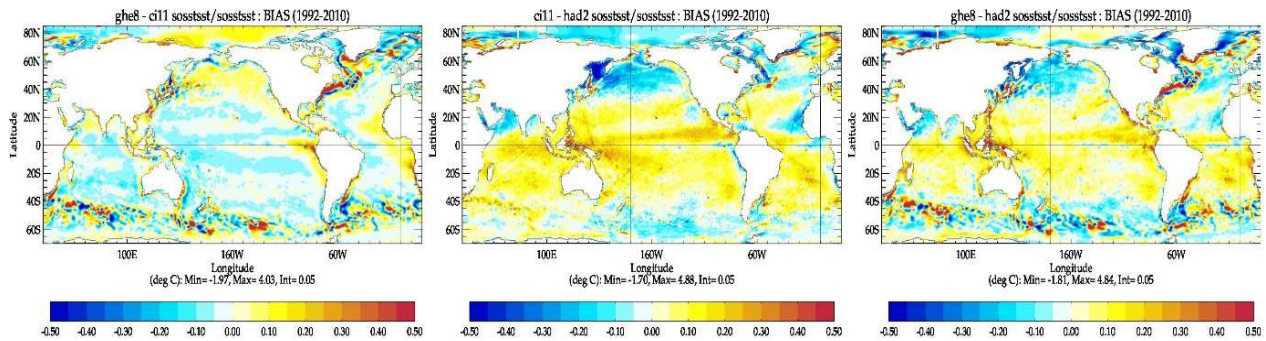


Figure 5: SST difference averaged over 1992-2010 between (left) ORA CCI-SST and CCI-SST, (middle) CCI-SST and HadISST2, and (right) ORA CCI-SST and HadISST2.

Despite these bias patterns, monthly-mean anomalies of SST are well correlated both between the two data sets, and between the model simulation and the data sets (Figure 6). Correlations between ORA CCI-SST and CCI-SST are generally 0.95 or higher, except in the presence of mesoscale eddies in the Southern Ocean and the western boundary currents, where correlations are degraded to values of 0.5 to 0.7. It is worth noting that the SST correlation between the observational data sets (Figure 6 middle) is actually weaker than between ORA CCI-SST and HadISST2. This might suggest that the assimilation system is able to reduce uncertainty of observed SST variability and/or trend by spreading information from non-SST fields to the SST.

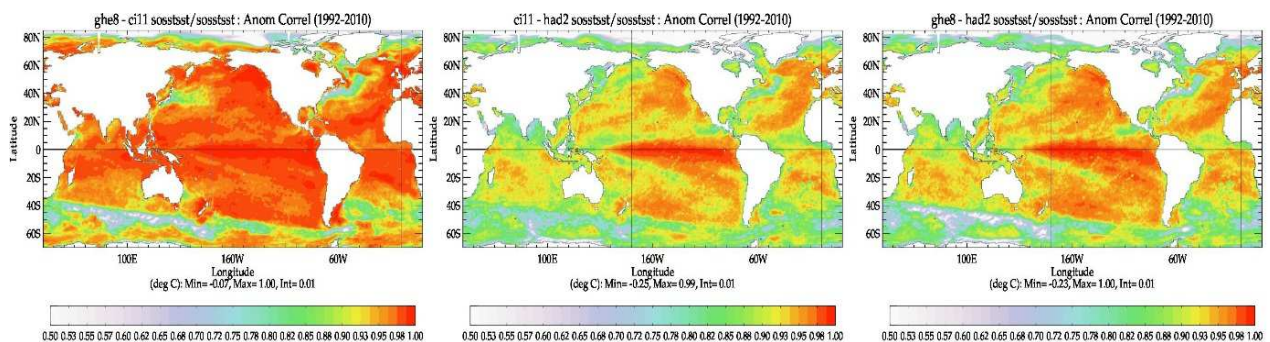


Figure 6: Correlation of monthly-mean SST anomalies (seasonal cycle removed) from 1992—2010 between (left) ORA CCI-SST and CCI-SST, (middle) CCI-SST and HadISST2, and (right) ORA CCI-SST and HadISST2.

CMUG Phase 2 Deliverable

Reference: D3.1: Quality Assessment Report
Due date: June 2016
Submission date: July 2016
Version: 2.0c



Ingesting CCI-SST in the ORA system has an impact on the simulation of some other important aspects of climate variability and change. We will limit the discussion to upper-ocean heat content (UOHC) and sea ice cover here; for these variables the impact is most pronounced.

The overall trend and variability of global-mean UOHC in ORA CCI-SST is close to that of ORA REF. However, UOHC is slightly higher for several periods, especially between 1994 and 2000 (Figure 7 left). This differences comes mainly from the tropical oceans (Figure 7 middle), while the UOHC in the North Pacific is lower in ORA CCI-SST than in ORA-REF (Figure 7 right). These UOHC differences are consistent with the SST differences shown in Figure 5.

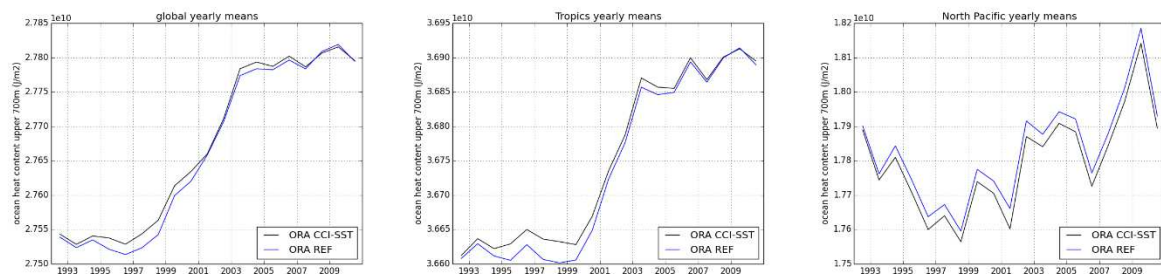


Figure 7: Upper 700m ocean heat content from 1992-2010, averaged over (left) the global ocean, (middle) tropical oceans, and (right) the North Pacific.

There is a significant and consistent impact of CCI-SST on Northern Hemisphere sea ice cover, as illustrated by Figure 8. Although trend and variability of Northern Hemisphere sea ice area fraction and Arctic sea ice thickness in ORA REF are reproduced in ORA CCI-SST, a rather constant positive offset is apparent. One might speculate that the on average colder SST in the northern extra tropics are responsible, but closer inspection of seasonal and regional signals (not shown) suggest there is not such a clear correspondence between SST and sea ice cover, and it appears that further investigation into the mechanisms of propagating the SST information to the sea ice would be useful. This will also connect to and enhance the already documented inconsistencies between SST and sea ice data sets.

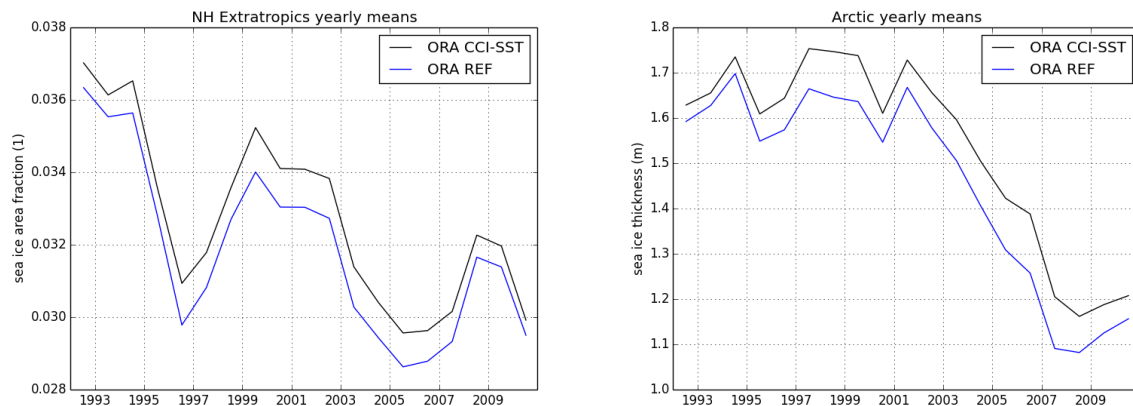


Figure 8: Northern Hemisphere annual-mean sea ice for ORA CCI-SST and ORA REF. (Left) average sea ice area fraction over northern extra-tropical oceans; (right) average sea ice thickness of the Arctic.

Technical comments on the data

Here, the following CCI data products were used:

- Sea surface temperature: level 4 data, analysed daily mean at 20cm depth on 1/20 degree regular grid, version 1.1, available 1992—2010
- Sea surface height: level 2 data, along-track anomalies referenced to DTU10 mean sea surface + level 4 data to calculate global mean sea level for freshwater budget corrections in assimilation, available 1993—2012
- Sea ice concentration: level 4 SSMI data, analysed daily means on EASE2 hemispheric grids with 25km resolution, available 1992—2008

When preparing the data, a few technical problems were found. For future use of the data in weather and climate models, it might be helpful to address these.

1. Due to the details of the analysis method, the MSLA gridded data contains spurious data over land points, but does not provide a land-sea mask. This is a well-known problem, but since it is not documented in the data themselves, it is easy to obtain wrong results when performing area averages. We suggest to either provide a land-sea mask in the files, or to remove the spurious data in future versions.
2. The gridded MSLA data are only available as monthly means. While this is sufficient for most applications, it poses a problem when the global mean sea level is needed on a daily basis to constrain the daily fresh-water balance. Therefore, for data assimilation purposes, it would be very helpful to have the gridded MSLA data as daily means.
3. The SSMI SIC data have a constant number of missing values (the land points), but on just three days, the 25th, 26th, and 27th August 2008, there are additional missing values in the Hudson Bay. The status flag indicates that the cause was missing satellite data. This can cause problems in interpolation routines which for efficiency reasons assume constant missing values over time. A warning in the data documentation about unusual missing values would be appreciated.

CMUG Phase 2 Deliverable

Reference: D3.1: Quality Assessment Report
Due date: June 2016
Submission date: July 2016
Version: 2.0c



3.3 Assimilation of several L2 ozone products in the ERA system [WP 3.2]

Aim

The aim of this study is to promote and facilitate the integration of as many O3-CCI products as possible in reanalysis systems in general and in the forthcoming ERA5 production in particular. A number of Observing System Experiments (OSEs) have been designed to provide a detailed assessment of the quality and of the impact of these O3-CCI products. The list of assessed datasets includes seven products encompassing the three lines of production of O3-CCI (total column, profiles from nadir instruments, and profiles from limb instruments).

A set of Round Robin (RR) assimilation exercises for algorithm selection were performed using ozone datasets retrieved alternative algorithms from the same radiance measurements. The aim of the RR exercise was to provide an objective and rigorous assessment of the impact of assimilating similar datasets, thus giving the reanalysis community feedback on which one to use.

By inter-comparison with the results from some of the performed experiments, it is possible to provide user recommendations to space agencies and retrieval teams on the most useful characteristics of future satellite instruments for ozone measurement.

Summary of Results

The results from this study were reported in the CMUG QAR (2015), and briefly summarized as follows:

- The structure of observation uncertainties generally compare well with estimates obtained using the Desroziers method (Desroziers et al., 2005). The differences between estimated and provided uncertainties show up to 60% overestimation in the tropical mid stratosphere for GOME-2 NPO3 (this accounts for less than 4% of the observation values) and up to 100% underestimation in the tropics for the total columns (this difference is about 8% of the global mean total column ozone value).
- All the products exhibit negligible to very small biases.
- All assessed O3-CCI datasets lead to improved ozone analyses.
- Regarding the RR assimilation exercises, with the exception of OMI TCO3, the O3-CCI retrievals seem to better constrain the ozone analyses than retrievals obtained from the same radiances using alternative algorithms.
- The assimilation of the GOME-2 NPO3 show a clear improvement in the internal consistency of the data assimilation system in terms of better fit to the AIRS ozone-sensitive IR channels that in turn leads to statistically significant reduction (i.e. improvement) in the RMS of the geopotential forecast errors in the tropics.
- Assimilation User Requirements to Space Agencies and retrieval teams:

CMUG Phase 2 Deliverable

Reference: D3.1: Quality Assessment Report
Due date: June 2016
Submission date: July 2016
Version: 2.0c



-
- ❖ The comparison of the impact generated by the GOME-2 TCO3 and that of the GOME-2 NPO3 shows that the latter dataset can lead to a greater positive impact on the ozone analyses than the former.
 - ❖ The comparison of the impact generated by the GOME-2 NPO3 and that of the MIPAS LPO3 shows that thanks to its higher vertical resolution limb observations can lead to a greater positive impact in the stratosphere and upper troposphere than the nadir ozone profiles. This is not always the case in the lower troposphere, where despite lacking visibility, the limb observations can still improve the ozone analyses compared to a control experiment if their synergy with other observations (in particular total column ozone products) can be exploited within the data assimilation system.

The recommendations that were formulated on the basis of the results and conclusions summarized above were un-controversially accepted by the C3S reanalysis team, and the following O3-CCI products are being assimilated in the ERA5 reanalysis currently in production: SCIAMACHY TCO3; GOME and GOME-2 NPO3; MIPAS LPO3.

A summary paper, Dragani (2016), has been accepted for publication in Atmospheric Chemistry and Physics Discussion, and it is now under review for Atmospheric Chemistry and Physics.

CMUG Phase 2 Deliverable

Reference: D3.1: Quality Assessment Report
Due date: June 2016
Submission date: July 2016
Version: 2.0c



3.4 Integrated assessment of the CCI Aerosols, GHG, and Ozone datasets [WP3.3]

Aim

WP3.3 aims at providing an integrated assessment of the impact of assimilating ozone, aerosol, and GHG datasets in the global atmospheric composition data assimilation system developed through a number of FP6, FP7, and H2020 projects (GEMS, MACC, MACC-II, and MACC-III) and currently operated by the Copernicus Atmosphere Monitoring Service (CAMS) to provide NRT monitoring of air quality relevant gases and their reanalyses. The results are expected to feed back into the decision process in preparation for the forthcoming, first reanalysis of the CAMS.

To maintain this WP aligned with the state-of-the-art research and understanding, as well as needs of both groups, further interactions with the CCI community and the MACC/CAMS ECV experts at ECMWF continued after the CMUG Phase 2 proposal was accepted. These interactions indicated that to best meet the evolving needs of both the CCI consortia, and the CAMS while still attempting at providing an indication of the consistency between the three ECVs the original experiment design had to be substantially modified. The new design is discussed below, and contrasted with the original one.

Summary of the results

The discussion presented here is based on preliminary results that will need to be carefully confirmed by further analysis. The significant changes adopted in the experiment design have caused some delays in the original schedule, so it is not possible at this stage to provide a full account for the three ECVs. At the time of writing, the experiments are still running and in cases, e.g. for the GHG, they are not fully spun-up yet making premature any discussion. For that reason, this initial assessment focus on the assimilation of two CCI Aerosol Optical Depth or Thickness (AOD or AOT) datasets retrieved with the SU (v4.2) and ADV (v1.42) algorithms. The results available thus far can be summarized as follows:

- Based on the period available, the SU algorithm seems to produce AOD retrievals with higher values than the ADV algorithm, but the latter provides a larger dataset than the former. (For comparison, MODIS observations show values between the SU and ADV datasets.)
- The two algorithms provide similar uncertainty estimates, which appear overestimated when compared with the first-guess and analysis departures. In a data assimilation system, an overestimation of the observation uncertainty has the only consequence of limiting the

CMUG Phase 2 Deliverable

Reference: D3.1: Quality Assessment Report
Due date: June 2016
Submission date: July 2016
Version: 2.0c



observations' impact on the analyses, thus contributing to a conservative assimilation, with no detrimental consequences.

- The data assimilation system seems to be able to exploit the synergy between MODIS and AATSR AOD datasets that results in a reduction of the analysis departures when they are jointly assimilated compared to the assimilation of only one of them (i.e. either MODIS or AATSR data).
- Comparisons with the AERONET data of the modelled AOD at 500 nm from an experiment assimilating MODIS only, one assimilating (SU) AATSR, and one assimilating both show that
 - ❖ Globally, the MODIS-constrained AODs have a positive bias compared to the in-situ dataset. In contrast, the CCI (SU) AATSR-constrained AODs show a negative bias.
 - ❖ The assimilation of AATSR and MODIS data together leads to the best fit to AERONET globally.
 - ❖ The level of agreement with the AERONET observations strongly depends on the geographical area.
 - In the South-East Asia, the MODIS-only experiment exhibits the best fit to the AERONET observations.
 - Over Europe, the two datasets lead to residuals from AERONET that are of similar magnitude, but opposite sign, clearly showing an inter-instrumental bias-related problem. Here, the combination of the two instruments, generally improves the agreement to the independent observations.
 - Over Africa, North and South America, the modelled AOD shows the best fit to the independent observations when only constrained by the CCI AATSR retrievals.

The data assimilation system

The data assimilation system used in this study consists in the most recent version of the global atmospheric composition data assimilation system operated at ECMWF for the CAMS. At present, this system uses a bin-model for aerosol that includes desert dust, sea salt, organic matter, black carbon and sulphates, as well as the greenhouse gases, allowing assimilation of CO₂ and CH₄. For the chemical reactive species (i.e. O₃, CO, NO₂, SO₂ and HCHO), the IFS data assimilation system was extended to include an integrated chemistry model (referred to as C-IFS), which provides emissions, deposition, and chemical tendencies for the species included in the system. These variables are all constrained by the assimilation of satellite observations, where possible.

The experiment design

CMUG Phase 2 Deliverable

Reference: D3.1: Quality Assessment Report
Due date: June 2016
Submission date: July 2016
Version: 2.0c



The assessment of the three CCI ECVs within the MACC-II system is performed in both passive and active modes.

An experiment design was originally proposed. It included four data assimilation experiments, with the first one used as a control that included all CCI data in passive mode and three additional, incremental active experiments (see Table 3).

Furthermore, in the submitted proposal it was suggested that the active assimilation of CCI datasets made use of:

- The GOME-2, SCIAMACHY and OMI TCO3 and MIPAS LP datasets from the O3-CCI;
- The AATSR AOD from one algorithm to be decided among those available from Aerosol-CCI;
- The XCO2 retrievals from one algorithm and one instrument from the GHG-CCI.

Experiment	CCI O3	CCI Aerosols	CCI GHG
Control	passive	passive	passive
Exp 1	active	passive	passive
Exp 2	active	active	passive
Exp 3	active	active	active

Table 3: Originally proposed experiment design for WP3.3.

As anticipated above, to maintain this WP aligned with the state-of-the-art research and understanding, as well as needs of both the CCI community and the CAMS, the original experiment design, presented above, had to be substantially modified. Below, we first report on the new requirements and needs and then provide a summary table of the new experiment set-up.

The new requirements from CAMS indicated that:

1. **On Ozone:** There was a good understanding on how to use the ozone products from the nadir instruments (in particular, SCIAMACHY nadir, OMI, GOME, GOME-2) but not enough on the use of the limb datasets, with the exception of MIPAS. A similar request on assessing other limb datasets was also made by members of the O3-CCI consortium.
2. **On Aerosols:** preliminary assimilation runs had been performed for 2008 with an earlier version of the data assimilation system using the ADV retrievals from AATSR. Interest was expressed in assessing the SU retrievals and contrasting the impact of the two datasets, and their synergy and consistency with MODIS data.
3. **On GHG:** an assessment of the difference in the impact of assimilating the proxy product and the full physics product was considered useful.

CMUG Phase 2 Deliverable

Reference: D3.1: Quality Assessment Report
Due date: June 2016
Submission date: July 2016
Version: 2.0c

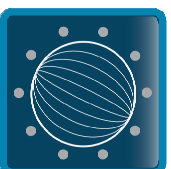


Additionally, at the time the new CAMS requirements were defined, it was noted that the GHG CCI had not yet finalized the baseline algorithm selection for some products.

To account for these new requirements, the modified experiment design includes six assimilation experiment instead of the four envisaged, and it is presented in Table 4. Experiments Exp 1 – Exp 4 are used to assess the individual aspects for each of the three ECVs with respect to the Ctrl while Exp 5 will help to assess the level of consistency between the three ECVs when contrasted with the results from the other five experiments.

All the experiments were started on 1 Jan 2010, and will run to cover the period till the end of September 2010, with the aim of analysing in detail the NH summer period (May-September 2010) after removing the period affected by spin-up. They make use of the branch currently used for preparing the next CAMS reanalysis and run with a resolution of T255 (about 80 km) on 60 vertical levels.

The changes in the experiment set-up required a much larger number of datasets to be processed than originally anticipated, with some of the ozone datasets being still pre-processed at the time of writing. This caused some delays on the schedule with some of the experiments not yet completed and others still within the spin-up period. This is particular critical for the GHG, for which a spin-up period is normally estimated in four to five months (S. Massart, personal communications), much longer than that for aerosols and ozone. It is also noted that the IASI CO₂ and CH₄ were assimilated in most experiments to improve the GHG background information, but also in an attempt of reducing the system spin-up. Based on these considerations, only preliminary results concerning the aerosols can be discussed as a proof of concept over the period available. These should also be carefully confirmed by further analysis.



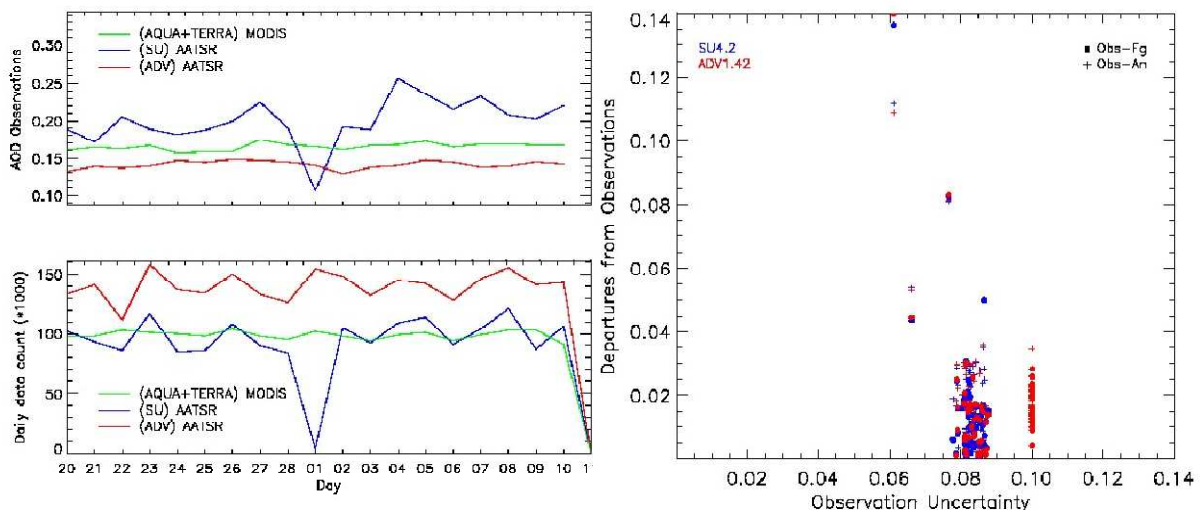
Experiment NAME / ID	Ozone		Aerosol		GHG			
	Passive	Active	Passive	Active	CO ₂		CH ₄	
					Passive	Active	Passive	Active
Control / gi90	SCIA limb OSIRIS SMR ACE-FTS	SBUV SCIA TCO3	SU AATSR	MODIS	BESD SCIA SRFP TANSO	IASI	SRFP TANSO	IASI
Exp 1 / gi91	OSIRIS SMR ACE-FTS	SBUV SCIA TCO3 SCIA limb	MODIS	SU AATSR	BESD SCIA	IASI OCFP TANSO	N/A	IASI SRFP TANSO
Exp 2 / gi92	SCIA limb OSIRIS SMR	SBUV SCIA TCO3 ACE-FTS	N/A	MODIS SU AATSR	BESD SCIA	IASI SRFP TANSO	N/A	IASI SRPR TANSO
Exp 3 / gi93	SCIA limb OSIRIS ACE-FTS	SBUV SCIA TCO3 SMR	MODIS	ADV AATSR	OCFP TANSO	IASI BESD SCIA	IASI	SRFP TANSO
Exp 4 / gi94	SCIA limb SMR ACE-FTS	SBUV SCIA TCO3 OSIRIS	N/A	MODIS ADV AATSR	N/A	IASI SRFP TANSO BESD SCIA	IASI	SRPR TANSO
Exp 5 / gi95	SCIA limb OSIRIS SMR	SBUV SCIA TCO3 ACE-FTS	ADV AATSR	MODIS	OCFP TANSO	IASI	SRPR TANSO	IASI

Table 4: New experiment design for WP3.3. The CCI data are given in bold. The experiment IDs as used in the following plots are provided in the first column together with their name.



Preliminary discussion on Aerosols:

Figure 9 (left panels) shows the global mean statistics for the CCI AATSR AOD data retrieved from the SU algorithm (v4.2) and ADV (v1.42) algorithm, and contrast it with that of MODIS retrievals during the period 20 February – 10 March. MODIS data here are taken with the same configuration used as default in the IFS that foresees a data thinning over a $0.5^\circ \times 0.5^\circ$ resolution grid. No thinning is instead applied to the AATSR retrievals. From the short period available, the SU algorithm leads to higher AOD values than the ADV algorithm, but the latter provides a larger dataset than the former.



*Figure 9: **Top left panel:** Time series of the global daily mean AOD statistics for MODIS (green lines), and the CCI AATSR retrieved with the ADV (v1.42) algorithm (red lines) and the SU (v4.2) algorithm (blue lines) during the period 20 February – 10 March. **Bottom left panel:** Data count for the three datasets. MODIS data is used in the default IFS configuration that foresees a thinning over a $0.5^\circ \times 0.5^\circ$ grid. **Right panel:** Scatter plot of the observation uncertainty derived from the SU algorithm (blue symbols) and ADV algorithm (red symbols) versus the absolute value of the first-guess and analysis departures from the observations. The filled circles refer to the first-guess departures, the crosses refer to the analysis departures.*

The uncertainty provided by the two AATSR algorithms is compared with the modelled AOD departures against the observations (right panel in Figure 9). The inspection would suggest that the two algorithms provide uncertainty estimates of similar magnitude that are larger than the first-guess and analysis departures. It is noted that in data assimilation, an overestimation of the observation uncertainty has the only consequence of limiting the observations' impact on the analyses, thus contributing to a conservative assimilation, generally desirable to avoid potential degradation in the analyses.

CMUG Phase 2 Deliverable

Reference: D3.1: Quality Assessment Report
Due date: June 2016
Submission date: July 2016
Version: 2.0c



Figure 10 shows the global mean statistics for AATSR AOD data from the CCI SU algorithm. In the left hand side panels, the AATSR data are passively monitored and MODIS observations from both AQUA and TERRA are assimilated. In the right hand side panels, the assimilation of MODIS AOD data was completely replaced by that of the AATSR AOD observations.

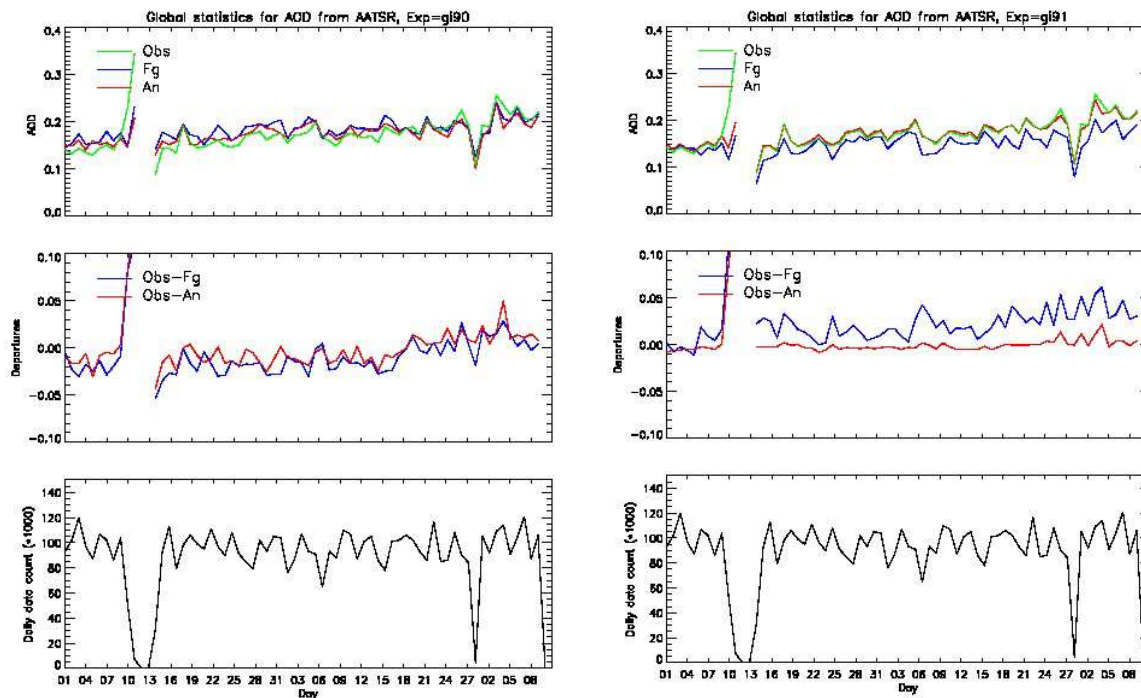


Figure 10: Time series of the global daily mean statistics computed from the experiments gi90 (Ctrl, i.e. assimilation of MODIS only, left hand side panels), and gi91 (Exp 1, i.e. assimilation of the CCI AATSR dataset retrieved from the SU algorithm, right hand side panels). The top panels show the mean modelled and observed AOD; the middle panels the first guess and analysis departures from the CCI AATSR observations, and the bottom panels the CCI AATSR AOD data count. The period is from 1 January to 10 March 2010.

The top left panel of Figure 10 shows that there is a general good agreement between the AATSR retrievals and the first guess and analyses constrained by MODIS AOD data, with a trend in the departures (mid left panel) that exhibit modelled values higher than AATSR until about 20 February and lower afterwards. When the assimilation of MODIS is replaced by that of AATSR, the analysis departures decrease as expected (mid right panel).

Figure 11 shows the AATSR global statistics similar to those in Figure 10, but obtained from Exp 2, which assimilated both MODIS and AATSR AOD observations. The most significant aspect is that the data assimilation system seems to be able to exploit the synergy between the two AOD datasets. A first indication of such a synergy is the reduction of the analysis departures in Exp 2 for both AATSR and MODIS (mid left panel of Figure 11 compared to Ctrl (mid-left panel of Figure 10 for AATSR).

CMUG Phase 2 Deliverable

Reference: D3.1: Quality Assessment Report

Due date: June 2016

Submission date: July 2016

Version: 2.0c

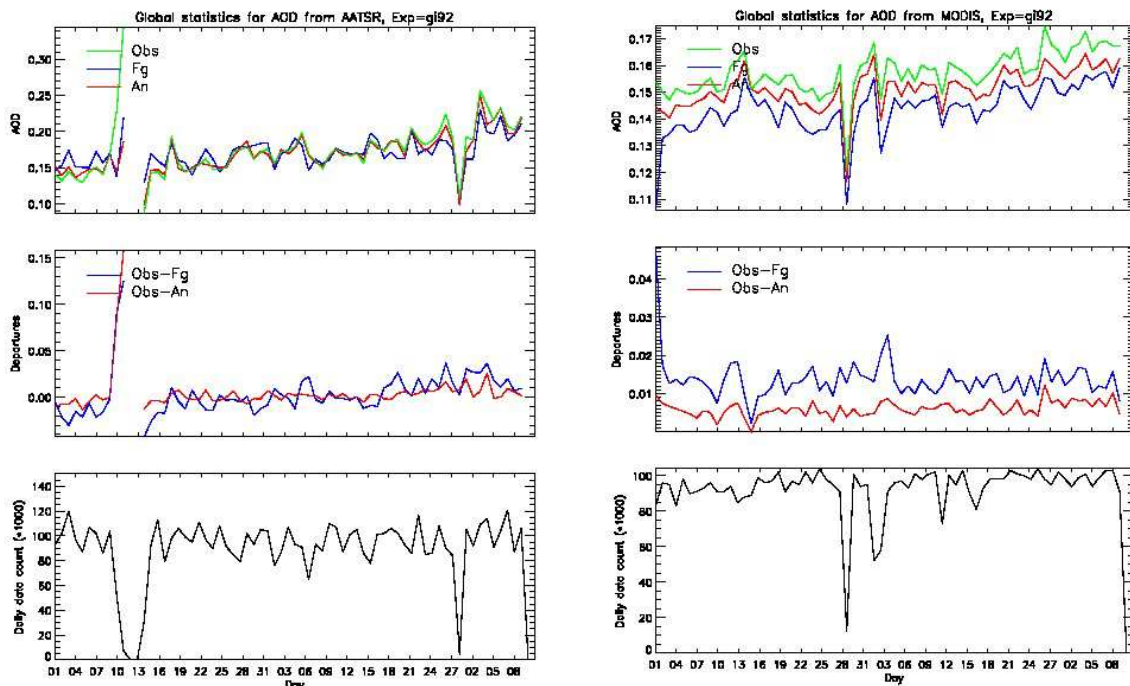


Figure 11: As in Figure 10 (left panels), but for Exp 2 constrained by the assimilation of both MODIS and (SU) AATSR AOD observations. The left hand side panels show the statistics for AATSR, the right hand side panels show similar statistics for MODIS.

The impact of assimilating AATSR either on its own or in addition to the MODIS data has been assessed by comparison with independent AOD observations obtained from the AERONET network. These preliminary comparisons refer to the period 15 January – 20 February 2010, after discarding the first two weeks of run, and refer to the AATSR AOD retrievals obtained with the SU algorithm. Figure 12 shows an example of verification of the modelled AOD at 500 nm (left) and at 1640 nm (right) against the AERONET dataset for three of the experiments detailed in Table 4. It is noted that only the 500nm is actively constrained. This means that changes are mostly expected at 500 nm, while only negligible to small impact should be noticed at the longest wavelength. Thus, the time series should be very similar to each other and they are only shown as a basic quality check.

Figure 12 (left hand side panels) shows that the information provided by MODIS tends to increase the global aerosol amount above the values measured by the AERONET stations, thus MODIS would have a positive bias compared to the in-situ dataset. In contrast, the CCI (SU) AATSR AOD assimilation tends to decrease the AOD distribution below that reported by the AERONET data, thus showing a negative bias. The assimilation of AATSR and MODIS data together leads to the best fit of the modelled aerosols to AERONET. The impact on the 1640 nm wavelength (Figure 13, right hand side panels) is as expected negligible to very small.

CMUG Phase 2 Deliverable

Reference: D3.1: Quality Assessment Report

Due date: June 2016

Submission date: July 2016

Version: 2.0c

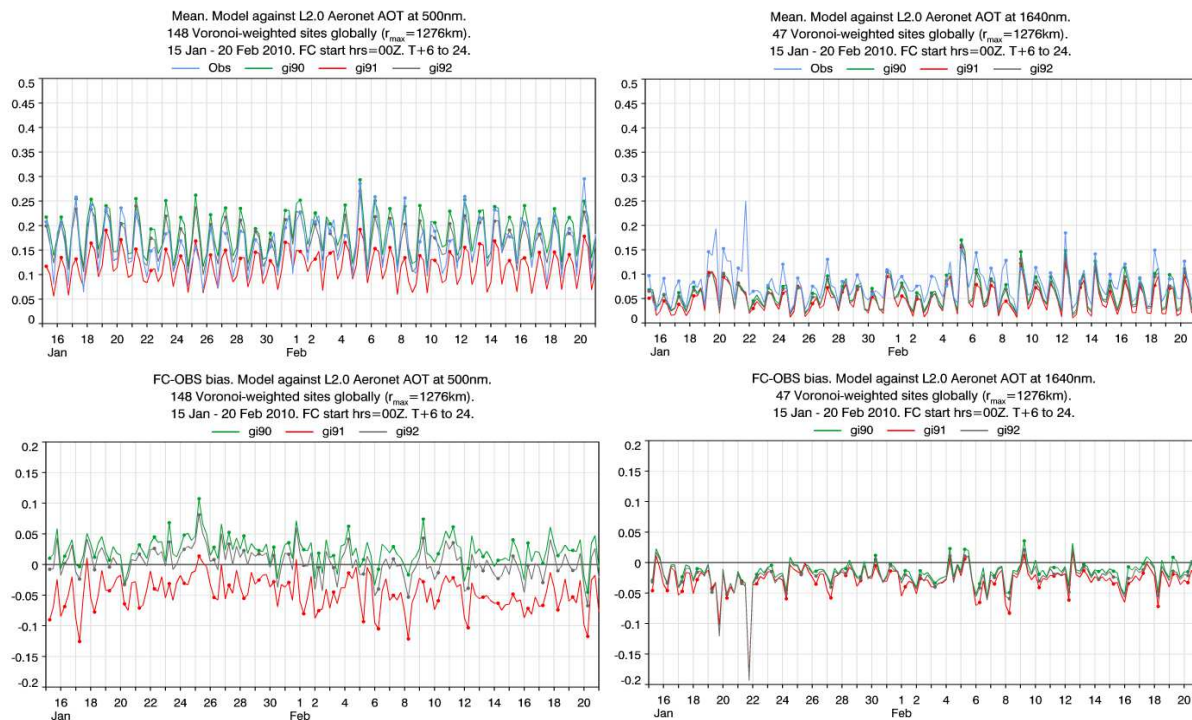


Figure 12: Top panels: Time series of the global mean modelled Aerosol Optical Depth at 500 nm from the experiments gi90 (Ctrl, i.e. assimilation of MODIS only in green), gi91 (Exp 1, i.e. assimilation of the CCI AATSR dataset retrieved from the SU algorithm in red), and gi92 (Exp 2, i.e. assimilation of both MODIS and CCI [SU] AATSR dataset in black), and the observation from the AERONET network (blue). The top left panel refers to the 500 nm wavelength; the top right panel refers to the 1640 nm wavelength. **Bottom panels:** Modelled AOD departures from the AERONET observations at 500 nm for the same three experiments presented in the top panels.

The level of agreement with the AERONET observations strongly depends on the geographical area. Figure 13 presents the area averaged time series of the modelled AOD departures from the AERONET observations for the same three experiments shown in Figure 12. Five areas are represented: Europe, Africa, North and South America, and South-East Asia.

- In the South-East Asia, the MODIS-only experiment exhibits the best fit to the AERONET observations.
- Over Europe, the two datasets lead to residuals from AERONET that are of similar magnitude, but opposite sign, clearly showing an inter-instrumental bias-related problem. Here, the combination of the two instruments, generally improves the agreement to the independent observations.
- Over Africa, North and South America, the modelled AOD shows the best fit to the independent observations when only constrained by the CCI AATSR retrievals. These differences could be due to a number of reasons, e.g. the ability of the two retrieval schemes to deal with specific aerosol types, their characterization, the AOD model bias,

CMUG Phase 2 Deliverable

Reference: D3.1: Quality Assessment Report

Due date: June 2016

Submission date: July 2016

Version: 2.0c



and the model's ability to efficiently extract the information in the assimilated observations.

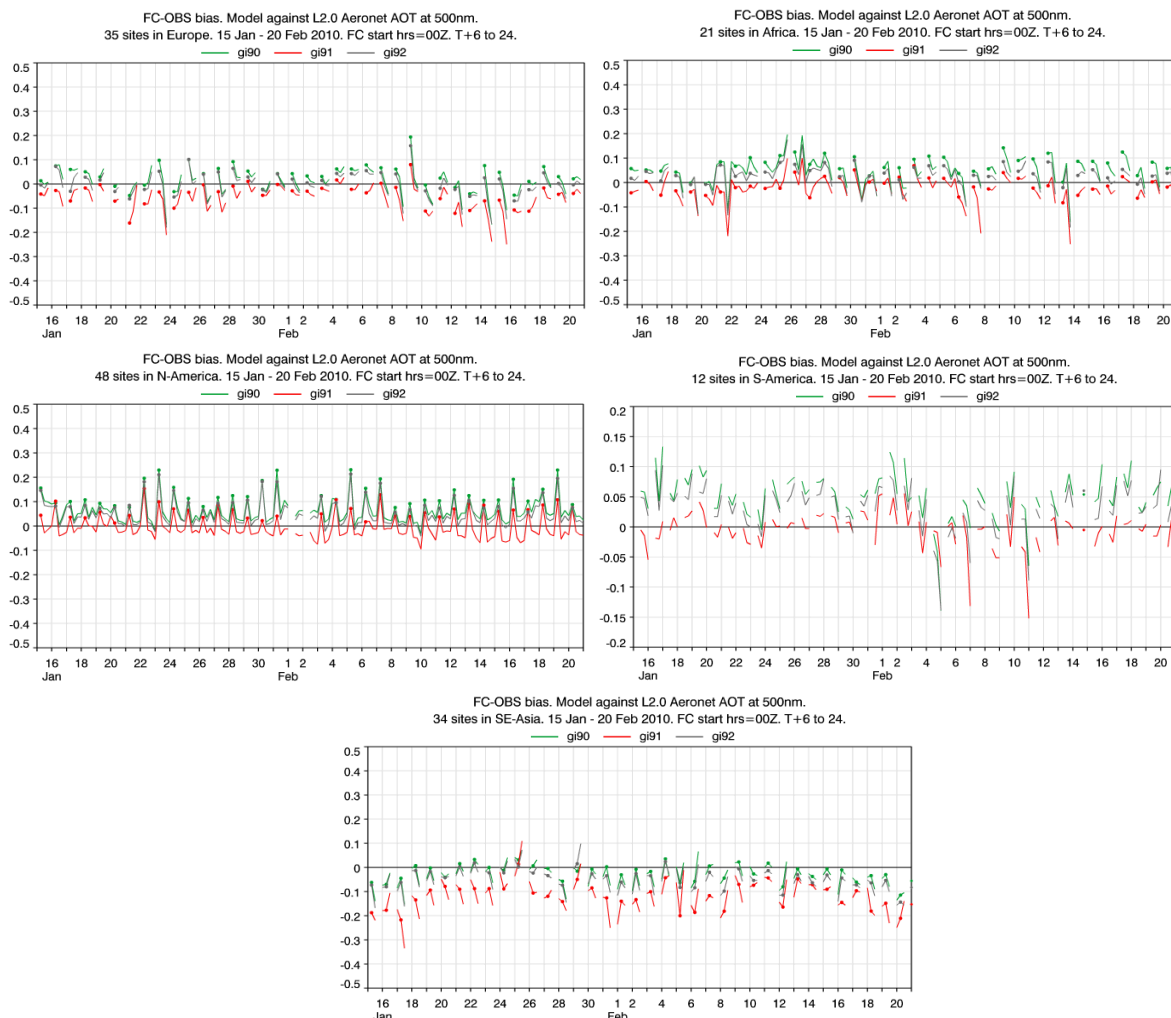


Figure 13: Time series of the departures between the modelled AOD and the AERONET observations for experiments Ctrl (green, MODIS only), Exp 1 (red, AATSR only) and Exp 2 (black, MODIS and AATSR) at 500 nm and for five regions: Europe (top left panel), Africa (top right panel), North and South America (middle left and middle right panel, respectively), and South-East Asia (bottom panel). The number of AERONET sites available in each region is reported in each title.

Further to Figure 13, Figure 14 shows the correlations between the modelled and AERONET AODs at 500nm by station for the three experiments discussed in Figures 12 and 13. It confirms that over the South-East Asia the assimilation of MODIS AOD produces modelled AODs that have higher correlation with the AERONET observations than those constrained with the CCI AATSR retrievals. In contrast, the latter show higher correlation with AERONET data than the former over the South America.

CMUG Phase 2 Deliverable

Reference: D3.1: Quality Assessment Report
Due date: June 2016
Submission date: July 2016
Version: 2.0c

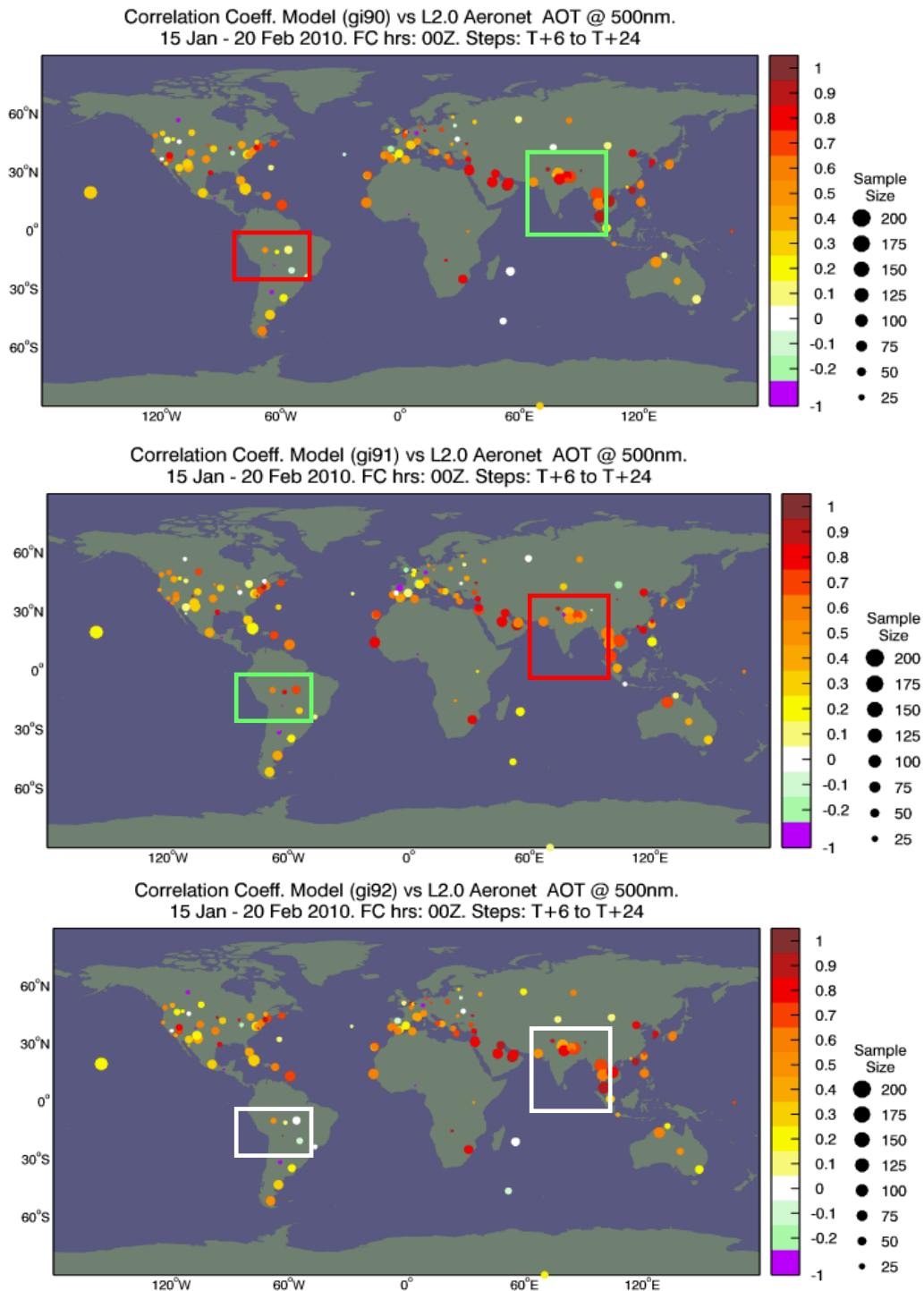


Figure 14: Correlation coefficient between the modelled AOD and the AERONET data at 500 nm at various sites for experiment Ctrl (MODIS only, top panel), Exp 1 (AATSR only, middle panel) and Exp 2 (MODIS and AATSR, bottom panel). The size of each circle refers to the size of sample used to estimate the correlations. The squares over the South-East Asia and South America refer to the area where the largest differences between the MODIS only and AATSR only experiments were found.

CMUG Phase 2 Deliverable

Reference: D3.1: Quality Assessment Report
Due date: June 2016
Submission date: July 2016
Version: 2.0c



3.5 Integrated assessment of CCI terrestrial ECVs impact in the MPI-ESM [WP3.4]

Aim

WP3.4 includes an integrated assessment of the terrestrial ECV variables available in the CCI with a joint analysis of the ECVs land cover, fire, soil moisture, and greenhouse gases (GHG). The ECVs were used to optimize uncertain parameters in the MPI-M ESM fire model process formulations using an optimum estimate framework, to make use of the uncertainty information provided with the ESA CCI datasets. The overarching questions to be addressed were:

- Are the four CCI data-sets consistent with each other and with model data so that modelled and observations data can be used directly for model validation and data assimilation?
- How can CCI data records be used to improve fire emission modelling in an earth system model?
- Do simulated carbon emissions improve using CCI datasets?

Summary of Results

SPITFIRE-JSBACH simulations were performed for the time period 1850 to 2010 in which burned area and fire carbon emissions are interactively simulated. Simulations were run with the standard model setup as described in detail in Lasslop et al., 2014. In addition, simulations were performed with a modified representation of the Nesterov-Index in SPITFIRE following Groisman et al. 2007. The modified version served as a first test case to use ESA CCI data in the evaluation of the SPITFIRE-JSBACH model. Simulated, FIRE_CCI burned area as well as burned area reported in GFEDv3/GFEDv4 based on MODIS (Giglio et al., 2006, Giglio et al., 2010) for the time period 2006-2008 are compared in Figure 15.

Contrasting the burned area with soil moisture reported from CCI_SM, we find a distinct relationship between burned area and soil moisture with low burned area for low soil moisture (fuel limitation) and low burned areas for high soil moisture (moisture limitation).

The comparison shows that all products have a very similar distribution. The CCI-MERIS product peaks at a higher soil moisture compared to GFED products and the distribution is wider. Both versions of JSBACH-SPITFIRE peak at a too high soil moisture and the distribution is too wide.

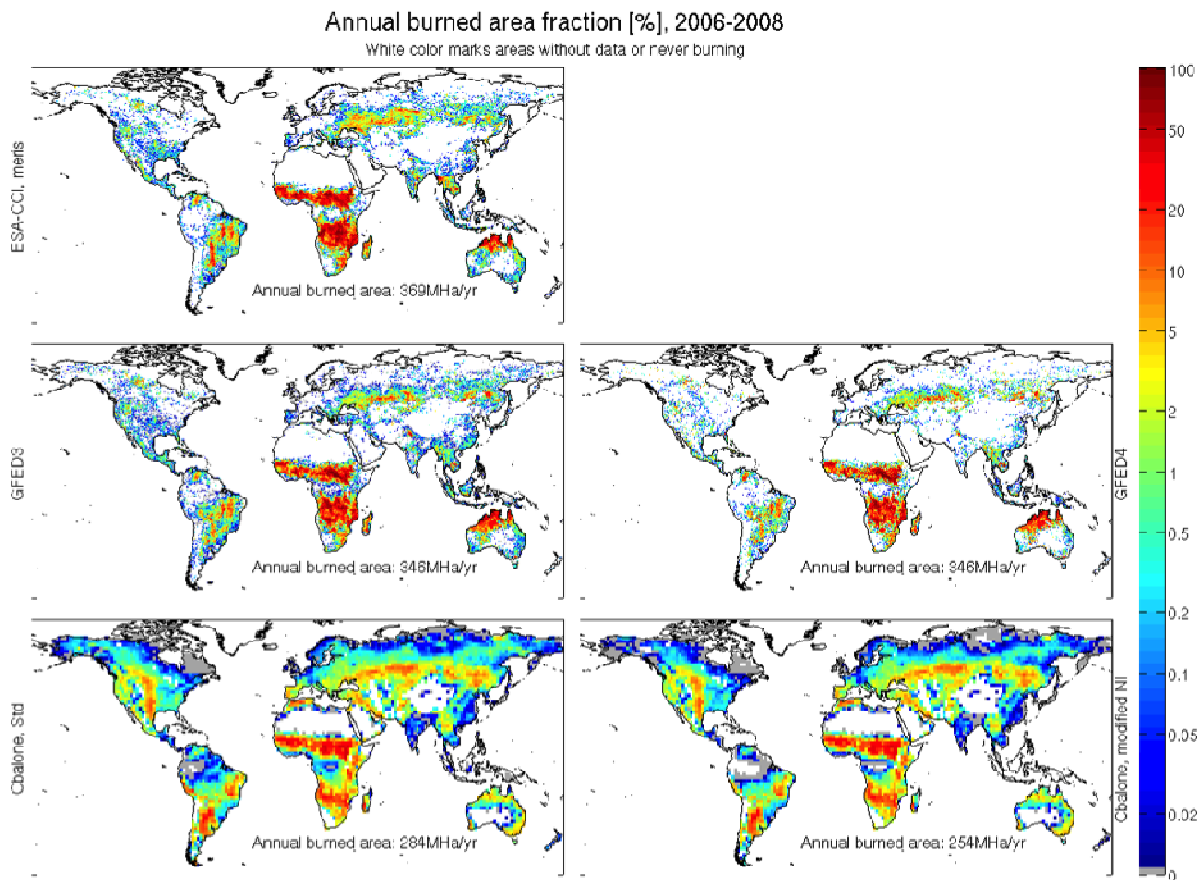


Figure 15: Burned area averaged for the years 2006-2008. FIRE_CCI (upper row), GFEDv3 and GFEDv4 (middle row), SPITFIRE-JSBACH standard and modified (lower row).

In a first step we identified two parameters (conversion soil moisture to fuel moisture and ignition rate) in SPITFIRE-JSBACH that are not well constrained by observations, which we systematically varied over a reasonable parameter space to optimize width and peak position of the soil moisture / burned area relationship. JSBACH-SPITFIRE was optimized to run a large number of experiments with varying parameter settings in a reasonable amount of time. Figure 16 shows the deviations in peak position and distribution width for 70 experiments with CCI-MERIS as reference.

Further analysis within FIREMIP will assess the differences in state-of-the-art global fire models applying CCI data.

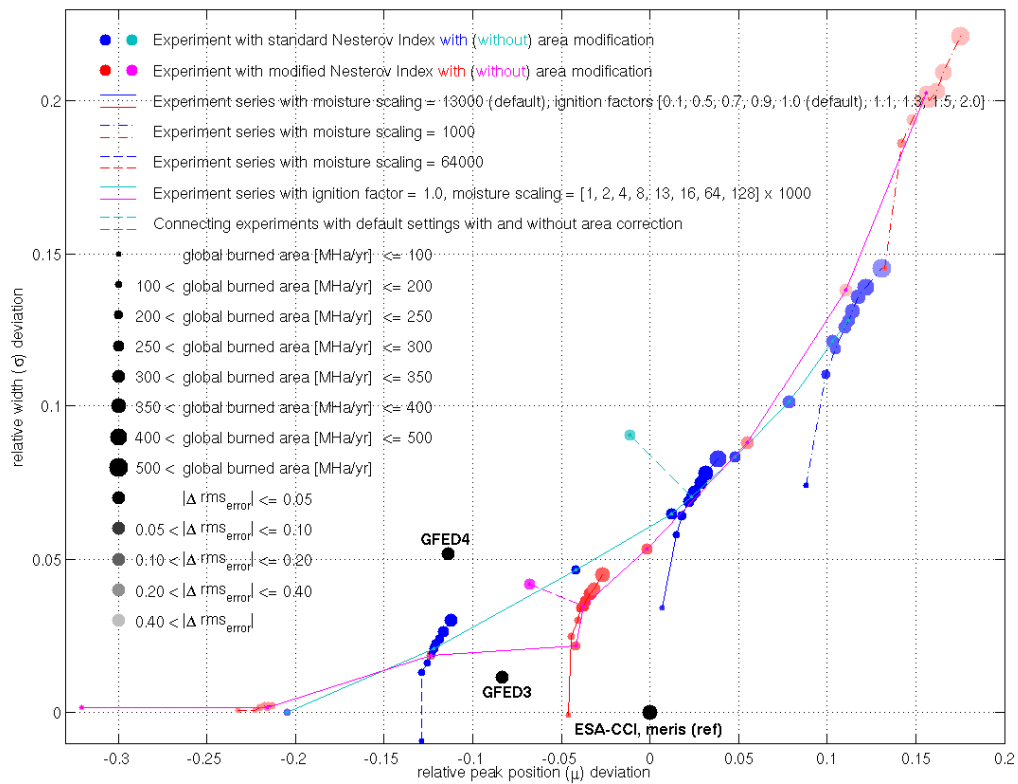


Figure 16: Relative difference in peak position and width of the burned area – soil moisture relationship for 70 experiments performed with JSBACH-SPITFIREv1/v2 compared to GFEDv3/v4 and CCI MERIS (reference).

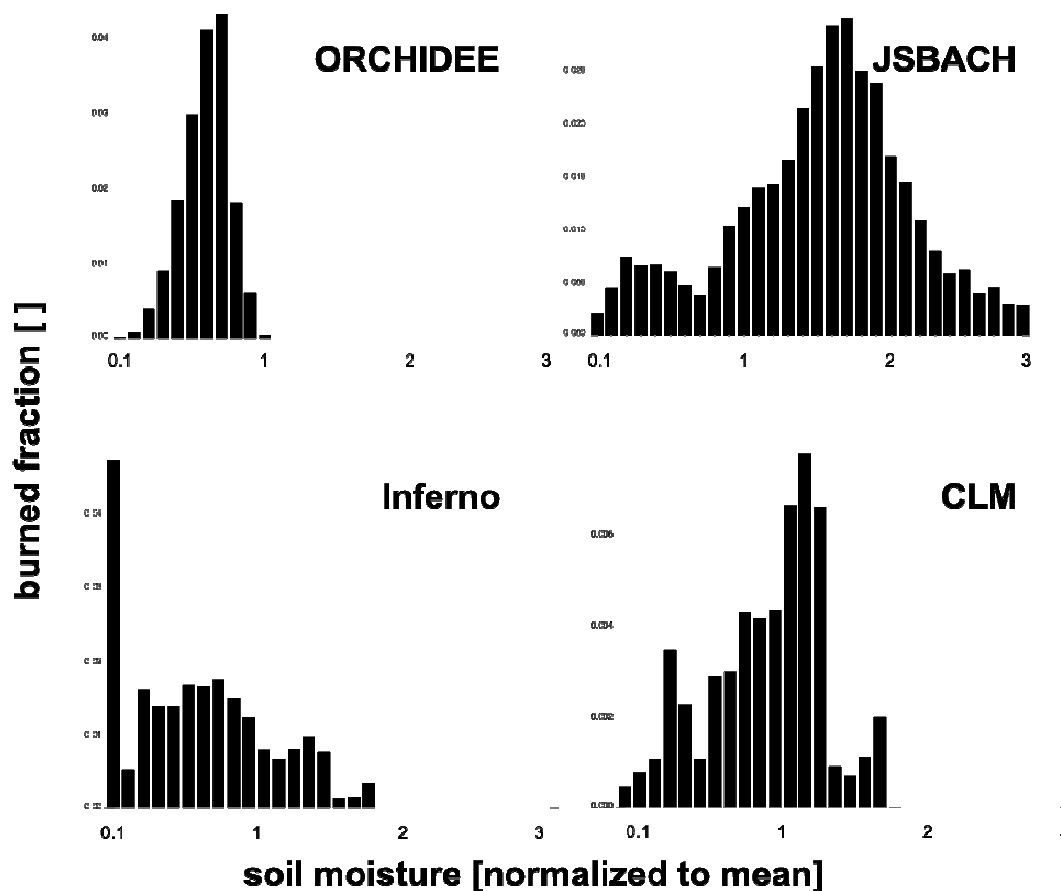


Figure 17: burned area – soil moisture relationship in four global fire models participating in FIREMIP.

Quality relevant outcomes

In WP3.4, only the gridded FIRE_CCI products were used. The FIRE_CCI gridded products from phase I were only available for a 3 year period (2006-2008), which limited their applicability for climate studies. To test the functional relationships, such as the relationship between burned area and soil moisture, global data coverage was available, reducing the dependency on having a long time series. Further assessment for fire model development will require categorization by land cover type to optimize land cover dependent parameters, which will benefit from a longer time series.

The CCI-MERIS product shows a very similar distribution of soil moisture dependency compared with the MODIS based GFEDv3/GFEDv4 product, which was applied in previous studies. These findings agree with the analysis of the FIRE CCI team reported in the Product Validation Report II and the Climate Assessment Report. The temporal stability of the product was not assessed due to the limited time period covered by the global product.



3.6 Cross assessment of clouds, water vapour, aerosols, ozone, GHG, SST, radiation and soil moisture impact on global climate variability and trends [WP_O3.4]

Aim

The aim of this WP is to make an integrated assessment of ECVs from CCI and other observations studying climate variability by investigating statistical relationships between co-varying variables and evaluate the same processes in global climate models, such as ENSO, IOD and NAO. The uncertainty information for the CCI data sets will be used when comparing to other observational data sets and associated model-generated variability. The scientific questions are:

- How are the observed ECV's related and what is the robustness of associated mechanisms across different observational data sets and climate model simulations?
- Can the models capture the relations between ECVs and the variability seen in observations?
- How do different representations of sea surface and sea ice impact on simulated variability and teleconnections?
- How do the results depend on the horizontal resolution of EC-Earth in capturing climate variability and teleconnection skills?

Key Outcomes of CMUG Research

- CCI SST, Cloud cover, sea level and ocean colour all capture the ENSO variability consistently. They ECV's are suitable for evaluating processes and climate models.
- ERA-Interim and EC-Earth AMIP simulations capture the observed ENSO variability.
- Coupled CMIP5 EC-Earth simulations are too cold over the Pacific Ocean and have too small variability for present day, towards the end of the century the model is warmer and have higher variability.
- This process study revealed issues with the NOAA satellites having problems with the scanning motor around 2000. This was known to the Cloud-CCI team but not how it could affect certain cloud products. This has been amended for in the latest Cloud-CCI v2.0 dataset, although some features remain and should be communicated to end users.

Summary of Results

The El Niño Southern Oscillation (ENSO) is the most important coupled ocean-atmosphere phenomenon affecting global climate variability on seasonal to inter-annual time scales. It is an irregularly periodical variation in winds and sea surface temperatures (SST) over the tropical eastern Pacific Ocean, affecting much of the tropics and subtropics. The warm (El Niño) phase is associated with large positive SST anomalies in eastern to central Pacific occurring on 3-7 years times-scales and the cold phase (La Niña) occurring every 2-4 years is less intense but longer

CMUG Phase 2 Deliverable

Reference: D3.1: Quality Assessment Report
Due date: June 2016
Submission date: July 2016
Version: 2.0c



lasting. The phases can be classified by calculating SST anomalies for different regions of the Equatorial Pacific, most typically the Niño3.4 region (190E-240E, 5S-5N) (Figure 18). More recently other variables, top of the atmosphere outgoing long-wave radiation and clouds have also been used to classify the ENSO events giving new perspective of the ENSO phase distributions.

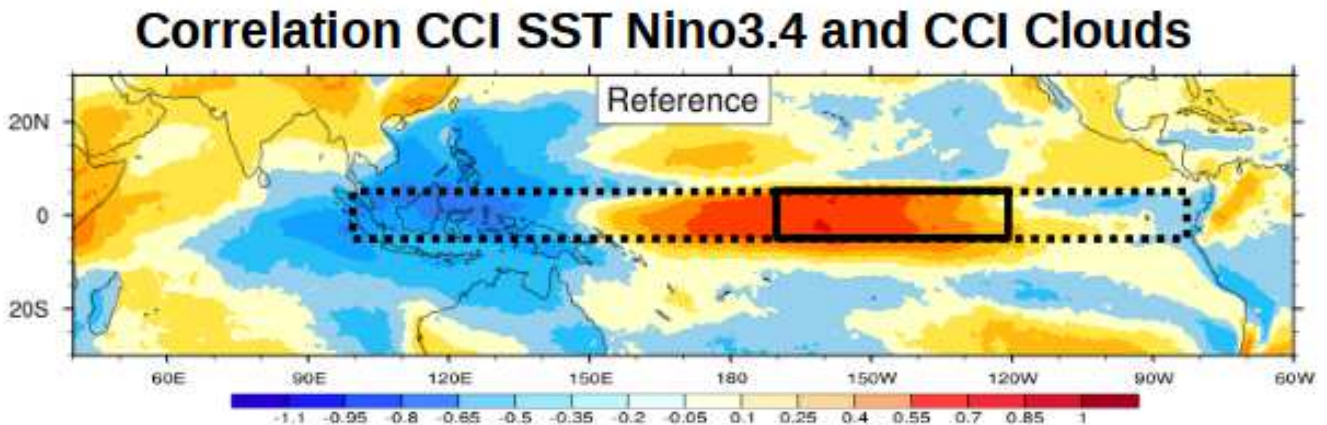


Figure 18: Correlation between CCI SST Niño 3.4 SST time series and CCI global Cloud cover for 1992-2008. The boxes show the Niño3.4 region (170W-120W, 5S-5N, black) and the Hovmöller region (100E-80W, 5S-5N, hatched) used in the other figures in this section.

The short time scale, large amplitude and multiple ECV's affected by ENSO makes it an ideal natural forcing to focus on for cross-assessment of multiple satellite records as the CCI data sets, albeit the records are too short for sampling the full ENSO diversity and the decadal ENSO variability. Climate models capture the basic ENSO features but the amplitude, life cycle and frequency are not properly reproduced and most models variability extends too far into the Western Pacific. To further understand model performances and biases, evaluating models with observational constraints derived from multiple variables can give new perspectives.

In this ongoing study we examine ENSO variability in satellite observations, CCI SST, sea level, ocean colour and clouds and the corresponding variables in climate models. Figure 19 shows the correlation between CCI SST Niño3.4 index and CCI global cloud cover. The warm El Niño phases are accompanied with deep convective clouds in the central or eastern Pacific and reduced cloudiness in the western Pacific. The maximum positive correlation is for the mid Pacific shifted west of the Niño3.4 box. We calculate Niño3.4 indices for CCI and other ECV's from their respective monthly anomalies and normalize by the standard deviation as shown for CCI and CLARA (Kaspar et al 2009) cloud cover and for HadISST (Rayner et al 2003). The cloud and SST indices co-vary especially for the positive ENSO phase. The lower panel show the Niño3.4 cloud cover indices calculated for ERA-Interim (ERA-Interim, Dee et al 2011) and for an

CMUG Phase 2 Deliverable

Reference: D3.1: Quality Assessment Report
 Due date: June 2016
 Submission date: July 2016
 Version: 2.0c

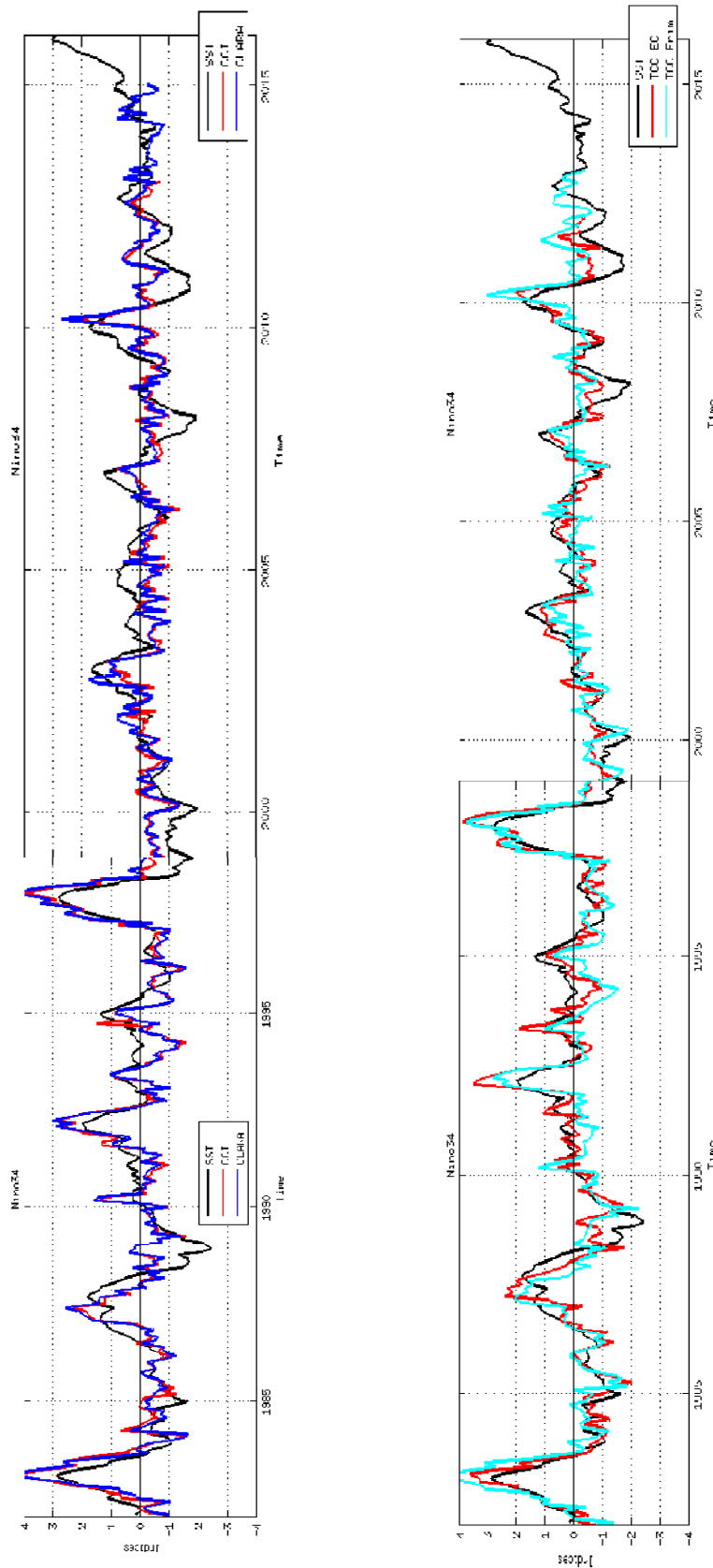


Figure 19: Niño3.4 index time series for a. HadISST (black), CCI (red) and CLARA (blue) Cloud cover and b. HadISST (black), EC-Earth (red) and ERAI (cyan) cloud cover.

CMUG Phase 2 Deliverable

Reference: D3.1: Quality Assessment Report
Due date: June 2016
Submission date: July 2016
Version: 2.0c



EC-Earth (Hazeleger et al 2010) AMIP simulation (a 30 year atmosphere only simulation with prescribed observed SST and Sea-Ice). EC-Earth atmospheric part is based on the ECMWF atmospheric model explaining the very good agreement with ERAI and that when driven by observed SST EC-Earth capture the natural variability.

For the CMUG cross-assessment and to find alternative ENSO indices, we investigate the variability for all CCI variables for the equatorial Pacific Ocean, by calculating normalized anomalies (5S to 5N) for all longitudes and months for CCI SST, Sea level, ocean color (chlorophyll) and cloud cover. The results are shown in Hovmöller diagrams (Figure 20 top row), where the positive and negative values show the deseasonalised monthly anomalies as function of longitude and time. For all variables we see the strong El Niño event 1997/1998 and the following longer La Nina period as well as other weaker El Niño's peaking further west. We note that the largest variability for the different ECV's occur at different longitudes as seen for the standard deviations (STD's) as function of longitude (lower row, Figure 20).

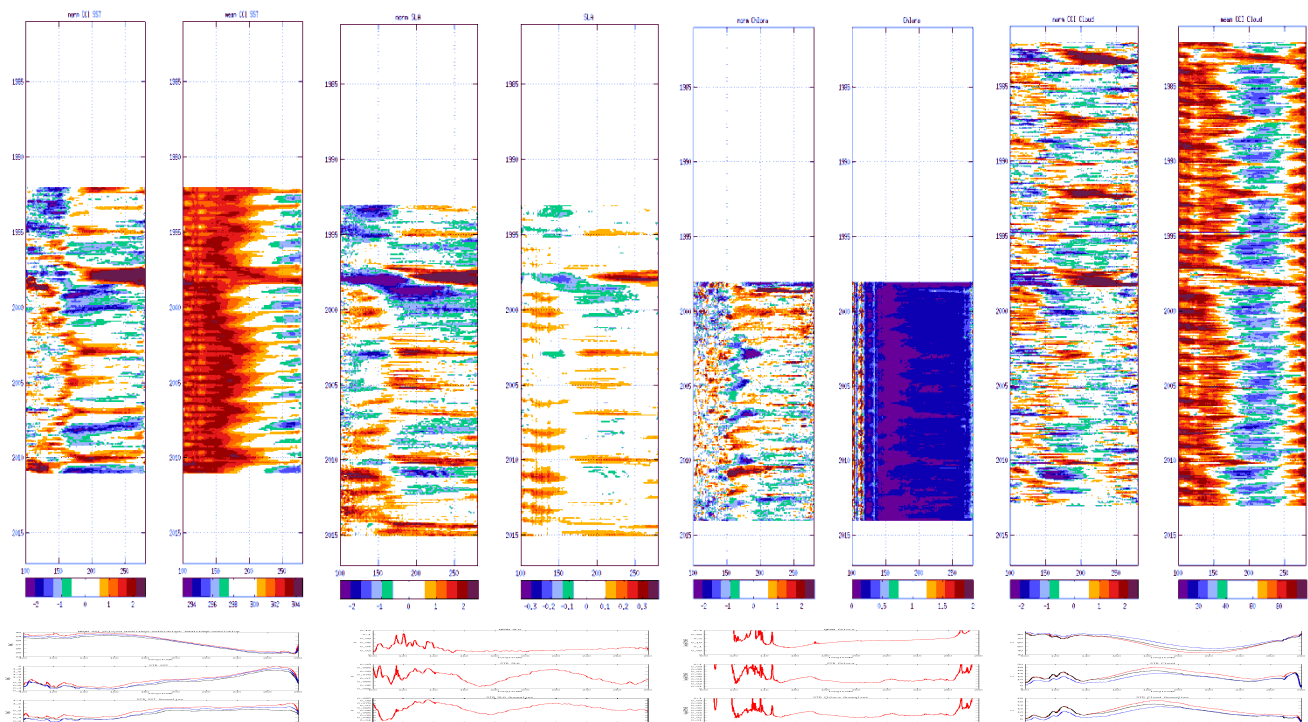


Figure 20: Hovmöller diagrams for Pacific Ocean 5S-5N normalized anomalies for CCI SST, Sea Level, Chlorophyll and Cloud cover as function of time and longitudes between 100E to 270E. Bottom row show the standard deviation for each variable as function of longitude.

SST has a wide flat peak in STD over the Pacific cold tongue region (enclosing the Niño3.4 region) in contrast the cloud variability having a peak just east of the dateline (~190E). For sea level variability there is a minima at the dateline and two maxima at 140W and 140 E. The OC-

CMUG Phase 2 Deliverable

Reference: D3.1: Quality Assessment Report
Due date: June 2016
Submission date: July 2016
Version: 2.0c



chlorophyll is anti-correlated with the other variables as expected (high chlorophyll for cold upwelling waters), the largest variability is seen near the South American coast and over the Indonesian islands. The spikes in chlorophyll STD could be due to missing values not masked properly or mixed in land points in our analysis, it will be further investigated. For this first analysis we have used the full time length of each variable, for the final evolution we will make the comparisons for the same time-period.

For the model comparisons as well as using AMIP simulations, that can be directly compared to the observations, we will also evaluate statistics of coupled climate models ENSO simulations. Figure 21 show an example of SST and cloud Niño3.4 time series from 1982 to 2100 for one EC-Earth RCP8.5 scenario, with the CCI observations included. We note the model is not in phase with the observations (as expected) and EC-Earth is too cold and has too small variabilities for SST and clouds for the “present” day climate. Towards the end of the century when the model is warmer the variabilities are larger and closer to the observations

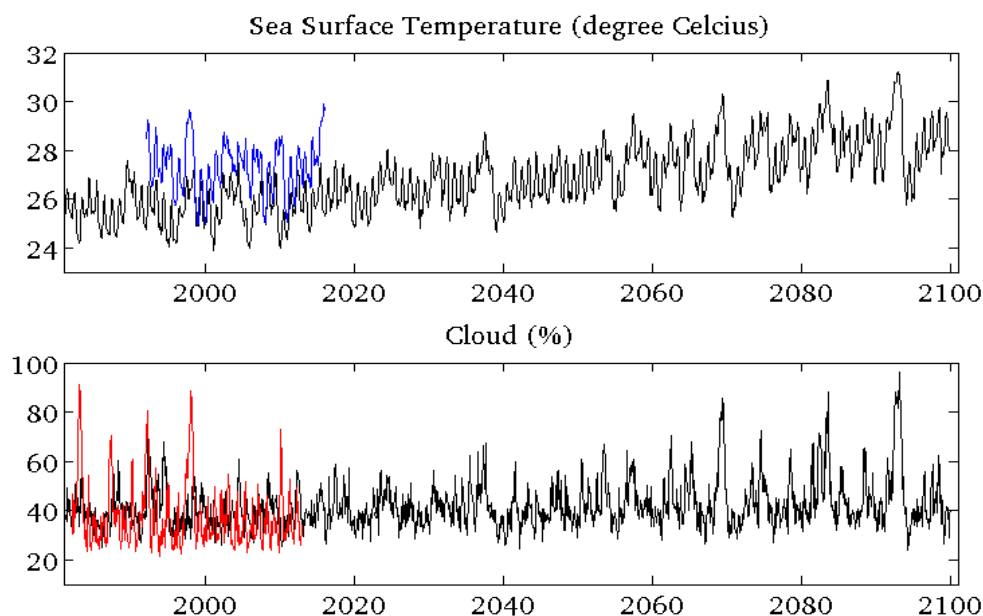


Figure 21: Niño3.4 index time series for (top) HadISST (black), CCI (red) and CLARA (blue) Cloud cover and (bottom) HadISST (black), EC-Earth (red) and ERAI (cyan) cloud cover.

Decadal variations in ENSO are visible in EC-Earth timeseries, with a plateau in the SST warming around 2040 after a strong El Niño 2038. This illustrate the problem of characterizing ENSO from “short” time periods, 20-30 years, which should be remembered when deriving constraints from observations. Using observations and models together can help to improve our understanding of ENSO and other large scale processes.

CMUG Phase 2 Deliverable

Reference: D3.1: Quality Assessment Report
Due date: June 2016
Submission date: July 2016
Version: 2.0c



Finally, in Figure 22, we show an example how this process study have revealed issues with the satellite data. We do not expect a strong ENSO signal in Cloud liquid water path (LWP) since it is mainly the high convective clouds with ice water that interact with ENSO. Still, we also made HVM diagrams for liquid water path (LWP) for Cloud-CCI, CLARA and PATMOS-x (Heidinger et al 2014) that revealed unrealistic high values for the anomalies after year 2000. This is due to problems with the scanning motor onboard the satellites. The Cloud-CCI and CLARA team were aware of this problem but it was not clear on how it could affect the ECV's. In the latest Cloud CCI data v2.0 corrections have been made that mitigated the issue but some features remain, which should be communicated to end users.

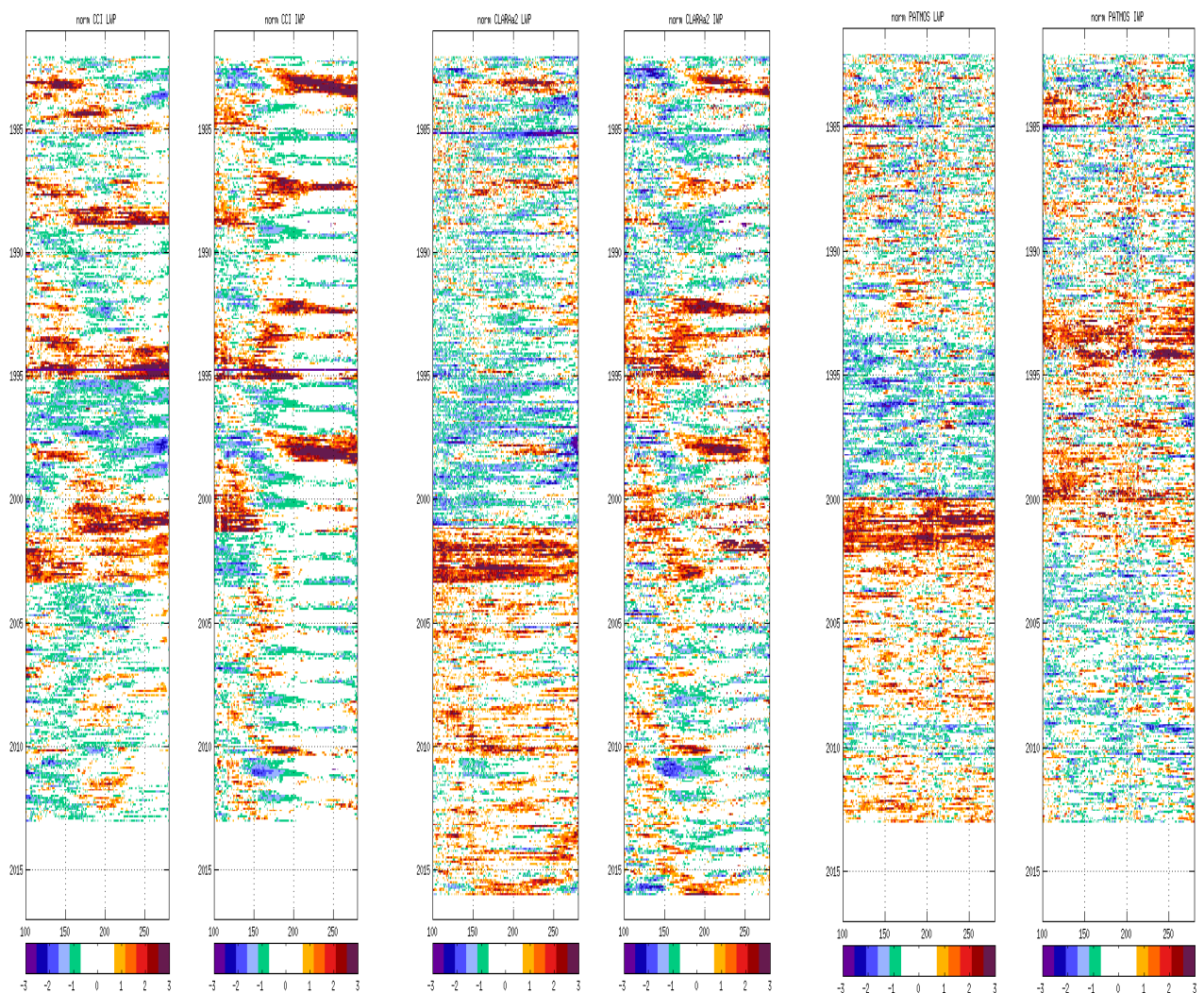


Figure 22: Hovmöller diagrams for CCI, CLRA and PATMOS-x LWP, anomalies for 5S-5N as a function of time and longitude, 100E-270E. see text for explanation of debugging application.



3.7 Coupled climate model assessment [WP3.5]

Aim

The aim of WP3.5 is to investigate the suitability of ESA-CCI products to constrain coupled climate model responses, especially the climate carbon feedback. In the last Coupled Model Intercomparison Project (CMIP5), all coupled climate models agree on the positive sign of this feedback, meaning a reduction of carbon uptake by ocean and land biosphere sinks under higher temperature, but the magnitude of this feedback is still subject to significant uncertainties, especially for the land components of the models.

The climate carbon feedback cannot be directly measured, but the concept of “emergent constraints” has flourished over the last years (Cox *et al.*, 2013 ; Wenzel *et al.*, 2014). The idea is to define an empirical relationship between long and short-term carbon sinks sensitivity to a given variable, and then to constrain the simulated future CO₂ fluxes thanks to the observed short-term sensitivity. The ESA-CCI products offer a great opportunity to look for this kind of relationships. We focus here on the ESA-CCI combined soil moisture product and the IPSL climate coupled model, with this specific question: How much soil moisture CCI data allow constraining carbon sinks sensitivity to climate change?

To answer this general question, the following questions are first addressed:

- What spatio-temporal resolutions are relevant to carry out this study?
- Are the ESA-CCI soil moisture spatio-temporal coverage sufficient to define such a relationship?
- Can the simulated relations between soil moisture and climate (precipitation and temperature), and between soil moisture and carbon fluxes, be observed?

Eventually, we plan to extend this study to the CCI GHG product, for use as an additional constraint.

Summary of results

3.7.1 Spatio-temporal coverage of data

The combined soil moisture product v02.2 is used in this study. This product was released in February 2016, and was developed from two types of instruments, active and passive microwave space borne instruments. It is available from 1979 to 2014 and provides daily data at 0.25° resolution. The surface soil moisture (SSM) data are supposed to stand for the SSM through the first 2 cm of the soil on average, expressed in m³/m³. (Dorigo *et al.*, 2015).

CMUG Phase 2 Deliverable

Reference: D3.1: Quality Assessment Report
Due date: June 2016
Submission date: July 2016
Version: 2.0c



The CCI-SM data were first aggregated at a larger spatial resolution of 1 degree, as the resolutions of coupled climate model are rarely higher than this. Then, as the relation between soil moisture and carbon fluxes is investigated at the global scale, and measures of GPP such as GPP from Jung *et al.*, 2014 are given at the monthly timescale, the CCI-SSM data were monthly averaged. This temporal aggregation allows a better global coverage of data as it is showed in Loew *et al.*, 2013, but we tested the impact of imposing a threshold of the minimum of observations per month necessary to compute the monthly mean. Figure 23 shows the evolution of the global coverage depending on this minimum of observation threshold taken from 1 to 10 daily observations per month. Demanding a minimum of 10 observations per month prevent from considering data before 1992, as less than 30% of land surfaces is covered. On the contrary, taking only 3 observations per month gives a good coverage from the beginning but shows an important gap between 1988 and 1990, coming from a change in constellation of satellites used to build the product. Eventually, the threshold of 5 observations per month shows an increasing improvement of the data coverage from 30% in 1978 to 65% in 2014. Therefore, we conclude that taking at least 5 observations in a month to compute monthly means stands for a good trade-off between sufficient data spatial coverage and mean “robustness”. Spatially, the difference between the different thresholds lies mainly in the high latitudes (see. Figure 24).

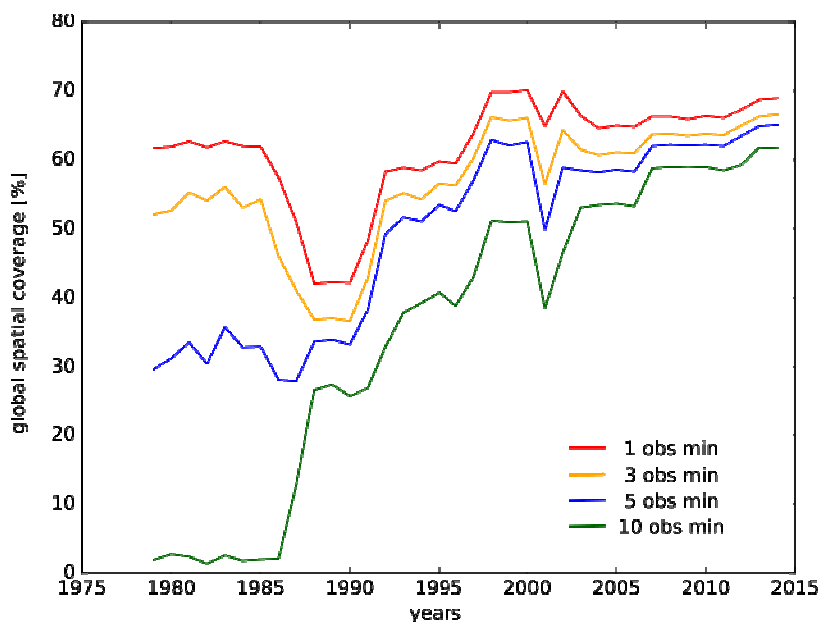


Figure 23: Evolution of the global spatial coverage depending on the threshold of observations per month taken.

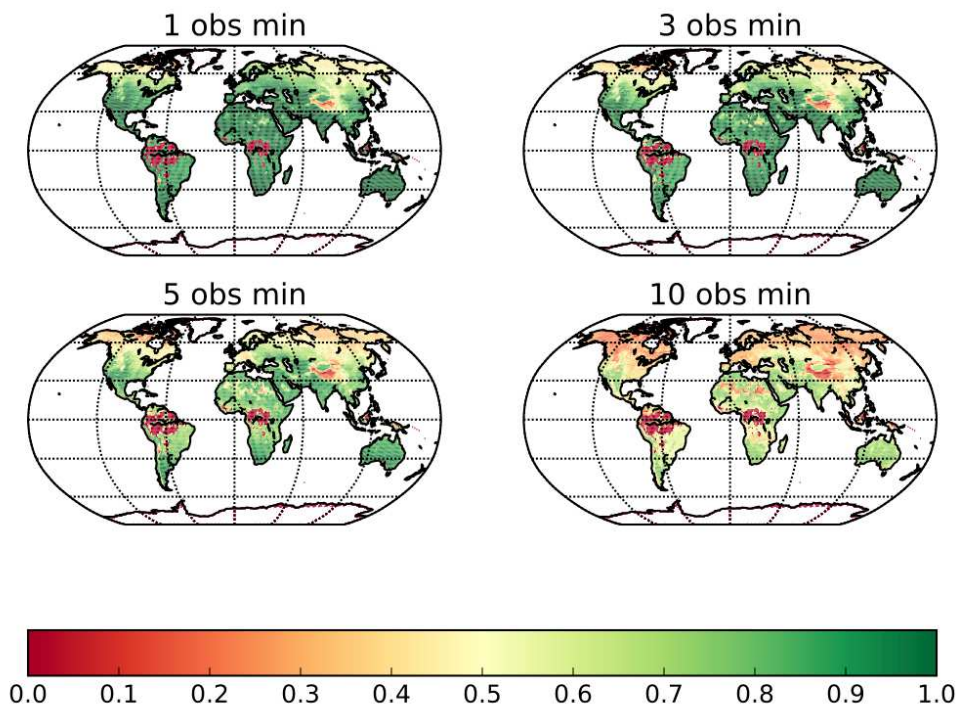


Figure 24: Mean monthly spatial coverage of CCI-SM data over 1979-2014, depending on the threshold of minimum daily observations per month (a) 1 day per month (62%), (b) 3 days per month (57%), (c) 5 days per month (49%), (d) 10 days per month (36%).

3.7.2 Comparison of the CCI-SM product with the IPSL model

Following the CMIP5 design, the simulated surface soil moisture by the IPSL model stand for the amount of water in the first 10 cm of the soil column whereas soil moisture from the ESA-CCI stand for the first 2 cm. These two variables are thus not directly comparable and need to be normalized by their mean (content of water) and their standard deviation (dynamic of soil hydrology), following Reichle et al. (2004). Once normalized, the spatial patterns of soil moisture are very similar between the model and the ESA-CCI product (not shown here).

3.7.3 Relationships between soil moisture, precipitations, air temperature and carbon fluxes

Soil moisture and climate

Annual correlations between soil moisture, precipitations, air temperature and Gross Primary Productivity (GPP) were calculated using an AMIP run of the IPSL-CM5A-LR (sea ice and SST imposed) from the CMIP5 experiment. The correlations simulated by the model are compared with correlations obtained from “observations” on a 96x96 grid resolution. The temperature and precipitation data come from the reanalysis CRU-NCEP.v2. The annual correlations are calculated from 1993 to 2009 because the CCI-SM data present a global coverage higher than 50 % from this year. Figure 25 shows that soil moisture and precipitation are positively correlated,

CMUG Phase 2 Deliverable

Reference: D3.1: Quality Assessment Report
Due date: June 2016
Submission date: July 2016
Version: 2.0c



with a larger proportion of significant correlation coefficient given by the IPSL-CM5A-LR model than by the observations, 63 % of grid cells are significantly correlated with $R=0.67$ using the model against 25% for the observations with $R =0.53$.

On contrary, soil moisture and temperature are negatively correlated, meaning that the hotter, the drier is the surface (cf. Figure 25). The strongest signal appears in the Northern Hemisphere during spring, but the sign of this correlation depends on the season and on the regions. Again, the signal given by then IPSL model is stronger than the one given by the observations. However, the differences are lower, 24% of grid cells are significantly correlated with $R=-0.57$ using the model against 22% with $R=-0.53$ using the observations.

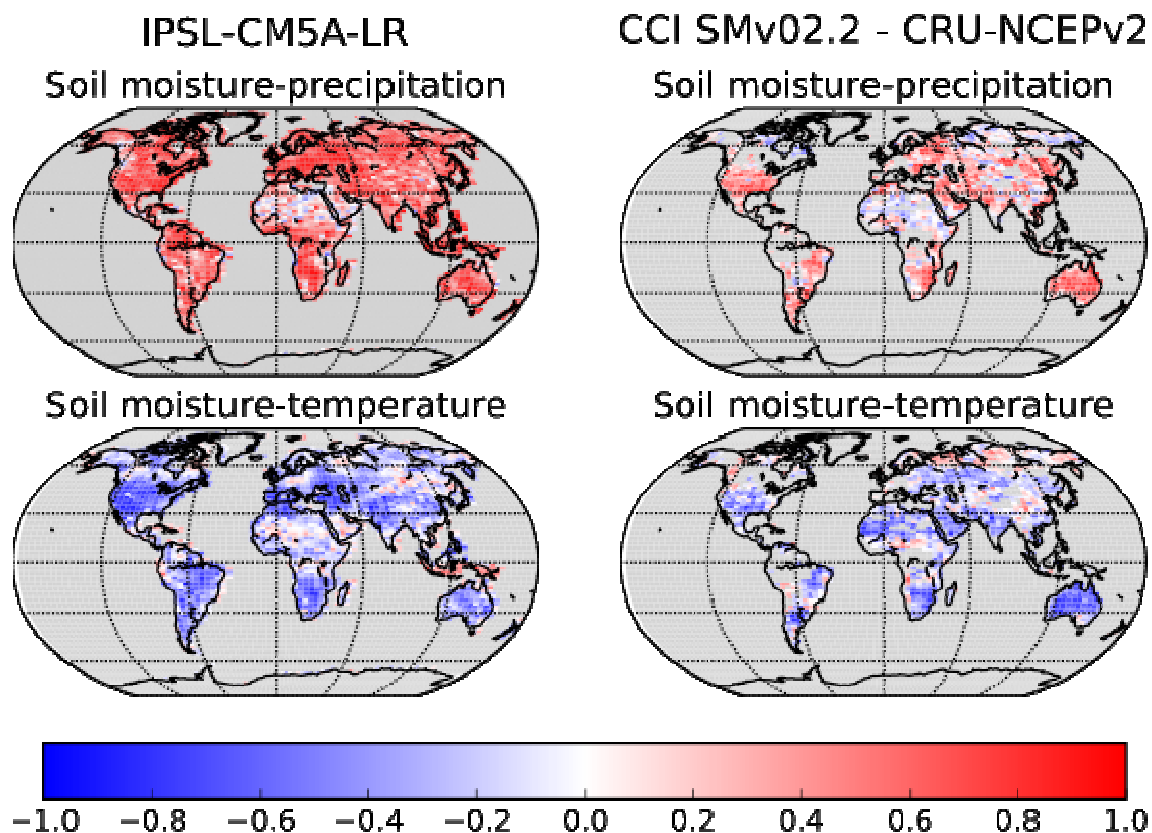


Figure 25: Annual correlations between soil moisture and precipitation (upper row), and between soil moisture and temperature (lower row), calculated over 1993-2009 on a 96x96 grid resolution, by the IPSL model and by CCI-SM and CRU-NCEP precipitations and temperature.

This analysis shows the importance of soil moisture as an integrator of climate information, not only of precipitation but also of temperature, and it is supported by the ESA-CCI data.

Soil moisture and carbon fluxes

The relationships between soil moisture and GPP, which is the rate at which photosynthesis occurs, are here investigated. The GPP come from Jung et al., 2013 and are provided at the monthly scale. The seasonal correlations using ESA-CCI SM and observed GPP are calculated if

CMUG Phase 2 Deliverable

Reference: D3.1: Quality Assessment Report
Due date: June 2016
Submission date: July 2016
Version: 2.0c



at least 10 values among 16 from 1993 to 2009 exist. The seasonal correlations, calculated by the IPSL model, between soil moisture and GPP shows interesting contrasts between spring and summer (Figure 25). Soil moisture is negatively correlated to GPP in spring whereas it is positively correlated in summer. These contrasts seem to highlight different vegetation processes. When plants photosynthesize, they pump water, inducing a reduction of soil moisture. However, water stress can break this mechanism by preventing photosynthesis to occur. The opposite signs of the correlations are thus likely to highlight two hydrological regimes inducing different plants behaviours. Spring is rarely subject to water stress, the first mechanism is thus followed: important GPP induces a reduction of soil moisture, illustrated by the negative correlation between these two variables. On the contrary, summer can be subject to water stress, and low soil moisture would reduce GPP. The positive correlation is thus likely to reflect a water-limited regime.

Figure 26 shows that the correlations in spring are mostly noisy and do not reflect the relationship highlighted in the simulations. The signal is a bit stronger in summer in central Europe. Besides, the contrasts between southeast Europe (positive correlation) and northwest Europe (negative correlation) in summer are similar as in the model and tend to support our analysis. The differences between the model and the observations could either come from missing processes that are not represented in the model and induce a signal that is too 'simple' than the reality, or an insufficient temporal coverage of the observations. Indeed, if we impose that all values in the time series (i.e. 16) must exist to compute the correlations, than Western Europe is not covered at all. Spatial contrasts at the global scale will also be investigated to understand more about these differences.

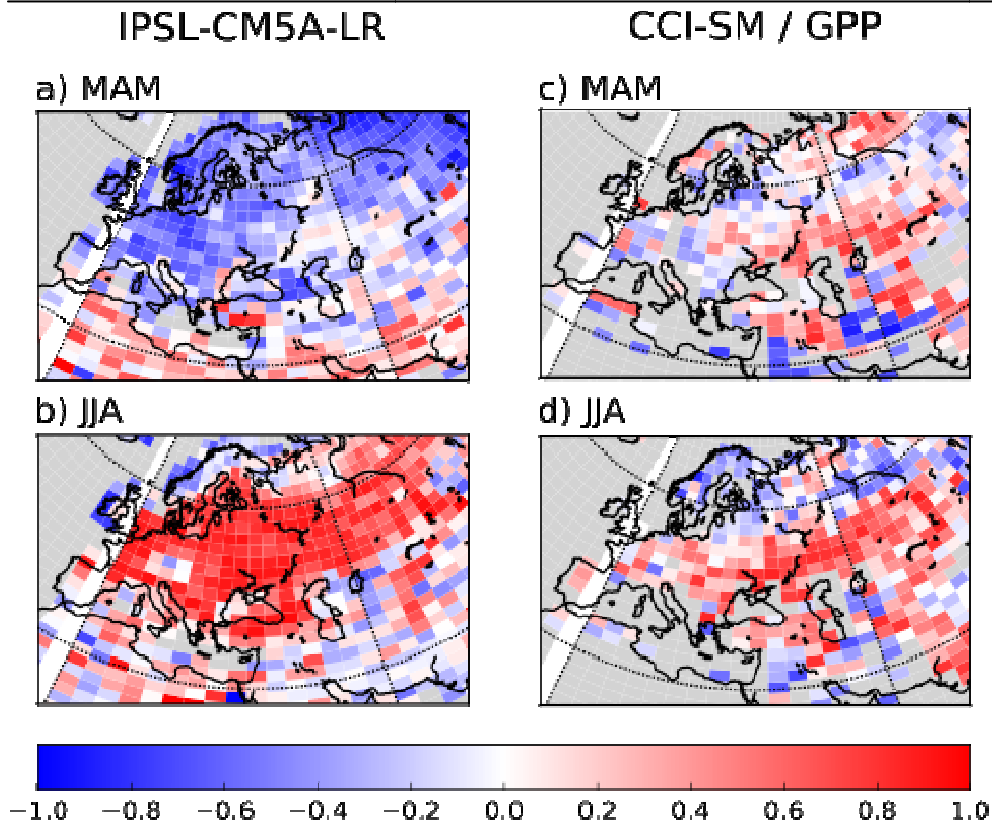


Figure 26: Spring and Summer correlations over 1993-2009, on a 96x96 grid resolution, between soil moisture and GPP using the IPSL-CM5A-LR (left column) and the CCI-SM data and GPP from Jung et al., 2014 (right column).

To conclude, soil moisture plays a key role in water and carbon cycles. It integrates information about climate (temperature and precipitation) and drives vegetation processes such as photosynthesis. These statements were already partly supported by the ESA-CCI soil moisture product and show good promises to identify a relationship between present and future carbon sinks sensitivities to soil moisture.

CMUG Phase 2 Deliverable

Reference: D3.1: Quality Assessment Report
Due date: June 2016
Submission date: July 2016
Version: 2.0c



3.8 Improved process understanding from Arctic and Antarctic cross ECV assessment [WP3.6]

ESA-CCI sea ice and sea surface temperature data products

We assess here the quality of sea ice concentration and sea ice thickness datasets compiled by the ESA Sea Ice CCI (SICCI) team, and perform a polar ECV cross assessment between ESA-CCI ice concentration and sea surface temperature datasets. To analyse the quality of the sea ice concentration and thickness products we assimilated these datasets into the Max Planck Institute Earth System Model (MPI-ESM; Stevens et al., 2013). In order to evaluate the SICCI ice concentration dataset we assimilated only SICCI ice concentration data into the model, and compared the performance of the simulated sea ice behaviour with identical experiments where ice concentration data from the National Snow and Ice Data Center (NSIDC) was assimilated. To evaluate the quality of the SICCI ice thickness dataset, we assimilated both SICCI ice concentration and thickness data into the model, and compared the simulated sea ice volume to other observational datasets as well as to the ice volume derived from the experiment where only ice concentration was assimilated. For the polar ECV cross assessment ESA-CCI sea ice concentrations and sea surface temperatures were assimilated into the model. For each of the two ECVs the assimilation run was repeated with a reference data product.

The assimilation technique we apply in our model system is Newtonian relaxation (or “nudging”), and besides sea ice also atmospheric and oceanic observations are assimilated into the model. In the atmosphere vorticity, divergence, temperature and surface pressure data provided by ERA-Interim reanalyses (Dee et al., 2011) are assimilated, while ocean temperature and salinity are nudged with ORA-S4 reanalysis data (Balmaseda et al., 2013). Relaxation times applied when data was assimilated into the model vary from 1 day for atmospheric nudging to 10 days for ocean nudging, and 20 days for nudging of sea ice. When only sea ice concentration is assimilated into the model, sea ice thickness is updated proportionally to sea ice concentration updates (Tietsche et al., 2013).

Results of our performance analysis for both SICCI sea ice concentration and thickness datasets, as well as for the polar ECV cross assessment, are given below.

3.8.1 ESA-CCI sea ice concentration dataset (version 1.1, daily data, 1991-2008)

A comparison of SICCI and NSIDC sea ice concentration products shows that the Arctic sea ice area computed from SICCI data lies between NASA-Team (Cavalieri et al., 1984) and Bootstrap (Comiso, 1995) datasets from NSIDC. While NASA-Team data shows lower Arctic sea ice area

CMUG Phase 2 Deliverable

Reference: D3.1: Quality Assessment Report
Due date: June 2016
Submission date: July 2016
Version: 2.0c



than SICCI, the Arctic sea ice area derived from Bootstrap data is larger than for SICCI. The difference between NASA-Team and Bootstrap products lies in the selection of tie points for brightness temperatures representing “fully ice-covered” grid boxes. In the Bootstrap retrieval algorithm 100% ice cover is obtained already for lower brightness temperatures compared to the NASA-Team algorithm. From computed Arctic sea ice areas we infer that the SICCI algorithm gives intermediate ice concentrations in the Arctic. This result also holds for simulated Arctic sea ice area in assimilation experiments with the different ice concentration datasets.

The Antarctic sea ice area derived from both the SICCI ice concentration dataset and the assimilation run performed with SICCI ice concentrations shows that in the Antarctic the SICCI product resembles the NSIDC Bootstrap product, while the NASA-Team product shows about 10% less sea ice area.

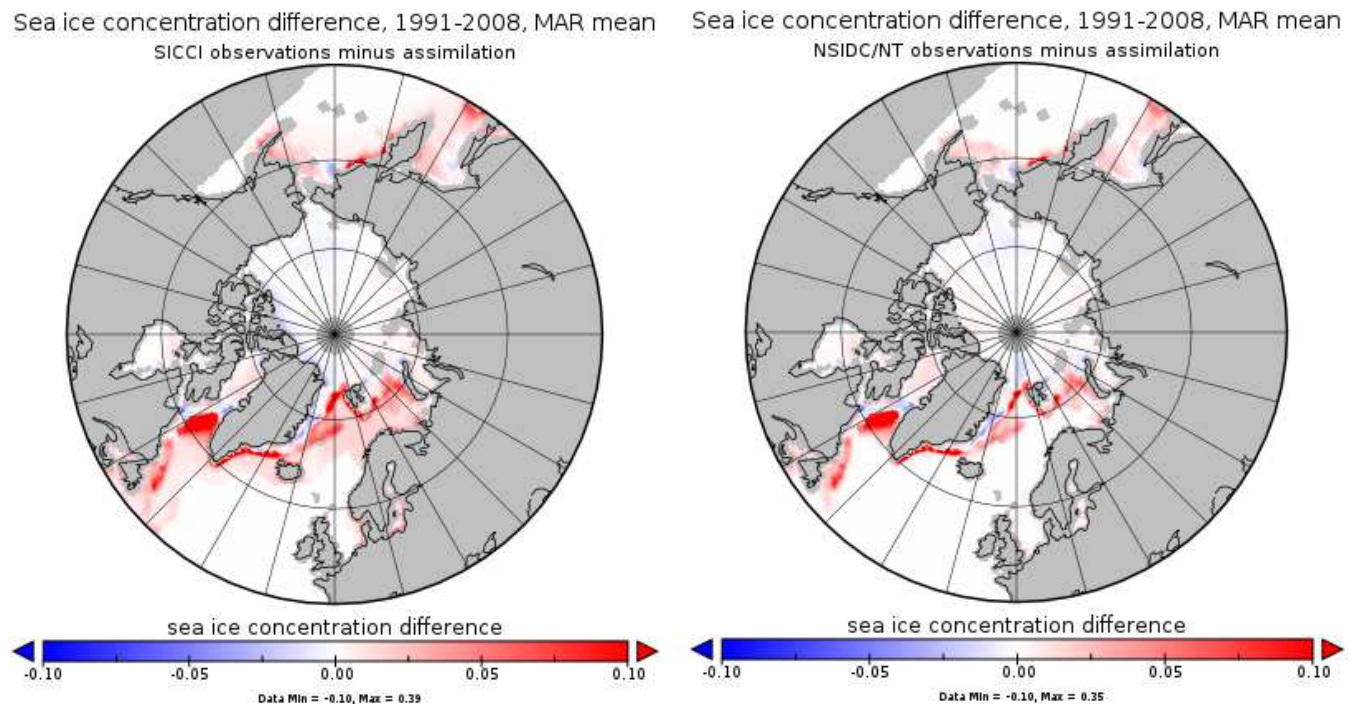


Figure 27: Sea ice concentration differences between observations and the associated assimilation runs are presented for SICCI (left) and NSIDC/NASA-Team (right) data products. March-mean values over the period 1991 to 2008 are shown.

A regional evaluation of the correspondence of the assimilated sea ice data product with the model physics indicates, however, a clear difference between SICCI and NSIDC data products. In many regions, especially in the Norwegian and Labrador Sea, low ice concentrations (< 3%) are obtained by the SICCI algorithm in grid boxes where observed sea surface temperatures as well as NSIDC ice concentration products indicate ice-free waters (see Figure 27). These

CMUG Phase 2 Deliverable

Reference: D3.1: Quality Assessment Report
Due date: June 2016
Submission date: July 2016
Version: 2.0c



spurious ice concentrations occur, because consciously no weather filter was applied in the SICCI algorithm. In NSIDC ice concentration products these low ice concentrations, which originate from the contribution of clouds to brightness temperatures recorded by the satellite, are removed by a weather filter. However, since it is not feasible to objectively distinguish between the origins of possible brightness temperature sources, weather filters are likely to filter out also contributions of actual sea ice. Thus, although not using a weather filter introduces spurious ice concentrations in the open ocean, it provides a more objective view on the satellite data, since no actual ice concentrations are removed and it is left to the user to discard spurious low ice concentrations over open waters, if intended.

The regional investigation of the assimilation performance also showed that a notable amount of sea ice in the marginal ice zone melts directly after assimilation into the model. The most prominent area for this to happen is the Davis Strait (see Figure 27). Sea ice observations show that in a few years (e.g. 1993) this area is largely covered by sea ice in March, however, model physics does not allow here for sea ice to exist. The model physics in a grid box where both sea ice and sea surface temperature are assimilated can be described as follows:

In a model grid box the temperature of the uppermost ocean layer needs to be at freezing point to allow even for small amounts of sea ice to exist. Thus, assimilated sea ice cannot persist if the heat content in a certain ocean model grid box plus the sum of heat contributions from the assimilated sea surface temperature and the assimilated sea ice adds up to an ocean surface temperature above freezing.

In many regions inconsistencies with the assimilated SST data also play an important role (see also Section 3.7.3).

In summary, we consider the SICCI sea ice concentration data product as adequate for use in climate modelling, and of comparable quality as NSIDC data products. A major advantage of the SICCI product with respect to other datasets is its error characteristics. The different types of uncertainties provided with the dataset allow for more accurate studies, e.g., on the evaluation of model physics.

3.8.2 ESA-CCI sea ice thickness dataset (version 0.9, Arctic-only, monthly data for October to March, 2003-2008)

A comparison of the SICCI ice thickness product with other data products derived from observational time series reveals a substantial positive bias in SICCI data. When besides sea ice concentration data also SICCI ice thickness data is assimilated into the model, the March-mean Arctic sea ice volume exceeds the ice volume derived from the assimilation run where only ice concentration is nudged by almost 100% (see Figure 28).



Reduced Arctic sea ice volume, MAR mean

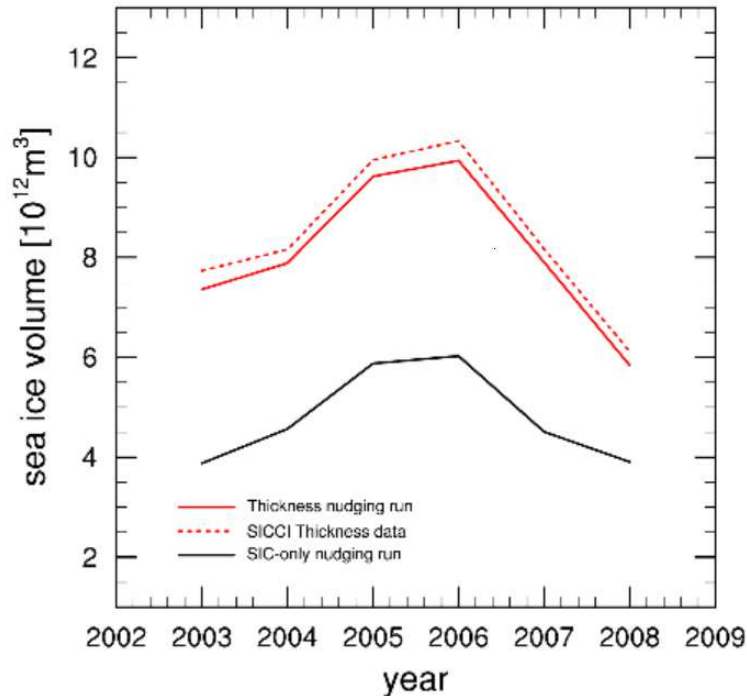


Figure 28: March-mean reduced Arctic sea ice volume over 2003-2008, as derived from SICCI ice thickness data (red dotted line), the combined SICCI ice thickness/concentration assimilation run (red solid line), as well as the SICCI ice concentration-only assimilation run (black line), is shown. The term “reduced” is introduced here, since only grid boxes, where the SICCI ice thickness dataset contains non-missing non-zero values, are considered.

A side effect of assimilating high SICCI ice thicknesses into the model is that almost no assimilated sea ice in the marginal ice zone is lost directly after assimilation due to sea surface temperatures above freezing (see section on SICCI ice concentration data). The additional cooling of the system due to the positive bias in assimilated ice thicknesses prevents assimilated sea ice from being melted. However, we find the positive bias in the SICCI sea ice thickness dataset to be too large to allow for the data product to be of adequate quality for climate modelling studies. Error characteristics were not provided with the SICCI ice thickness data product.



3.8.3 Cross assessment ESA-CCI sea surface temperature and ice concentration (SST data version 1.1, daily data, 1992-2008)

A comparison between ESA-CCI sea surface temperature (SST) and sea ice concentration (SIC) datasets reveals that inconsistencies among the data products exist in many regions close to the ice edge. Figure 29 shows the ESA-CCI sea surface temperature for March 1998 in all grid boxes where the ESA-CCI ice concentration is larger than 5%. Particularly in the Denmark Strait, but also in other regions such as the Baltic Sea, sea surface temperatures exceed 2°C over large areas, although ice concentrations above 5% are found in the same grid boxes. This result does not change qualitatively in other years.

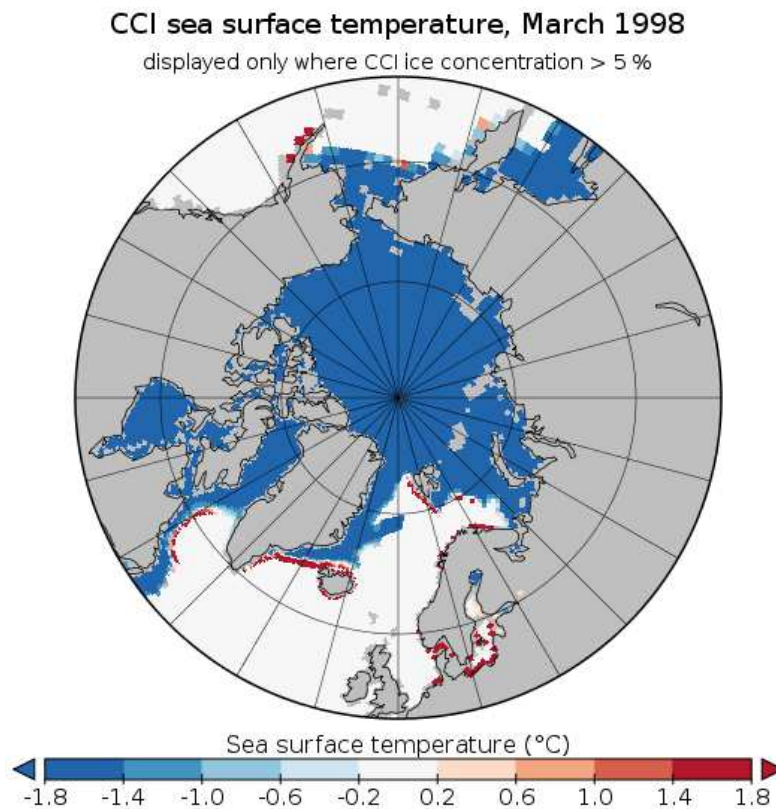


Figure 29: ESA-CCI sea surface temperatures are shown for March 1998. Grid boxes with less than 5% ice concentration were set to 0°C.

The reason for these inconsistencies is likely that for the compilation of the ESA-CCI SST product another sea ice dataset, the OSI-SAF SIC product, was used to determine the exact position of the ice edge. Thus, ESA-CCI SST and SIC datasets are two independent data products, each showing the location of the ice edge as retrieved from the respective algorithm. In order to test how MPI-ESM model physics agrees with both ESA-CCI SST and SIC data, we assimilated both datasets simultaneously into the model. To assess the quality of the

CMUG Phase 2 Deliverable

Reference: D3.1: Quality Assessment Report
Due date: June 2016
Submission date: July 2016
Version: 2.0c



correspondence between the model and the data products, we repeated the assimilation run once with ERA-Interim (instead of ESA-CCI) SST data, and once with NSIDC/Bootstrap (instead of ESA-CCI) SIC data. For reference, we also performed an assimilation run without any ESA-CCI data by using the respective SST and SIC reference products.

The impact of the assimilated SST data product on the simulated total Arctic sea-ice area is almost undetectable. Figure 30 shows that both SST products assimilated into the model give very similar Arctic sea-ice area. This result holds, independent of the SIC product assimilated simultaneously. The total Arctic ice area reduces, however, after assimilation into the model. This reduction is slightly higher for the ESA-CCI compared to the NSIDC/Bootstrap SIC product, and is generally more prominent in March than in September (see Figure 30). The cause for this reduction is twofold. On the one hand, SSTs above freezing overlapping with the marginal ice zone cause ice melt in the respective regions (compare Figure 29). On the other hand, in regions such as the Davis Strait MPI-ESM model physics does not allow for ice being formed. The reduction is higher for ESA-CCI SIC than NSIDC/Bootstrap sea ice data, since the ESA-CCI algorithm does not apply a weather filter, so that clouds over open water are interpreted as ice concentrations by the algorithm (compare Figure 27).

The general offset between ESA-CCI and NSIDC/Bootstrap SIC data is likely to originate from a different setting of the ice tie points in the different retrieval algorithms.

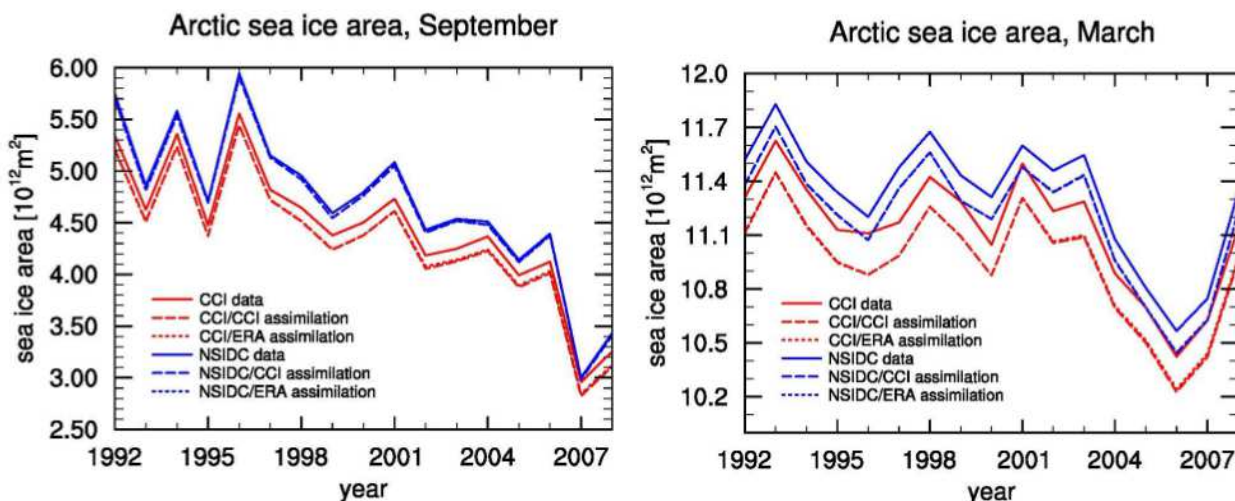


Figure 30: Arctic sea-ice area in March (left) and September (right) as derived from observational datasets (solid lines) and assimilation runs (dashed and dotted lines). Only grid boxes with non-missing values in all datasets were considered for the computation.

CMUG Phase 2 Deliverable

Reference: D3.1: Quality Assessment Report
Due date: June 2016
Submission date: July 2016
Version: 2.0c



3.9 Cross-Assessment of Aerosols, Cloud and Radiation CCI ECVs [WP3.7]

Aim

The aim of this work package is to complement the work of the Aerosol CCI Climate Research Group by providing a cross-assessment in the ESA CCI ECVs and in the CMIP5 climate models. We also aim at providing an improved process understanding by performing additional, more-detailed studies with the global aerosol model EMAC. The following scientific questions shall be addressed:

- What is the interrelation between different aerosol, cloud and radiation ECVs in CCI data and Earth System Models?
- How do the CMIP5 models perform in comparison to a more detailed aerosol global model (EMACMADE) in the representation of processes related to aerosol-radiation and aerosol-clouds interactions?

Summary of Results

A first working version of the EMAC model, coupled with a new version of the aerosol sub-model MADE (MADE3) has been set up. The MADE3 sub-model is able to simulate the main aerosol microphysical processes, such as nucleation, condensation and coagulation, as well as the equilibrium between the gas and the aerosol phases. In the current version of EMAC-MADE3, it is also possible to calculate aerosol optical properties using the aerosol quantities calculated by MADE3 (particle number, mass and radius) combined with pre-calculated lookup tables of optical parameters. This allows us to couple MADE3 to the radiation scheme of the model. An additional coupling of MADE3 to the cloud scheme (including aerosol interactions with liquid, mixed-phase and ice clouds) is currently being developed and will be used to perform the planned experiments if a working version is available by the end of the project.

Several test simulations have been conducted with the new model system. Using the ESMValTool, which is being developed within WP5.1, the model has been extensively evaluated by comparison with several observational datasets, including the ESA-CCI aerosol products for aerosol optical properties. In particular, we compared the simulated aerosol optical depth (AOD) at 550 nm against the ESA-CCI satellite products (Figure 31). The simulated AOD is higher than that derived from ESA-CCI satellite measurements, especially over the southern oceans, which may indicate too high sea spray emissions, and in East Asia, where an incorrect estimate of the input emissions may play a role. As mentioned in the previous quarterly report, however, differences exist also in the observational data, e.g. when comparing the ESA product with MODIS. Furthermore, deviations in the simulated AOD compared to measurements are common also in other models. The relative error of MADE3 in this experiment is comparable to or smaller than those of other global models.

CMUG Phase 2 Deliverable

Reference: D3.1: Quality Assessment Report
Due date: June 2016
Submission date: July 2016
Version: 2.0c



In order to perform a full transient simulation with EMAC-MADE3 and to compare its performance to that of the CMIP5 models, a similar emission setup has been developed, covering the period 1950-2010. It makes use of the MACCity inventory, which builds on the original CMIP5 emission data, but considers yearly-resolved emissions (using a linear interpolation between the decades) and a sector-specific seasonal cycle based on RETRO. This should allow a more precise representation of the emissions with respect to the CMIP5 models, which is particularly important for aerosol and aerosol precursors given the relatively short lifetime of these species.

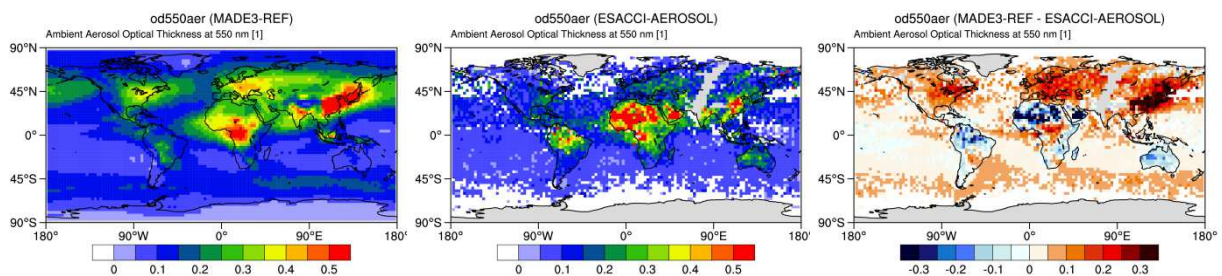


Figure 31: aerosol optical depth at 550 nm ($od550aer$) as simulated by EMAC-MADE3 (left panel) and from the ESA-CCI satellite product (middle panel). The right panel shows the difference model minus observations. Average values for the year 2001 are depicted in all panels.

CMUG Phase 2 Deliverable

Reference: D3.1: Quality Assessment Report
Due date: June 2016
Submission date: July 2016
Version: 2.0c



3.10 Cross assessments of clouds, water vapour, radiation, soil moisture for regional climate models [WP3.8]

Aim

The aim of this work package is to make an integrated assessment of ECV's related to regional moisture processes - clouds, soil moisture, precipitation and water vapour, to assess their consistency for African monsoons and European rainfall as simulated by regional climate models. The assessment will include an estimation of the usability of the corresponding CCI uncertainties. It will address the following scientific questions:

- How do the CORDEX regional climate models simulate cloudiness and soil moisture for the African and European regions?
- Are observed soil moisture and extreme precipitation relationships captured by regional climate simulations at different horizontal resolutions?
- Investigate moisture related feedbacks in observations which are important in the African monsoon development. This involves local feedback mechanisms, lagged regional correlations in time and space and large scale forcing.
- Identify key processes in regional climate models affecting the simulated rainfall and monsoon systems that can lead to improvements in their representations in the climate simulations.

Key Outcomes

For Europe,

- The observed variabilities of CCI cloud cover, CCI soil moisture (SM) and EOBS precipitation are consistent over Europe and suitable for climate model evaluations. The regional model anomalies are of similar magnitude as the observed anomalies.
- The climate model output (SM and Clouds) differ in absolute values compared to the observations. For SM it is due to difference in what is possible to compare, for cloudiness it is due to observational and model errors, as listed in the 3 points below.
- SM-CCI absolute values representing the top 2cm cannot be compared directly to model fields (see SM FAQ <http://www.esa-soilmoisture-cci.org/node/136>). However, comparisons of absolute values can help to identify seasonal model shortcomings. For comparisons with models, the model data should be sampled in time and space according to the availability of the satellite data (also stated in SM FAQ).
- Cloud-CCI prototype data v1.4 cloud cover is overestimated over North Atlantic and Mediterranean Sea. Feedback to the Cloud-CCI team has led to changes in thresholds for the cloud mask, which has improved the cloud cover in the final v2.0 data.

CMUG Phase 2 Deliverable

Reference: D3.1: Quality Assessment Report
Due date: June 2016
Submission date: July 2016
Version: 2.0c



- ERA-Interim underestimate cloud fraction in southern Europe. The regional climate model HCLIM agrees better with the satellite observations.

For Africa,

- The observed variabilities of CCI and other satellite datasets and surface based observations are consistent over Africa and suitable for climate model evaluations.
- Cloud-CCI and other cloud satellite data reveal that cloud cover in the CRU surface observations have “country shaped” errors.
- CCI Cloud prototype data v1.4 overestimate cloud cover over sea for latitudes north and south of 20°, here the Mediterranean Sea and Southern Ocean (improved for v2.0).
- RCA4 overestimate clouds over seas compared to the satellite observations, for regions with thin clouds as the stratocumulus region off the African west coast and cloudiness over sea East of Africa horn.

Summary of Results

The work so far for WP3.8 include evaluation of cloudiness, soil moisture and precipitation simulated by two Regional Climate Models (RCMs) utilizing the ESA CCI data soil moisture remote sensing product (Wagner et al., 2012) and CCI-clouds (prototype v1.4, Stengel et al 2013) and EOBS precipitation (Haylock et al 2008). In addition we use satellite cloud data from CLARA-A1 (Caspar et al 2009) and PATMOS-x (Heidinger et al 2014) and land surface based cloud data from CRU (Haylock et al 2008). Simulations were performed using two different RCM systems, the Rossby Centre Regional Climate model (RCA4) and a climate version of the non-hydrostatic meso-scale modelling system HARMONIE (HCLIM). Both models are driven by ERA-Interim (ERA-Interim, Dee and co-authors, 2011) lateral boundary fields of winds, temperature and humidity and sea surface temperature, every six hours.

All comparisons have been made for monthly mean values. Since the CCI-SM data is available on daily bases with spatial and temporal gaps, we used a simplistic simulator interpolating the regional models daily values of soil moisture to the observational grid. A daily mask represented by the grid boxes which have valid CCI-SM values was applied to the interpolated model SM fields. From these daily values monthly mean values were calculated for the RCM's and CCI-SM, respectively.

HCLIM over Europe

The aim is to evaluate moisture processes for Europe in the high resolution model HCLIM for a 30 year, 6km horizontal resolution simulation (work not yet completed). Here, we show preliminary results from a four year (2003-2007) HCLIM simulation at 15km horizontal resolution over Europe (Figure 31). An example of the co-variability of the moisture related variables is shown for the Mediterranean region in Figure 32. Time series of absolute values (left column) and de-seasonalised anomalies (monthly mean removed, right column) are shown for cloudiness, precipitation and soil moisture.

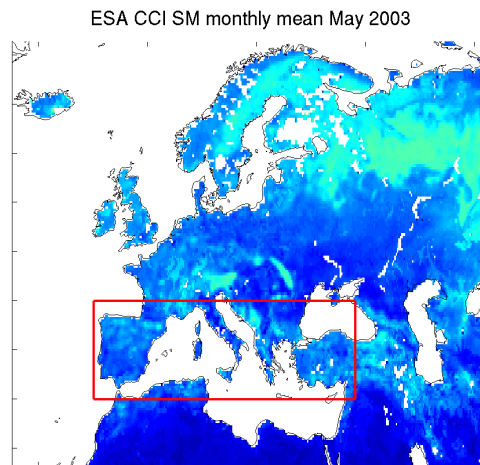


Figure 31: Map of the HCLIM area, the red box show the region for the time series in Figure 32.

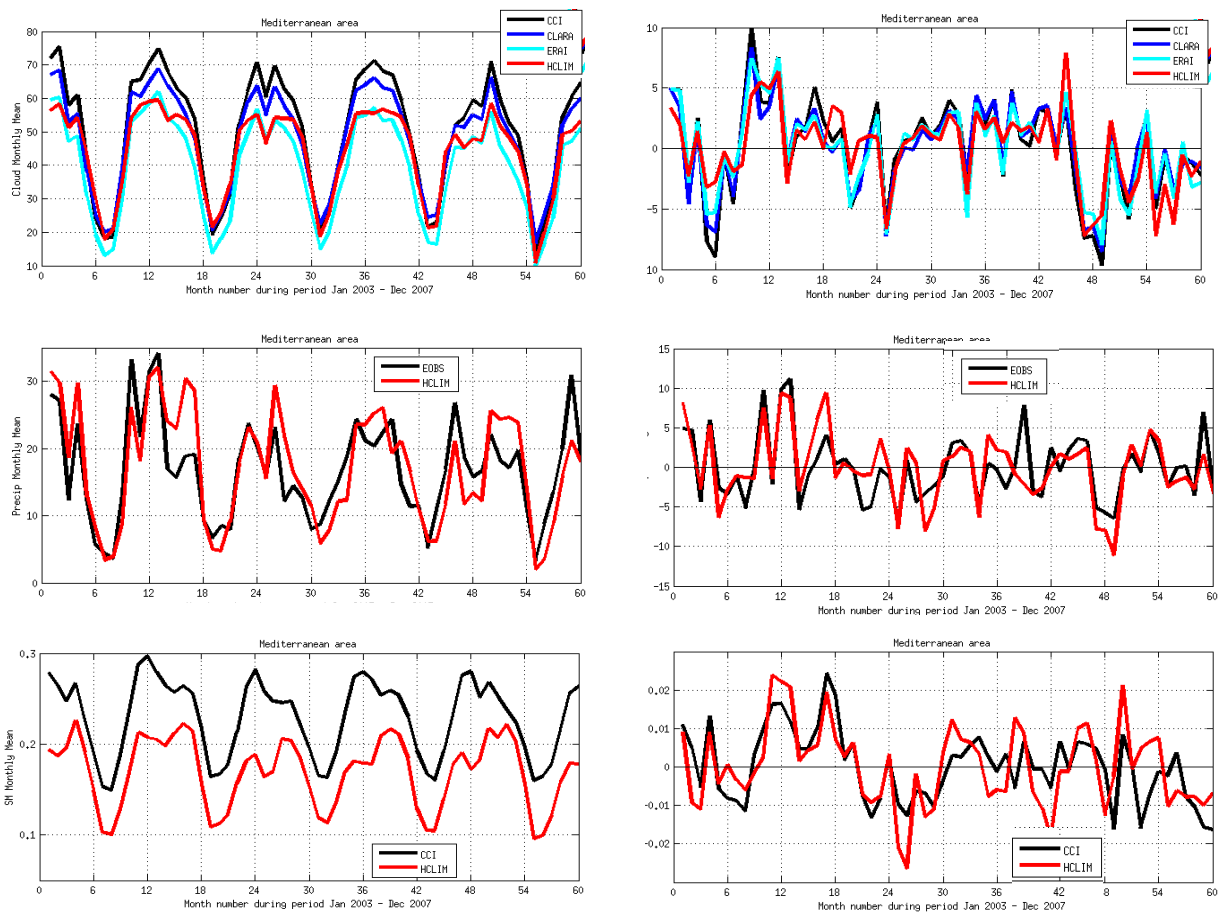


Figure 32: Monthly mean time series 2003-2007 for the Mediterranean region marked in the previous figure. Left column show absolute values for clouds (top), precipitation (middle) and soil moisture (bottom). Right column show de-seasonalised anomalies for clouds (top), precipitation (middle) and soil moisture (bottom). Black lines CCI data, red lines HCLIM, blue lines CLARA data and cyan lines ERA-Interim.

CMUG Phase 2 Deliverable

Reference: D3.1: Quality Assessment Report
Due date: June 2016
Submission date: July 2016
Version: 2.0c



The different observations show consistent variations in time with higher cloud fraction, precipitation and soil moisture in winter and lower values in summer (left column). The regional model anomalies are of similar magnitude as the observed anomalies (right column). Both observations and model anomalies have the wettest winter 2003/04 and the driest 2006/07.

ERA-Interim underestimate cloud cover all year but especially in autumn to spring (top left), as also found in other studies for Southern Europe (Calbó et al 2016). HCLIM is similar to ERAI and does not manage to produce more clouds than ERAI, except in summer when the regional model is less influenced by the inflow from the lateral boundaries. Both HCLIM and ERAI reproduce the observed cloud monthly variability (right top panel) but HCLIM has smaller variations than observed. Cloud-CCI v1.4 overestimate cloud cover over the Mediterranean Sea compared to CLARA and PATMOS-x data (top left) and over the Atlantic (not shown). This issue was reported to the Cloud-CCI team and was found to be due to too low thresholds over sea in the Neural Network cloud mask. In the latest v2.0 Cloud-CCI data the cloud cover bias over sea has been reduced.

HCLIM surface scheme has three layers of soil moisture, here we used the top 1cm to compare with the satellite observation. SM-CCI absolute values representing the top 2cm cannot be compared directly to models as known (<http://www.esa-soilmoisture-cci.org/node/136>). However, comparisons of absolute values can help to identify seasonal model short comings. As an example we note SM-CCI has a peak value each December while the simulated SM peaks later during the spring (lower left panel). This model SM bias can be explained by an overestimation of precipitation in spring as seen in the middle left panel in Figure 32. Further analysis into the moisture ECV's relationships will be made for the longer simulation.

CORDEX RCA4 simulations over Africa

The analysis of African monsoon and relationships between clouds, precipitation and soil moisture, in observations and CORDEX (Coordinated Regional Climate Down-scaling Experiment) simulations is ongoing. Here, we show examples comparing cloud cover from different observational data sets and RCA4 (Strandberg et al., 2014) run at 50 km horizontal resolution for the time period 1982-2010 driven by ERA-Interim and different CMIP5 models at the lateral boundaries.

The East African Monsoon is associated with the ITCZ moving south of the equator. The so-called long rains prevail during spring (MAM) and the short rains during autumn (OND). The transition season (JFM) bring most rainfall and cloudiness to East Africa. Figure 33 show the mean cloud fraction for January to March for the satellite observations, Cloud-CCI, CLARA, PATMOS-x and land surface observations CRU and three reanalysis datasets (ERAI, MERRRA2 and JRA25). For now, we use CLARA as the reference cloud data set, since the Cloud-CCI prototype data v1.4 has some known errors, the analysis will be remade for the final

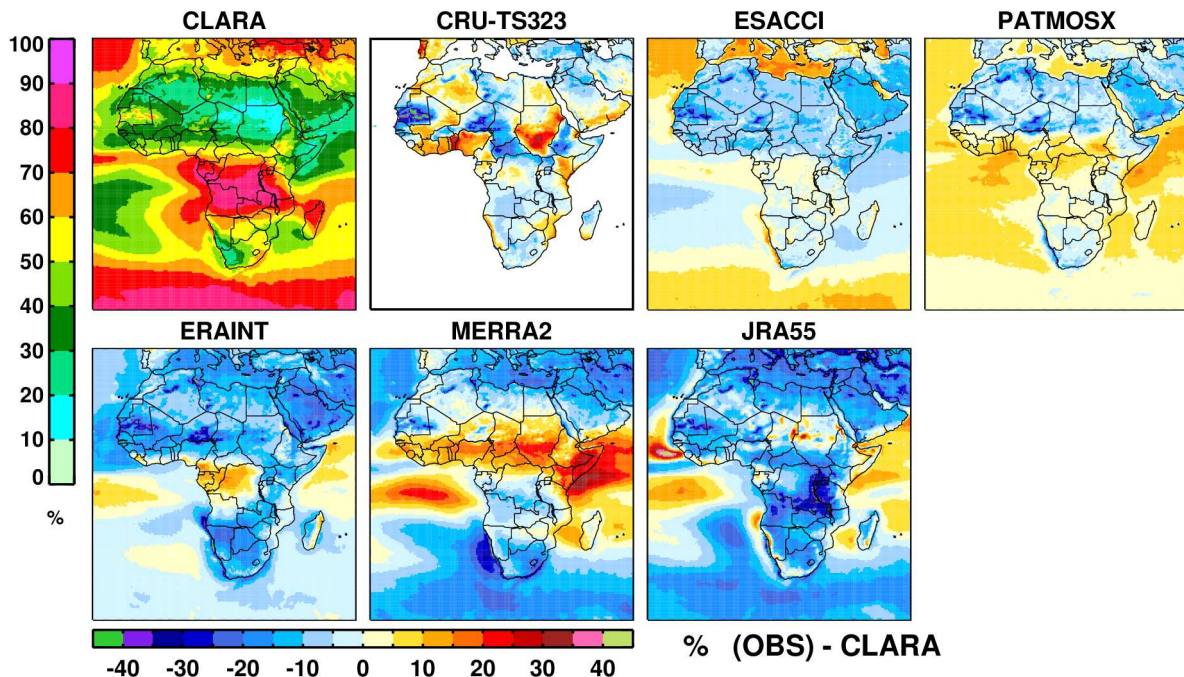
CMUG Phase 2 Deliverable

Reference: D3.1: Quality Assessment Report
Due date: June 2016
Submission date: July 2016
Version: 2.0c



phase 2 Cloud-CCI v2.0 dataset. All observational datasets have a maximum in cloud cover over East Africa consistent with the region of large amounts of rainfall. The reanalysis models underestimate the East-African cloud cover maxima, ERAI being closest to the observations.

Cloud Fraction (clt) | JFM | 1982-2012 | AFR-44



Cloud Fraction (clt) | JFM | 1982-2012 | AFR-44

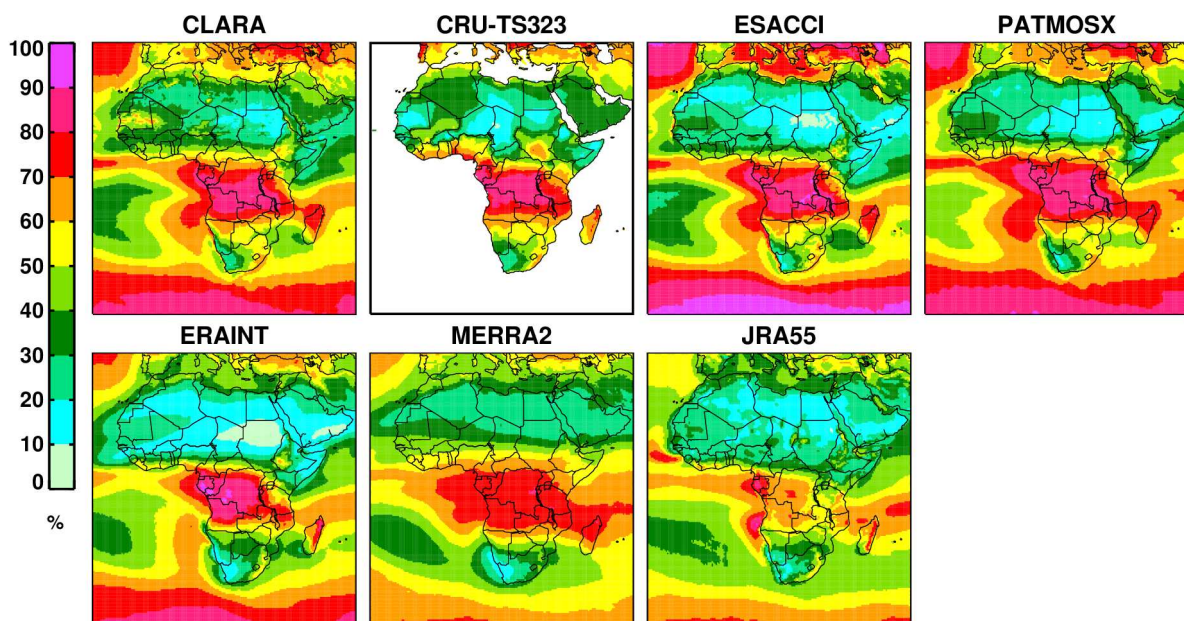


Figure 33: Top panel: Cloud fraction for observations and reanalysis over Africa. Bottom panel: CLARA cloud fraction and differences for satellite and reanalysis data compared to CLARA. All figures for January-March 1982-2012 (%).

CMUG Phase 2 Deliverable

Reference: D3.1: Quality Assessment Report
Due date: June 2016
Submission date: July 2016
Version: 2.0c



We note some problem regions for CRU, Cloud-CCI and CLARA cloud fraction. CRU surface observations have “country shaped” differences compared to CLARA (Fig 33 lower panel) and compared to the other satellite and reanalysis data sets (not shown). CCI Cloud prototype data v1.4 overestimate cloud cover over sea for latitudes north and south of 20°, as seen here over the Mediterranean Sea and Southern Ocean. The biases have been reduced in the latest Cloud-CCI v2.0 datasets. CLARA cloud cover is about 10% smaller than Cloud CCI, PATMOS and the reanalysis over Sahel and the desert regions in North Africa. This could be due to problems over-detecting clouds over desert surfaces for CLARA.

Figure 34 (top panel) show the cloud fraction for CLARA and the bias for RCA4 driven by ERA-Interim and 10 CMIP5 GCM models (resolution 200-300km) at the lateral boundaries. RCA4 overestimate clouds over sea; for the stratocumulus region off the African west coast and for seas East of Africa horn, the biases are very similar for all RCA simulations indicating problems with RCA thin cloud formation over sea that needs to be looked into. RCA4 driven by ERAI has the smallest bias over land compared to RCA4 driven by the atmosphere-ocean coupled CMIP5 models and the highest correlation compared to the observations (lower panel). This is expected since the coupled model climate do not reproduce the climate of a certain year, for coupled models other statistics is needed. To compare directly with the observations we will evaluate RCA4 driven by CMIP5 AMIP simulations (GCM's driven by observed SST and Sea-Ice at the lower boundary) which can reproduce the climate natural variability. We will also extend this study to include all moisture variables and other CORDEX RCM's for the final CMUG QAR report.

Quality relevant outcomes (updates from CMUG QAR 2015)

We found from these preliminary results assessing CCI SM and cloud cover that both variables are of “climate quality”. CCI clouds and soil moisture are consistent on a regional scale. Listed below are some remarks and recommendations for the individual variables and some general thoughts on observed versus modelled soil moisture.

Cloud-CCI Quality

The Cloud-CCI prototype data v1.4 was obtained directly from the Cloud-CCI team in December 2015, some issues were found and are listed below. These issues have been corrected and reduced in the final version that will be available summer 2016 from ftp://ftp-cmsaf-projects.dwd.de/ESA_Cloud_CCI/CLD_PRODUCTS/L3C/.

- Cloud-CCI prototype data had too much cloud fraction over sea compared to other satellite data (CLARA, PATMOS) and models (ERA-Interim, EC-Earth) as communicated to the Cloud-CCI team and since improved in the latest v2.0 dataset.

CMUG Phase 2 Deliverable

Reference: D3.1: Quality Assessment Report
 Due date: June 2016
 Submission date: July 2016
 Version: 2.0c



- For the NOAA satellites there are overlapping L3C data for same time periods. What is the Cloud-CCI recommendation on how to make one single time series, to minimize the drift and any artificial trend?

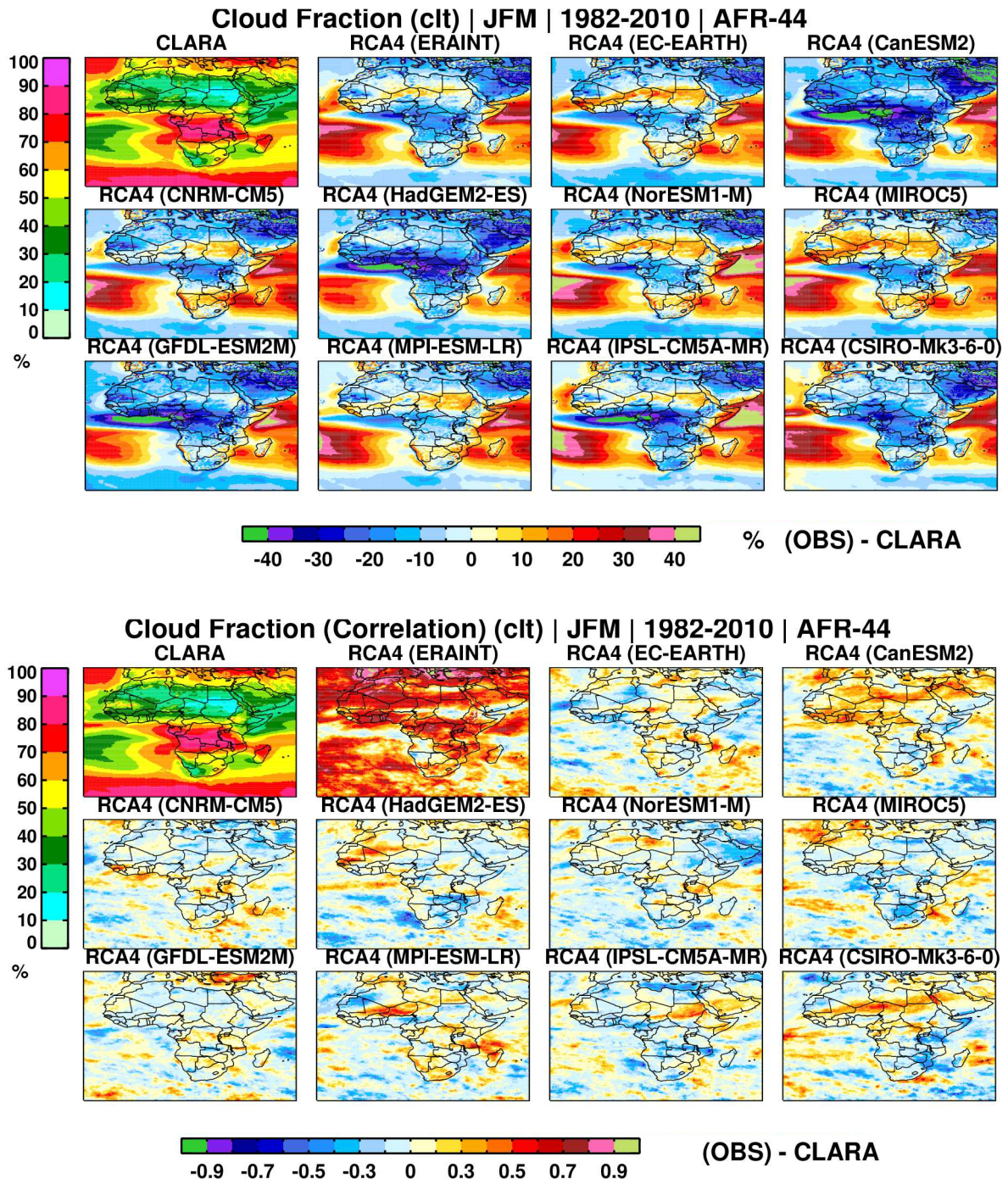


Figure 34: Top panel: Cloud fraction for CLARA and differences RCA4 (driven by ERA-Interim and 10 CMIP5 models) - CLARA. Bottom panel: CLARA cloud cover and correlation CLARA and RCA4 cloud cover. All figures for January-March 1982-2010 (%).

CMUG Phase 2 Deliverable

Reference: D3.1: Quality Assessment Report
Due date: June 2016
Submission date: July 2016
Version: 2.0c



SM-CCI Quality

The Frequently Asked Questions on the SM website (<http://www.esa-soilmoisture-cci.org/node/136>) was very useful. **It is recommended that a FAQ page be set up for all CCI ECVs, and any bugs can be listed under known issues/errors.** The following points should be added to the SM FAQ to avoid misuse under ‘Do’, ‘Don’t’ or ‘Data usage in models’.

- Do not compare (or take care when comparing) your model total SM directly with these products, the satellite observes the top ~2cm”.
- Any model data should be masked (“simplistic simulator approach”) when compared to the observations. This is indirectly implied in the spatial and temporal availability SM FAQ's. It was less important in this study but for other regions and time periods the differences can be much larger. Any user comparing with model data should strongly be recommended to do mask the model data.
- It would be useful to have a presentation similar to that presented at the CMUG 5th integration meeting available at the FAQ link or somewhere else at the website.

General thoughts on satellite and model soil moisture comparisons

The CCI-SM represents a very shallow layer corresponding to approximately the top two centimeters of the soil, however, the observed depth depends on the soil moisture content (deeper for drier soils). It is not easy to characterize this top soil layer but in many regions it is some combination of active or dormant vegetation mixed by some dead vegetation material mixed with mineral soil. In the model, depending on the exact parameterization applied, the top SSM layer may be purely mineral soil or some weighted value between mineral soil, soil carbon and vegetation material.

As stated on the CCI-SM web page “the statistical comparison metrics like root-mean-square-difference and bias based on our combined dataset are scientifically not meaningful. However, the CCI SM products can be used as a reference for computing correlation statistics or the unbiased root-mean-square-difference”. This would support the anomaly analysis of SM in the 2015 CMUG Quality Assessment Report (CMUG 2015), although the absolute simulated SM values are sometimes at the uncertainty limit of the CCI-SM. The most important soil moisture in models is represented by the layer occupied by roots since this is the soil moisture limiting the transpiration. Methods do exist which can be used to integrate CCI-SM in time to reach a soil moisture representing a thicker layer but assumptions, sometimes difficult to control, are needed for such methods. CCI-SM can be nudged or assimilated in a land-surface model to compile a deep soil moisture product but such a product will always be model dependent and must be used carefully when compared to other models. **A soil moisture product representing the degree of saturation rather than volumetric soil moisture would limit, or even exclude, any model dependence. We argue that such a product is preferable.** The SM team at the CMUG 5th integration meeting informed that such products are planned to be made, we support that work.



3.11 Cross assessments of ESA CCI glacier, land cover and sea level data for hydrological modelling of the Arctic Ocean drainage basin [WP3.9]

Aim

The aim of this study is to assess the use of the CCI Glacier and Land cover data in hydrological modelling of the Arctic Ocean drainage basin. The main underlying question is if the use of CCI Glacier and Land cover can improve hydrological models and simulated river runoff to the Arctic Ocean? The current assessment is focused on the usefulness of the data as input for model parameterization, initialization, and evaluation compared to pre-cursor datasets, as well as on the ‘climate quality’ of the products in terms of understanding long term trends and seasonal variation in the Arctic hydrological system.

Use of Land cover and Glacier data in the Pan-Arctic hydrological model Arctic-HYPE

A pan-arctic application of the hydrological model HYPE (Hydrological Predictions for the Environment) developed by SMHI (e.g. Lindström et al., 2010; Arheimer et al., 2012) is used in the analysis. The model is based on a semi-distributed multi-basin approach, with each river basin divided into sub-basins, and each such sub-basin divided into a set of soil-type/land-cover classes. The model domain includes the land area draining into the Arctic Ocean (excluding Greenland) and covers 23 million km², divided into 32,599 sub-basins with an average size of 715 km² (see further on). The model simulates processes including for instance accumulation and melt of snow and glaciers, evapotranspiration, surface runoff, and drainage from individual soil layers, routing in lakes and rivers, and accumulated water discharge through the mouth of each sub-basin. Arctic-HYPE version 2.5 was developed without any CCI data using GlobCover 2004-2006. A first model version 3.0 based on CCI data was developed during 2015-2016 including information from CCI Land cover (v1.4) and CCI Glacier (Randolph Glacier Inventory, RGI v4.0). Included in the current analysis is also some initial assessments of CCI Land Cover v1.6 and RGI v5.0.

Land cover information is used in the partitioning of the hydrological model sub-basin areas into the runoff-generating sub-units representing unique combination of soil types and land cover types. The original land cover data is re-classified to a smaller number of classes in order to represent only the most important hydrological responses and processes. The current land cover classes in Arctic-HYPE are: lake, glacier, urban, wetland, crops, forest, open vegetation, and bare soil. This may be a oversimplification, since we know for instance that different types of forest tend to grow in different hydrological and permafrost conditions (deciduous needle leaf and evergreen needle leaf, respectively). It should be noted that land cover classes are fixed and their areal extent cannot be changed during the HYPE model simulation. The exception is the glacier

CMUG Phase 2 Deliverable

Reference: D3.1: Quality Assessment Report
Due date: June 2016
Submission date: July 2016
Version: 2.0c



land cover class, for which the glacier covered areal fraction is calculated based on the glacier ice volume (see further below). Lakes and rivers are also given special attention in HYPE: surface water area can be separated into rivers, lakes on the main river course, and internal lakes connected to the main river through local rivers. However, none of the land cover data used for Arctic HYPE – neither GlobCover nor CCI land cover - contains information to separate the surface water area into rivers and lakes. Currently, all surface water area is attributed to lakes. Lake polygons from the Global Lake and Wetlands Database (GLWD) are used to identify lakes situated on the main river, whereas the remaining water area from the land cover data is considered as internal lakes in the model sub-basins.

Glacier information is used to initialize and parameterize a simplified glacier area and mass balance sub-model in HYPE, representing all glaciers within a hydrological model sub-basin by a single storage of ice. **Total glacier area** within each sub-basin is the main input information, whereas the **total glacier volume** is the main state variable in the model. Glacier area and volume is related using area-volume relationships following Bahr et al. (2015). The initial volume is calculated from the input glacier area, whereas during the simulation, the glacier area is updated as a function of the simulated glacier volume. In summary, there are at least 4 major issues related to glacier modelling in HYPE that has been assessed using the CCI Glacier data:

- The use of glacier area-volume scaling is actually not intended for dynamic modelling of individual glaciers, but rather for volume estimates of populations of glaciers. It has been suggested by the CCI Glacier scientific leader to instead use glacier models or glacier volume estimates by Huss and Farinotti (2012). On the other hand, the more simple area-volume scaling models might still be motivated for large-scale hydrological models, since the interest is mass balance and runoff generation of the population of glaciers within a river basin and not of individual glaciers. As a compromise for Arctic-HYPE v3 and later, the linear coefficients in the area-volume relationships are calibrated by fitting the total glacier volume per RGI zone to the values reported in Huss and Farinotti (2012). The glacier type data field in the RGI v4 was used to separate into glaciers and ice caps.
- When area-volume scaling is used, it should be applied on the individual glacier areas; otherwise the total volume will be different due to the non-linear properties of the scaling-functions. This poses a problem for the lumped model structure in HYPE where smaller glaciers within the same sub-basin are lumped together, and larger glaciers and ice caps covering several sub-basins are divided in smaller sections. This problem was solved using the RGI v4 glacier outlines by deriving sub-basin-specific corrections of the linear area-volume coefficients. The exponential coefficients are kept constant with different values for glaciers and ice caps, as discussed by Bahr et al., 2015).
- In previous versions of Arctic-HYPE (version 2.5 and earlier), the glacier area was derived from GlobCover's land cover class "Permanent snow and ice". First of all, this land cover class largely overestimate the glacier area (both using GlobCover and CCI Land Cover; Figure 35; Table 5), and obviously, land cover data does not provide

CMUG Phase 2 Deliverable

Reference: D3.1: Quality Assessment Report
Due date: June 2016
Submission date: July 2016
Version: 2.0c



information on individual glacier basis, which is needed for the area-volume coefficient estimations as described above - only the total area of (permanent snow and) ice.

- A major issue is the problem of: How to initialize glacier area and volume for historical time periods? The mean year of the RGI v4 glacier outline source data is 1996 and the CCI land cover data is representing the period 1998-2012, whereas we would like to start model simulations around 1960. The World Glacier Monitoring Service (WGMS) provide annual glacier mass balance from a large number of glaciers, but still that information need to be generalized through some sort of modelling in order to be applied on all glaciers in the RGI database. The following method was developed solve this problem for the Arctic-HYPE model:
 - We used annual mass balance data from 74 WGMS glaciers within the Arctic-HYPE model domain (Figure 36). The data was used to derive statistical models for the annual glacier mass balance at any point in the Arctic-HYPE model domain as a function of a) a 9 year centered running mean of all annual mass balance data points within the same RGI zone plus b) a linear regression model for the annual deviation from the regional running mean taking into account annual precipitation and temperature
 - An example of the statistical annual glacier mass balance model from the RGI zone Scandinavia is shown in Figure 37.
 - The annual mass balance was integrated backwards to 1961 from the RGI source data year, for each glacier in the model to obtain the initial ice volume. In total over the Arctic-HYPE model domain, the initial ice volume increased only by 2% by this procedure. But there were large regional differences: For the regions Iceland, Svalbard and Western Canada/US the initial glacier volume increased by 5%, 10%, and 30% respectively, whereas for Scandinavia and North Asia the initial glacier volume decreased by 17% and 36%, respectively.

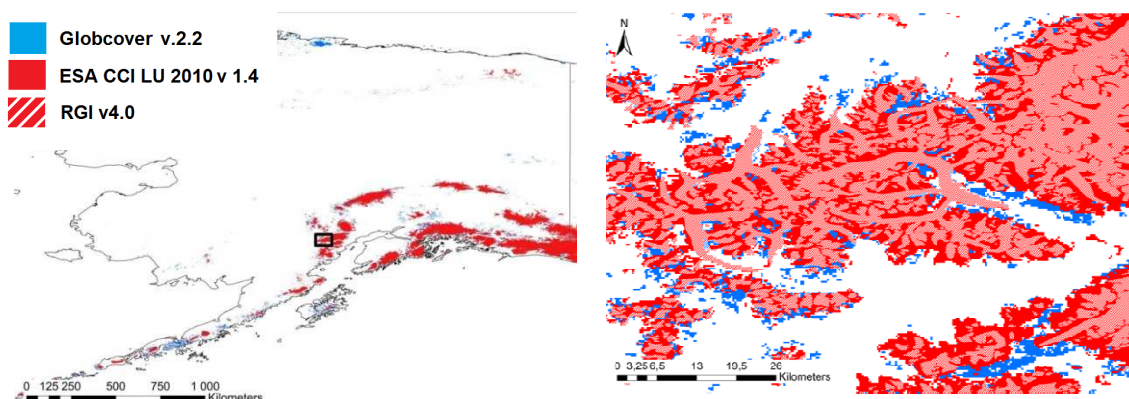


Figure 35: Comparison of glacier area in Alaska derived from CCI land cover and ESA GlobCover 2004-2006 (permanent snow and ice) and the glacier outlines from CCI Glacier (RGIv4).

CMUG Phase 2 Deliverable

Reference: D3.1: Quality Assessment Report
 Due date: June 2016
 Submission date: July 2016
 Version: 2.0c



Table 5: Glacier area in the Arctic-HYPE model per RGI region, comparing data from CCI glacier (RGI v4), Huss and Farinotti (2012), and estimations based on the land cover class “permanent snow and ice” in CCI land cover v1.4 and GlobCover 2004-2006.

RGI region	All glacier areas		ArcticHYPE model domain			
	RGIv4	HF2012	Based on RGIv4		Based on LCv1.4	Based on GlobCover
	km2	% of RGIv4	km2	% of region	% of area based on RGIv4	
01 Alaska	86723	104%	10346	12%	140%	157%
02 Western Canada/US	14559	100%	2151	15%	325%	1711%
03 Arctic Canada North	104873	100%	104716	100%	123%	240%
04 Arctic Canada South	40883	100%	40875	100%	159%	265%
06 Iceland	11060	100%	11060	100%	101%	208%
07 Svalbard	33959	100%	33458	99%	117%	165%
08 Scandinavia	2851	100%	2268	80%	157%	131%
09 Russian Arctic	51592	100%	50844	99%	121%	229%
10 North Asia	3435	82%	1613	47%	235%	860%
Total	349934	101%	257330	74%	130%	242%

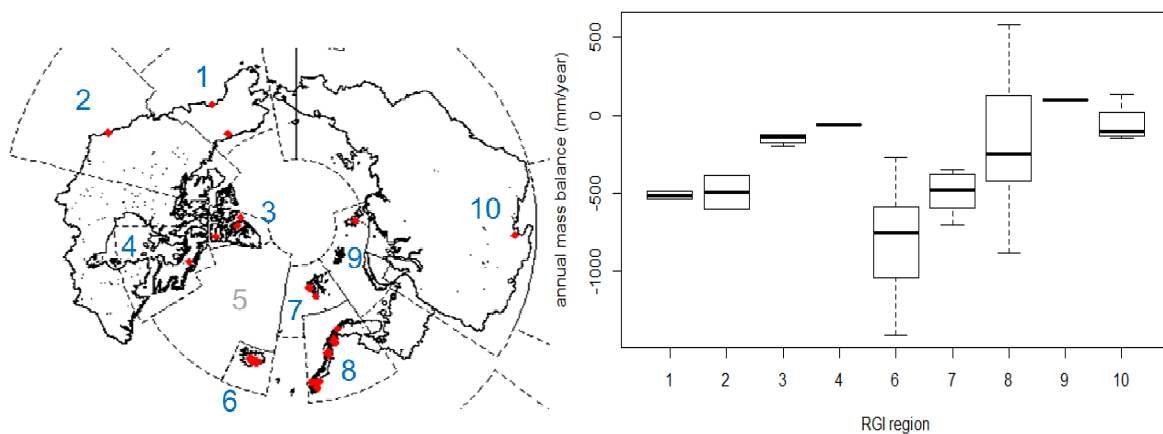


Figure 36: Left: Location of 74 WGMS glaciers with mass balance data within the Arctic-HYPE model domain and RGI regions 1-10 (Greenland zone 5 excluded from the model), Right: average annual glacier mass balance per RGI region.

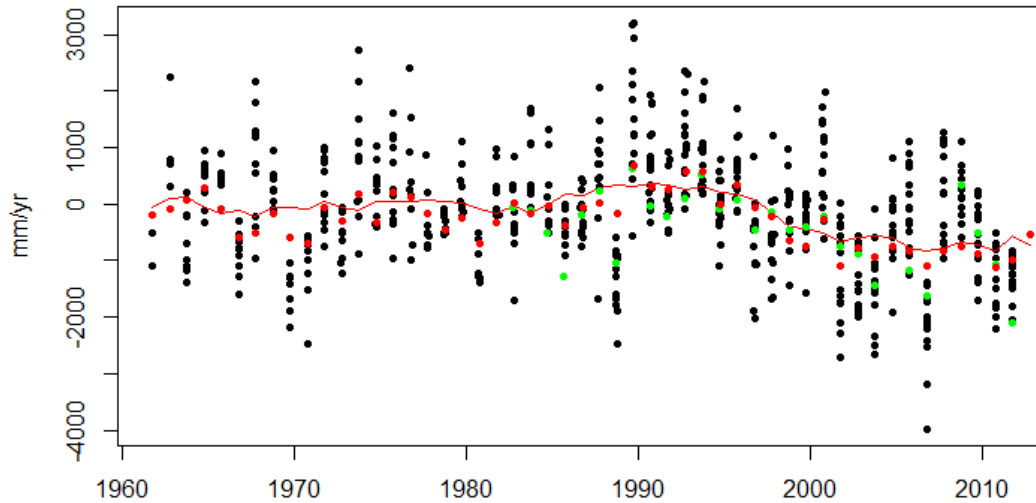


Figure 37: Annual glacier mass balance data from WGMS database for all glaciers in RGI zone 8 (black dots) (Scandinavia), simulated and observed for one of the glaciers (green and red dots, respectively) and the centered running average using a 9 year window (red line).

Summary of Results

CCI Glacier

CCI Glacier data (Randolph Glacier Inventory, RGI v4 and v5) was found to be very useful for evaluating and improving the setup of the glacier sub-model in the Arctic-HYPE model, especially in combination with additional information from other data on glacier mass balance (WGMS) and glacier volume (Huss and Farinotti, 2012):

1. The use of CCI glacier data drastically changed the total area of glaciers compared to previous model versions. Glacier area estimated from the class “permanent snow and ice” from CCI Land cover v1.4 and GlobCover 2004-2006 was found to overestimate the glacier area derived from RGIv4 by 30 % and 140 %, respectively (Figure 35; Table 5).
2. The individual RGI (v4) glacier areas and glacier type information were used to calibrate the area-volume scaling parameters used in the Arctic-HYPE model, by fitting the total glacier volume per RGI region in the Arctic area versus regional glacier volume estimates from Huss and Farinotti (2012).
3. Furthermore, the RGI data enabled the derivation of basin specific corrections of the area-volume scaling coefficients to correct for errors in the volume estimation when lumping or dividing individual glaciers by the hydrological model sub-basin delineation.
4. Compared to estimates with the scaling parameters used in Arctic-HYPE version 2.5, the new scaling parameters implies a decreased glacier volume by 8% when applied on the individual RGI glacier areas for all glaciers in the arctic RGI regions (Table 6). However, when applied on the total glacier area within the Arctic-HYPE sub-basins, the area-volume

CMUG Phase 2 Deliverable

Reference: D3.1: Quality Assessment Report
Due date: June 2016
Submission date: July 2016
Version: 2.0c



scaling resulted in a 37% overestimation of the total glacier volume if the new sub-basin corrections without the scaling parameters.

5. If the overestimation of glacier area in previous model version is also taken into account, the total overestimation of glacier volume in previous model version was even larger (44%, Table 4).
6. RGI glacier outlines could probably also be further used for improving sub-basin delineation following the glacier outlines. The data also includes additional information that could be further used to improve the glacier sub-model parameterizations: mean, maximum and minimum elevation, slope and length, as well as the detailed hypsography, but none of these potential values of the CCI glacier data have been assessed yet.

A first preliminary analysis of RGI v5 showed substantial improvements in North Asia, where previously many glaciers were only marked by a circle area without a real outline (Figure 38). Previous glaciers outlines were also improved and many of them shifted laterally in this region – some glaciers rather large shifts. It has not been not assessed if these updates have been adopted in the CCI Land cover data v1.6.

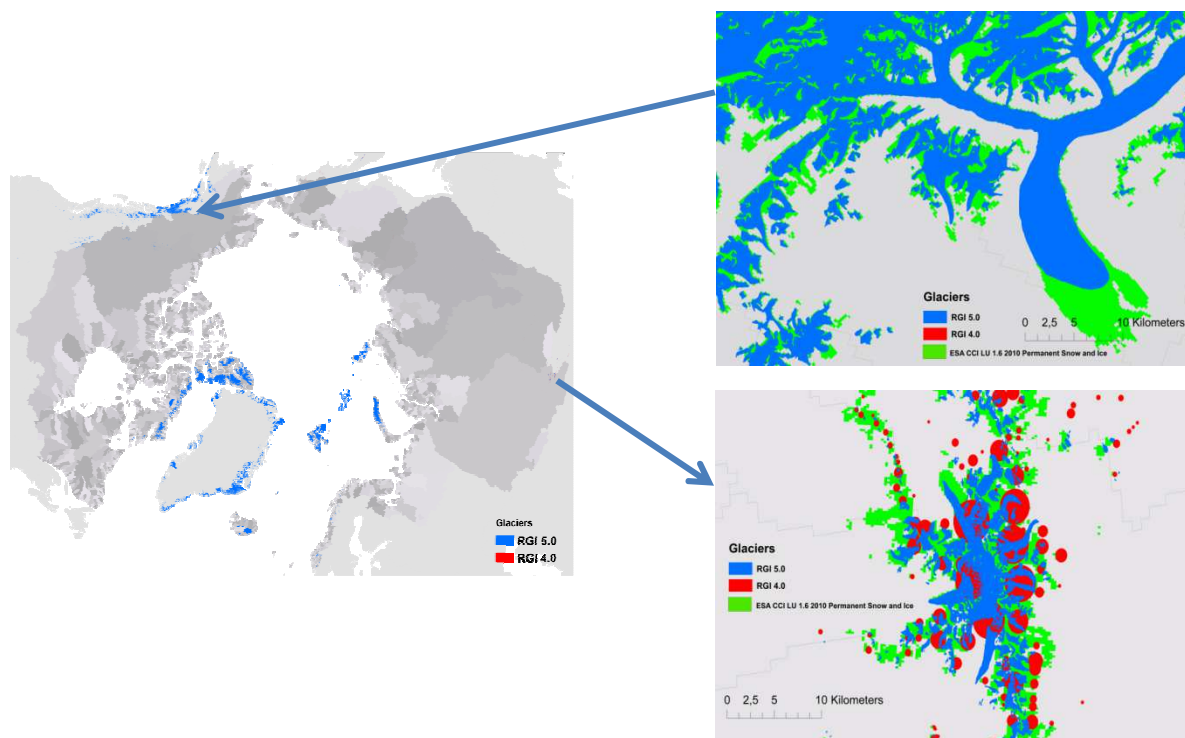


Figure 38: Comparison of Glacier area derived from CCI Glacier (RGI v4 and v5) and CCI Land cover 'permanent snow and ice' v 1.6. Glaciers with unknown outline but known existence and known area were represented by circles in RGI 4.0 (example in lower right panel from upper part of River Ob basin).

CMUG Phase 2 Deliverable

Reference: D3.1: Quality Assessment Report
 Due date: June 2016
 Submission date: July 2016
 Version: 2.0c



Table 6: Glacier volume estimated for RGI regions in the arctic region and in the Arctic-HYPE model per RGI region, comparing data from Huss and Farinotti (2012) with data estimated by area-volume scaling with glacier areas based on CCI glacier (RGI v4), CCI land cover v1.4 and GlobCover 2004-2006.

RGI region	All glacier areas			Arctic-HYPE model domain			
	HF2012	Area-volume scaling based on RGI v4		Area-volume scaling Based on RGI v4			Based on Land Cover v1.4
		Calibrated parameters	Reference parameters	calibrated	calibrated	reference	reference
	km3	% of HF2012		subbasin corrected	uncorr.	uncorr.	uncorr.
01 Alaska	20402	99%	118%	2112	153%	182%	212%
02 Western Canada/US	1025	96%	115%	109	298%	356%	1463%
03 Arctic Canada North	34399	101%	94%	34705	123%	114%	127%
04 Arctic Canada South	9814	97%	79%	9476	134%	114%	210%
06 Iceland	4441	103%	61%	4555	104%	62%	74%
07 Svalbard	9685	95%	80%	9015	166%	140%	155%
08 Scandinavia	256	99%	78%	216	200%	148%	276%
09 Russian Arctic	16839	99%	74%	16516	158%	112%	133%
10 North Asia	140	118%	141%	71	288%	344%	922%
Total	97001	99%	92%	76777	137%	116%	144%

CCI Land cover

CCI land cover v1.4 was compared to the precursor data GlobCover 2004-2006 with regard to differences in land cover distribution. The “climate quality” of the information in the land cover time series (2000, 2005, 2010) was of special interest, since the on-going changes in the Arctic regions (mainly climate related) are expected to be expressed for instance in the distribution of vegetation, surface water, and snow and ice. Furthermore, a initial assessment was made comparing CCI land cover v1.4 and v1.6 for the Arctic region.

Results to date:

- More surface water area in CCI Land cover data sets compared to the pre-cursor GlobCover 2004-2006):
 1. Arctic-HYPE water surface area based on CCI Land cover v1.4 increased with about 6-20% compared to the precursor based on GlobCover 2004-2006 (Figure 39), with ranges depending on how the land cover data was combined with the GLWD lake vector data. This is a very important improvement for understanding Arctic hydrology which is dominated by large rivers and a large number of small and large lakes. The

CMUG Phase 2 Deliverable

Reference: D3.1: Quality Assessment Report
Due date: June 2016
Submission date: July 2016
Version: 2.0c



- total water body area in the Arctic domain further increased with about 1% from v1.4 to v1.6.
2. More realistic distribution and higher resolution of water bodies in CCI Land cover v1.6:
 3. CCI Land cover v1.6 includes a new water body mask with higher spatial resolution (150m), which represented small lakes and river outlines much realistically than v1.4.
 4. The new 150 m resolution water mask has also been re-sampled in the v1.6 300 m land cover products with similar improvements in the representations of water bodies compared to v1.4 (Figure 40).
 5. By vectorizing the water body pixels, statistics on number of lakes and lake size distribution within the hydrological model sub-basins were further used to regionalize lake runoff generating parameters, which was helpful for improving the river discharge simulations in the model.

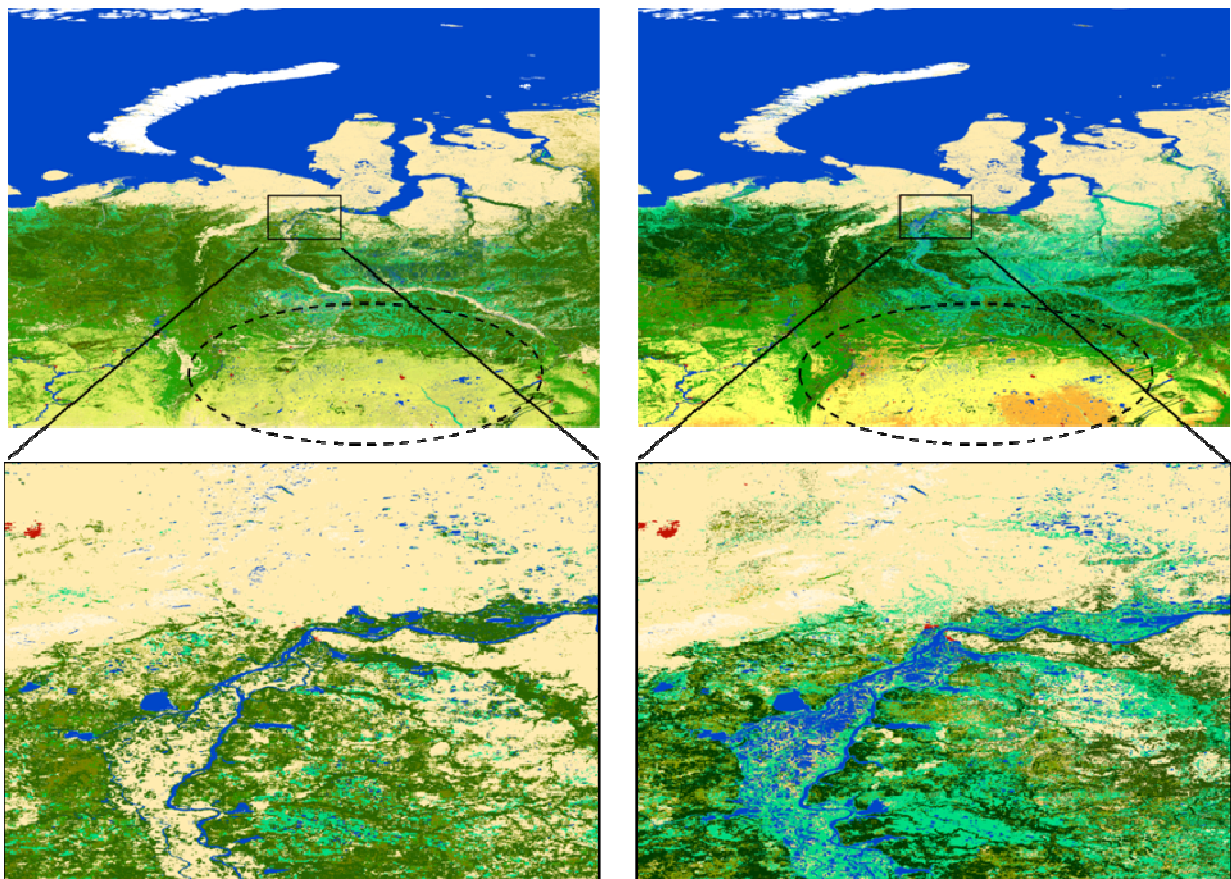


Figure 39: Land cover data from the area around the Ob River showing a clear increase in surface water area from Left: GlobCover to Right: CCI land cover.

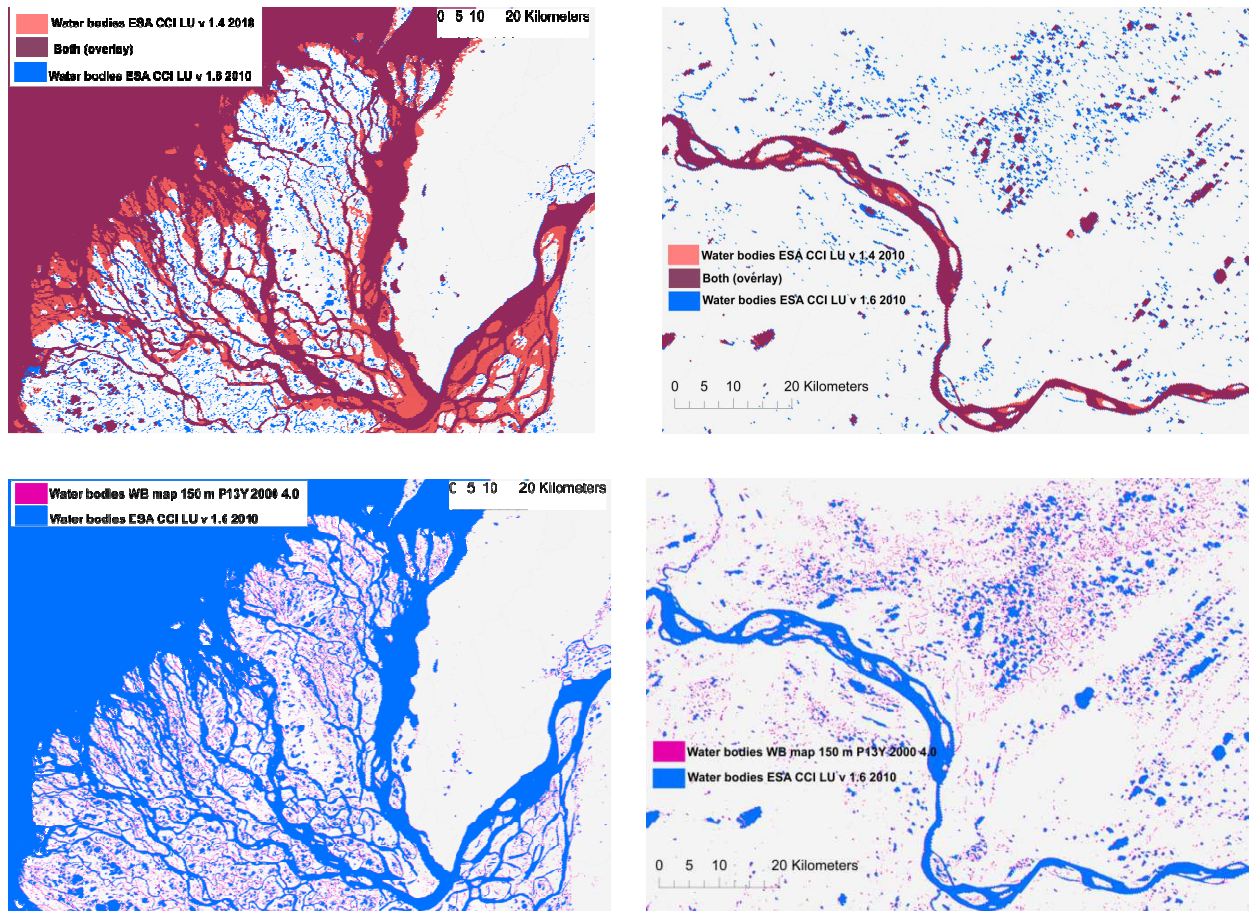


Figure 40: ESA CCI Land Cover Water bodies 2010 showing the difference between (top panels) v1.4 and (bottom panels) v1.6, as well as the difference between the 150 m resolution water body mask (ESACCI-LC-L4-WB-Map-150m) and the 300m land cover product in v1.6 (ESA CCI LU v 1.6), with examples from the Lena River delta (left panels) and the Mackenzie River (right panels).

- The class “water bodies” is constant throughout the three epochs and water bodies are not included in the seasonal products.
 1. From a “climate quality” perspective, it would be interesting to get information on the trends and seasonal variation in the spatial distribution of surface water. Variation in small water bodies is a relevant ECV related to permafrost melting, which is of highest interest in the Arctic region.
- The fraction of deciduous needle leaf trees was reduced in the latest epoch (2008-2012) compared to previous periods in eastern Siberia (based on v1.4, still to be evaluated in v1.6).
 1. Field observations suggest that this might be due to increasing precipitation during the period.
 2. This will affect the ‘climate quality’ of the land cover time-series data.

CMUG Phase 2 Deliverable

Reference: D3.1: Quality Assessment Report
Due date: June 2016
Submission date: July 2016
Version: 2.0c



3. Analysis of relation to observed and simulated river discharge still to be analyzed.
4. Improved distribution of lichens and mosses in v1.6 compared to v1.4:
5. In Land cover v1.4 there was no lichens and mosses in the Eurasian part of the Arctic region. In v1.6 this is improved (Figure 41), mainly by replacing sparse vegetation and bare soils. Summarized over the entire Arctic-HYPE model domain, water bodies and lichens and mosses increased by 1% and 2% respectively, between v1.4 and v1.6, whereas sparse vegetation and bare soil classes were reduced by 1.5% and almost 1% respectively. There were also minor reductions in forests and other remaining classes (Figure 41).

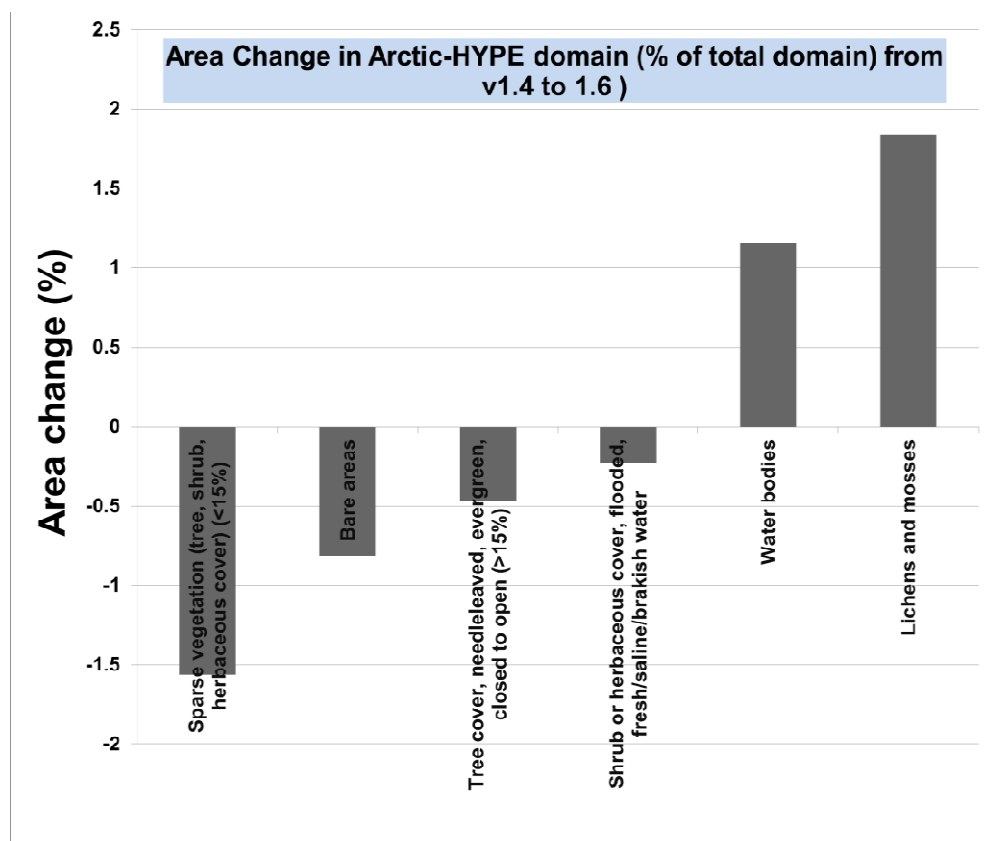


Figure 41: Changes in some aggregated land cover classes between CCI land cover v1.4 and v1.6, summarized over the Arctic-HYPE model domain.

Quality relevant outcomes

- Disagreement between CCI Glacier and CCI Land cover:
 - The CCI Land cover class “permanent snow and ice” is larger than the glacier area derived from the glacier outlines in CCI Glacier - in total over the Arctic-HYPE model domain 30% too large (Figure 24; Table 5).

CMUG Phase 2 Deliverable

Reference: D3.1: Quality Assessment Report
Due date: June 2016
Submission date: July 2016
Version: 2.0c



- The CCI Land cover documentation reveals that the CCI Glacier outlines have been used to assign “permanent snow and ice” to all land cover pixels within the outlines – however, areas outside of the CCI Glacier outlines classified as “permanent snow and ice” have not been reset to “unclassified” or any other land cover class. In addition, the latest version of land cover (v1.6) does not seem to be updated to the latest version of glacier data (RGI v5).
- Previous discussions with Science Leaders from CCI Glacier and Land cover confirmed that CCI glacier area was added to “permanent snow and ice”. It was suggested to include a sub-class under “permanent snow and ice” separating pixels under ice and other snow pixels. But as we can see, it has not been implemented yet in CCI LandCover v1.6.
- No ice thickness in CCI Glacier data (RGI v4 or v5):
 - Glacier thickness is not included in RGI even though estimates of each glacier exist based on modelling and observations (Farinotti and Huss, 2012).
 - The model estimates can be requested from the CCI Glacier team on request. However this information is not yet clear in the CCI Glacier documentation.
- No temporal information in CCI Glacier (RGI v4 or v5):
 - The RGI data provide the date of the source data, but information is still needed for proper initialisation of glacier models for previous time periods. Recommended practices on how to model historical glacier extents and volumes would be useful as an extension of the CCI Glacier.
- The need for a CCI Hydrography
 - Hydrography data (river network, sub-basin delineation, lake and water delineation, flow directions, man-made and natural diversions, dams, etc) is one of the most important inputs for hydrological models. Arctic-HYPE uses a polygon based partitioning of the landscape into sub-basins derived from digital elevation data (Hydro1K), vectorised lake delineation (GLWD) and discharge station metadata (location and upstream area). Other models uses gridded hydrography (Flow directions), but the importance for model development and evaluation is nevertheless essential. The most used datasets on the global scale are the USGS Hydro1K (1km² resolution) and only available below 60°N HydroSheds (90 m² resolution), which both provide hydrologically constrained digital elevation and flow direction data.
 - Just like land cover, the river and lake network may change as a result of hydrological, climatological, morphological and anthropogenic processes. Both river morphology, flow directions, number and extend of lakes is changing in the Arctic region and in other regions of the world.
 - The CCI Land Cover mask include excellent information of water bodies and the latest version 1.6 provide a major improvement of identified water bodies and spatial detail. However, water pixels are not linked to lakes and river network data. For instance, separating water pixels into lake and river pixels would be a

CMUG Phase 2 Deliverable

Reference: D3.1: Quality Assessment Report
Due date: June 2016
Submission date: July 2016
Version: 2.0c



important first step towards and improved usefulness of the CCO water mask data in hydrological modelling. The ultimate goal of a CCI Hydrography could be to contribute to a global high resolution hydrography dataset, including lakes and river outline data, and gridded hydrologically constrained elevation and flow direction data.

CMUG Phase 2 Deliverable

Reference: D3.1: Quality Assessment Report
Due date: June 2016
Submission date: July 2016
Version: 2.0c



3.12 Cross-assessment of CCI-ECVs over the Mediterranean domain [WP3.10]

Some key outcomes of the CMUG research activity on this topic are that:

- The CCI Sea-Level ECV is adequate to assess the performance of the state of the art regional climate models over the Mediterranean basin.
- There is a significant positive impact of the assimilation of the CCI Sea Level ECV in the ocean reanalyses that are used for the Atlantic lateral boundary conditions of the Mediterranean regional climate models.
- The uncertainty on the ECV local trends seems to be over-estimated.

Aim

The activity within the context of this Work Package is in the continuity of the Météo-France activity in the context of CMUG Phase 1. Its main objective is to evaluate the performances (mean climate, variability and trends) of the Med-CORDEX regional climate system models over the Mediterranean domain with a sub-set of atmosphere, marine and surface CCI-ECVs. The first scientific question to address is the following: are the state of the art RCSMs able to reproduce observed Mediterranean climate trends and variability over the last decades?

Summary of results

During CMUG Phase 1, the SSH simulated by the so-called RCSM4 coupled regional climate model (Sevault et al., 2009) developed at CNRM and applied in the Med-CORDEX international simulation exercise, was confronted with the CCI Sea Level ECV and its precursor over the 1993-2010 period (see Phase 1 deliverable 3.1). Some results of this confrontation have been recently published in the scientific literature as part of a presentation of the evaluation of the ocean component of the RCSM4 model (Sevault et al, 2014).

One main conclusion from this confrontation was that the CCI SSH is suitable for regional climate studies over the Mediterranean basin, even at a scale of a few tens of kilometres. The results of the model concerning trends of sea level change are encouraging. It also let some open questions concerning the way to facilitate the comparison between the modelled and observed sea levels. These questions come from the fact that climate models are not directly calculating the contributions to sea level changes that are due to mass changes implied by glaciers and ice sheet melting or by changes in continental water storage. In addition, in the specific case of regional climate models simulating the Mediterranean domain, the contribution to mass change in the Mediterranean Sea due to the mass flux at the Gibraltar Strait need also to be carefully taken into account.

CMUG Phase 2 Deliverable

Reference: D3.1: Quality Assessment Report
Due date: June 2016
Submission date: July 2016
Version: 2.0c



Since the beginning of CMUG Phase 2, thanks to the development of a new version of the Mediterranean Sea model, and thanks to the availability of a new ocean reanalysis, it was possible to improve the comparison between the modelled and the satellite-derived SSH.

The operational ocean reanalysis system (ORAS4; Balmaseda et al., 2013) has been implemented at ECMWF and it spans the period 1958 to the present. This makes this reanalysis suitable for MedCORDEX simulations since it can be used to constrain the oceanic component of a regional climate model in the Atlantic buffer zone over the ERA-Interim period (1980-2013). Contrary to the so-called COMBINE reanalysis previously used, ORAS4 assimilates satellite-derived SSH anomalies from the AVISO dataset (the precursor used in Phase 1). It also includes sea level contributions from ice sheet mass loss, glaciers ice melt, changes in land water storage and global thermal expansion. This makes great difference because this potentially allows to account for sea level changes due to mass changes in the simulated Mediterranean sea level through the boundary condition applied in the Atlantic buffer zone (see Phase 1 deliverable 3.1). The results presented below confirm that this is indeed the case.

The new version of the Mediterranean Sea model is NEMOMED12, a regional version of NEMO v3.2 model simulating the free surface evolution associated to the convergence of the oceanic current and to the fresh water flux at the ocean surface, as this was the case for NEMOMED8 used during Phase 1. Compared to this last, the resolution is improved on the horizontal ($1/12^\circ$ versus $1/8^\circ$) and on the vertical (75 vertical levels versus 43). The model was integrated over the period 1980-2013 with an atmospheric forcing from ALDERA (a dynamical downscaling of ERA-Interim using the ALADIN-Climat regional climate model) and a relaxation toward ORAS4 in the Atlantic buffer zone of the model (3D for temperature and salinity, 2D for SSH). However, since ORAS4 underestimate the mean seasonal cycle of the SSH over the basin (see Figure 42), it has been previously corrected in the Atlantic buffer zone in order to reproduce on average the mean annual cycle obtained from the CCI-ECV over the 1993-2010 period. This correction also applies before the satellite observing period.

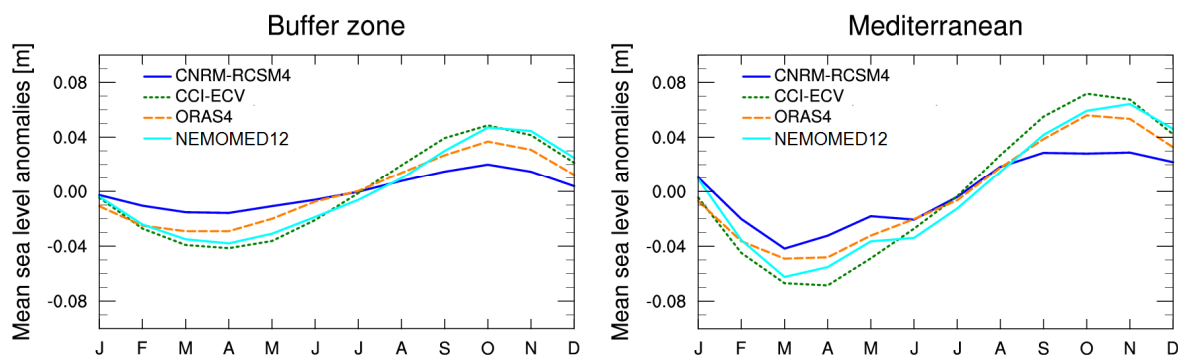


Figure 42: Seasonal cycle of mean sea level anomaly over the buffer zone (left) and over the Mediterranean Sea (right) for the CCI sea level (green dotted line), ORAS4 ocean reanalysis (orange dashed line), the coupled regional climate system model RCSM4 (dark blue line) and the Nemomed12 Mediterranean sea model (light blue line).



The results presented in Figure 43 show that the NEMOMED12 model reproduces correctly the mean seasonal cycle from the CCI-ECV over the buffer zone, small differences coming from the fact that the relaxation coefficients toward the corrected ORAS4 are decreasing in the eastern part of this zone. But NEMOMED12 also reproduces fairly well the Mediterranean Sea mean sea level inferred from the CCI-ECV, and with a much better agreement than the RSCM4 free surface (in Phase 1 deliverable 3.1, RSCM4 sea level was presented after adding the thermosteric component of sea level inferred from the simulated temperature changes only over the basin to account for missing terms in the model equations).

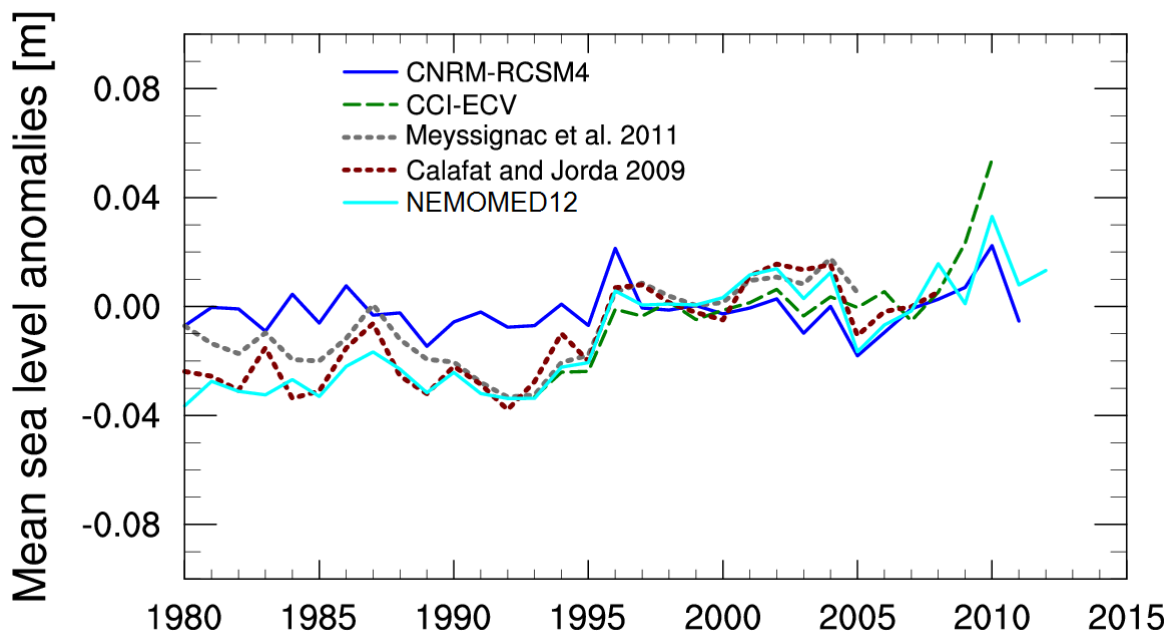


Figure 43: Time series of mean sea level anomalies averaged over the Mediterranean Sea over the period 1980-2013 for the CCI sea level (dashed green line), the tide gauge derived sea level reconstructions of Meyssignac et al. (dotted grey line) and Calafat and Jordà (dotted brown line), for the coupled regional climate system model RSCM4 (dark blue line) and the Nemomed12 Mediterranean sea model (light blue line).

The positive impact of the assimilation of satellite-derived sea level in the ocean reanalysis used to constrain the ocean model in the Atlantic is also illustrated in Figure 43 showing the time series of mean sea level over the Mediterranean Sea. NEMOMED12 is indeed able to reproduce the sea level change over the period as observed from tide gauges and by the CCI-ECV. This also illustrates that the mean sea level change in the Mediterranean Sea mainly depends on the mass flux change at the Gibraltar Strait. Here again, without the thermosteric term contribution, the RSCM4 model has low performance due to the absence of SSH assimilation in the COMBINE reanalysis used to constrain the model in the Atlantic.

CMUG Phase 2 Deliverable

Reference: D3.1: Quality Assessment Report
Due date: June 2016
Submission date: July 2016
Version: 2.0c



This analysis of the added-value of the CCI Sea Level ECV using the CNRM regional climate coupled and uncoupled models was completed by a multi-model intercomparison, considering two additional coupled regional climate system models used within the context of the Med-Cordex project (Adloff et al., 2016). The first one is the so-called LMDZ-MED model (L'Hévéder et al., 2013) coupling the LMDz4 regional atmospheric component with the NEMOMED8 regional configuration of the NEMO ocean model with a horizontal resolution of 9 to 12km. For this model, the mean sea level in the Atlantic buffer zone is kept constant. The second is the MORCE-MED model (Lebeaupin-Brossier et al., 2013) coupling the WRF atmospheric model with NEMOMED12. As for the CNRM-RCSM4 and the NEMOMED12 models, the simulated SSH is here relaxed toward a reference dataset in an Atlantic buffer zone. Over the period 2002-2008, it comes from the GLORYS-1 reanalysis (Ferry et al., 2010) which assimilates the AVISO satellite sea level. Over the period 1989-2001, the reference SSH varies seasonally but not interannually.

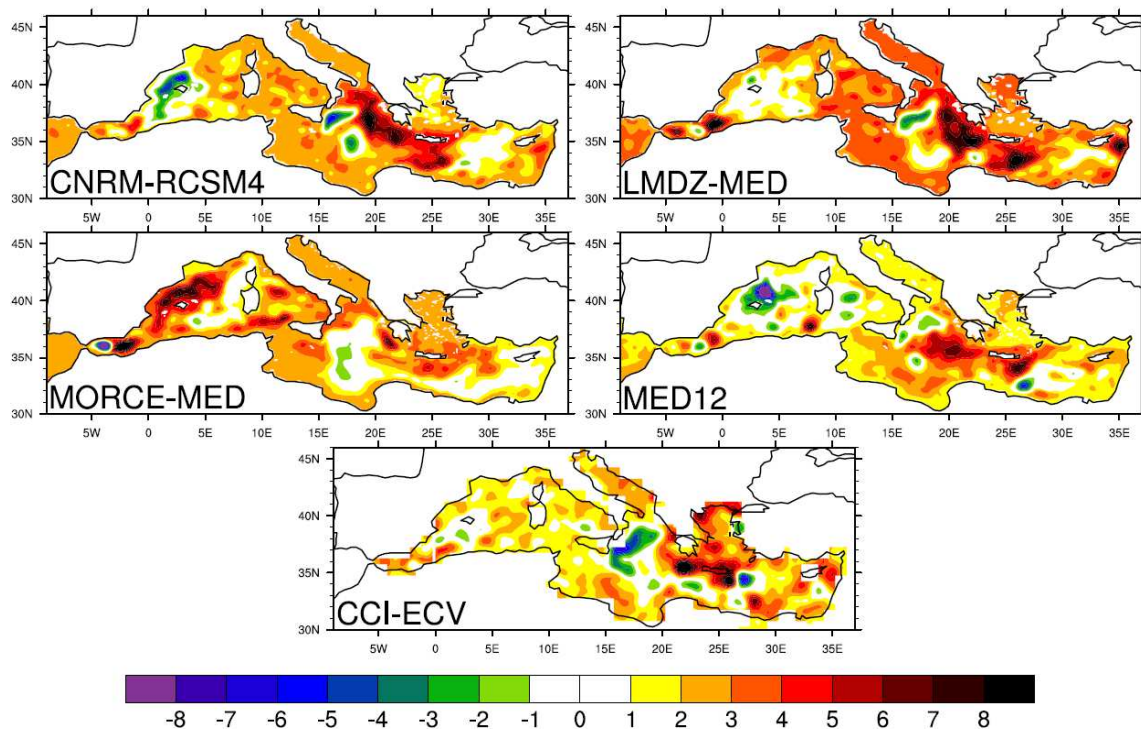


Figure 44: Trends in mm/year of Mediterranean sea surface height anomalies over the period 1993-2008 for the three coupled regional climate system model (RCSM4, LMDZ-MED and MORCE-MED), the NEMOMED12 Mediterranean Sea model (MED12) and the CCI Sea Level (CCI-ECV).

We have also reproduced in Figure 44 the simulated and observed sea level trends for the 16-year of the simulations common period (1993-2008). For the three coupled models, to account for the imperfect boundary conditions applied to the sea level in the Atlantic buffer zone, the

CMUG Phase 2 Deliverable

Reference: D3.1: Quality Assessment Report
Due date: June 2016
Submission date: July 2016
Version: 2.0c



reproduced trends are calculated as the sum of the calculated dynamic component and a spatially constant thermosteric component of the sea level change. This consists in neglecting the contribution of salinity changes in the computation of modeled sea level change at the Mediterranean basin scale as justified by previous analyses (see Phase 1 deliverable 3.1). However, whatever the hypothesis made to correct the trend averaged at the basin scale, the spatial trend variability reproduced in Figure 44 only results from the simulated dynamical processes and sea surface fresh water fluxes.

Here RCSM4 and NEMOMED12 display very similar performances because the different boundary conditions have little impact on the spatial trend variability. But this also proves that this variability is not too much affected by the coupling between the atmosphere and the Mediterranean Sea. The LMDZ-MED model also shows important similarities with the observations, showing that the spatial variability of the local trends is not significantly affected by the specification of the lateral boundary conditions. The difficulties of the models to reproduce the observed trends in the western part of the Mediterranean basin can be attributed to their difficulty to reproduce the circulation in the Alboran region (Adloff et al., 2016). The patterns are differently reproduced by the different models in this region. The patterns are better reproduced in the eastern part of the basin and in particular due to their ability to reproduce the recovery following the so-called “Eastern Mediterranean Transient” (EMT) anomaly. There is thus a model dependence of the results and the CCI-ECV can be used to assess the performances of the models.

In addition, the level of agreement between the models and the CCI-ECV observations shows that the uncertainty on local trends estimated to be 3mm/yr, might have been overestimated by the CCI Sea level team. The models are indeed consistent between them and with the observations in many regions with differences that have the same order of magnitude than this estimated error.



3.13 Assessment of sea ice concentration observational uncertainty from a data assimilation point of view [WPO3.11]

Sea ice concentration (SIC) is arguably one of the best-monitored essential climate variables (ECV) at high latitudes. SIC records date back to the late 1970s and are global (Cavalieri et al, 1996), which makes them central for climate studies. In addition, SIC is an essential term in the sea ice mass budget and is the primary information on which the skill of contemporary climate models is estimated in polar regions (e.g. Guemas et al, 2014). However, satellites do not measure SIC directly. Rather, they sense sea surface brightness temperature; since water and ice have different passive microwave signatures at a certain frequency, it is possible to estimate the relative amount of sea ice in a grid cell (that is, sea ice concentration) given the brightness temperature information. This conversion between brightness temperature and SIC comes at the price of numerous assumptions which, added to the instrumental uncertainty, make SIC products intrinsically uncertain. The comprehensive review by Ivanova et al. (2016) documents advantages and pitfalls of different algorithms for SIC retrieval and discusses these issues in detail.

By contrast, sea ice thickness (SIT) is a poorly observed variable, although it is thought to carry a significant share of sea ice predictability, at least for the summer season. Indeed, thin ice melts more easily, so that SIT anomalies are directly related to SIC anomalies a few months later, with possible re-emergence up to a year later (see Guemas et al., 2014). Defining SIT anomalies is not trivial, given the sparsity and intermittency of existing records. Efforts from many projects, including ESA-CCI, to make these products routinely available are therefore more than welcome, given the valuable information that they represent for the climate community.

The quality of observational sea ice products is critical for accurate initialization of climate predictions. Within the CMUG phase 2, the Earth Sciences Department of the Barcelona Supercomputing Center (BSC-ES) is implementing a sophisticated method of data assimilation for SIC, namely the ensemble Kalman Filter (EnKF; Evensen, 2003, 2007). The assimilation of SIT is currently under investigation and will be assessed in a later stage of this project. The EnKF works in two steps: (1) a *forecast step*, during which an ensemble of N ($N=24$ in our case) climate simulations is forwarded in time, each element (“member”) of the ensemble being subject to a perturbation and (2) an *analysis step*, during which all members are updated based on new information available from observations (Figure 45).

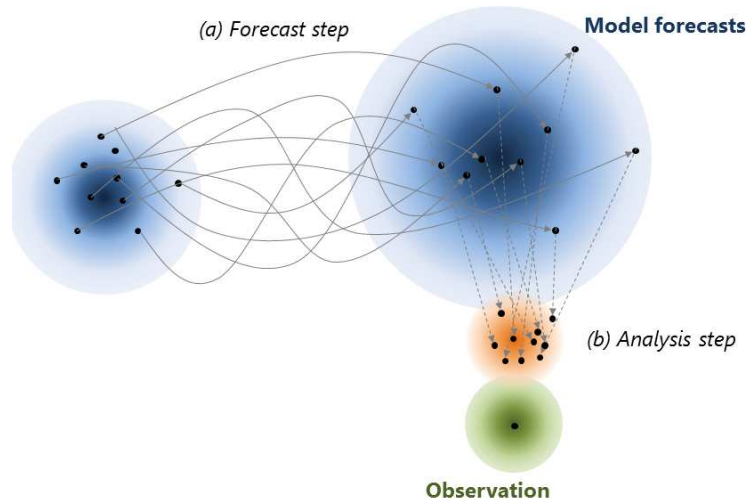


Figure 45: Principle of the ensemble Kalman Filter (EnKF). During the forecast step, model error is explored by integrating N model versions, each subject to a perturbation. The ensemble is then updated during the analysis step. The update is proportional to the misfit of forecasts to the observation, and is weighted by the relative uncertainties in observations and forecasts. A new forecast cycle is then started using the result of the analysis step as initial conditions for the new forecast step.

The EnKF can be considered as a sophisticated data assimilation method for two reasons. First, it is multivariate: partial observations will have a global impact. For example, the observation of SIC alone can lead to a substantial correction of other, non-observed variables including SIT but also sea surface temperature, salinity or even currents. The mechanism for updating these “non-observables” will not be discussed here in detail but illustrated in several examples. The other strength of the EnKF is the fact that this filter accounts for both model and observational uncertainties. In regions where the model is relatively confident (e.g., the interior of the Arctic sea ice pack in winter), updates will be minor; while they will be larger in the marginal ice zone where the position of modelled ice edge is usually uncertain. At the same time, updates will be large where observations are relatively confident. The specification of SIC uncertainties is therefore a key piece of information for data assimilation with the EnKF.

To the best of our knowledge, only two products provide estimates of uncertainty²: the OSI-SAF reprocessed sea ice concentration product (Eastwood et al., 2014) and the ESA-CCI sea ice concentration product, abbreviated SICCI hereinafter (Sea Ice CCI). In this deliverable, we compare uncertainties in these two products and assess the impact on updates from the EnKF.

Comparison of sea ice concentration uncertainty

The two products mentioned above, OSI-SAF and SICCI, both deliver SIC uncertainty as the

² The term « uncertainty » is here used to refer to the statistics of errors in modeled/observed SIC.

CMUG Phase 2 Deliverable

Reference: D3.1: Quality Assessment Report
Due date: June 2016
Submission date: July 2016
Version: 2.0c



grid-point standard deviation of the probability distribution of SIC errors. However, the products come at different resolutions: 10 km for OSI-SAF and 25 km for SICCI. Because of this difference, a direct comparison of uncertainty in SIC retrievals from the two sources is difficult, since error statistics are scale-dependent. A thorough regridding of the errors would require knowledge of the spatial correlation of these errors, which is neither provided by OSI-SAF nor SICCI. We assume therefore uncorrelated errors.

The OSI-SAF and SICCI standard deviation in SIC were gridded using a bilinear scheme to a common grid, that of the ocean sea ice model NEMO3.6 (Madec et al, 2016) used for assimilation. The target grid (ORCA1) is tripolar and has a resolution of ~50km in the Arctic and the Antarctic. From analyses of several pairs of SIC data during the overlapping period where both products are available (1992-2008), a systematic pattern emerges (Figure 47):

- The SICCI product provides lower uncertainty (i.e., is more confident) inside the sea ice pack and over the open ocean, while
- The OSI-SAF product provides lower uncertainty around the marginal ice zone. The example of September 2007 is striking in that respect (the tongue pattern of that year is standing out).

We now compare this uncertainty to the one provided by a 24-member ensemble of simulations carried with the ocean sea ice model NEMO3.6-LIM3, for which a CMIP6 version has recently been released (Madec et al 2016). LIM3 (Vancoppenolle et al, 2009), the sea ice component of the model, is a dynamic-thermodynamic sea ice model that simulates SIC and SIT, among others. The model features an explicit ice thickness distribution (ITD), meaning that SIC and SIT are modelled for different categories of sea ice thickness, in order to resolve the non-linear thermodynamic processes more accurately. How to transfer information from total SIC (available from observations) to each category is a separate question that we do not treat here; the interested reader is redirected to Massonnet et al (2015) for further information.

NEMO3.6-LIM3 is run with perturbed versions of the atmospheric Drakkar Forcing Set 5.2 (DFS5.2, Dussin and Barnier, 2015). In this pilot experiment, only the 2m temperature is perturbed, but perturbations are generated to match the spatial and temporal covariances of the original data set. All simulations start on the first of January 1993. Data of SIC is assimilated at the end of each month, either from the OSISAF SIC or the SICCI SIC.

CMUG Phase 2 Deliverable

Reference: D3.1: Quality Assessment Report
Due date: June 2016
Submission date: July 2016
Version: 2.0c

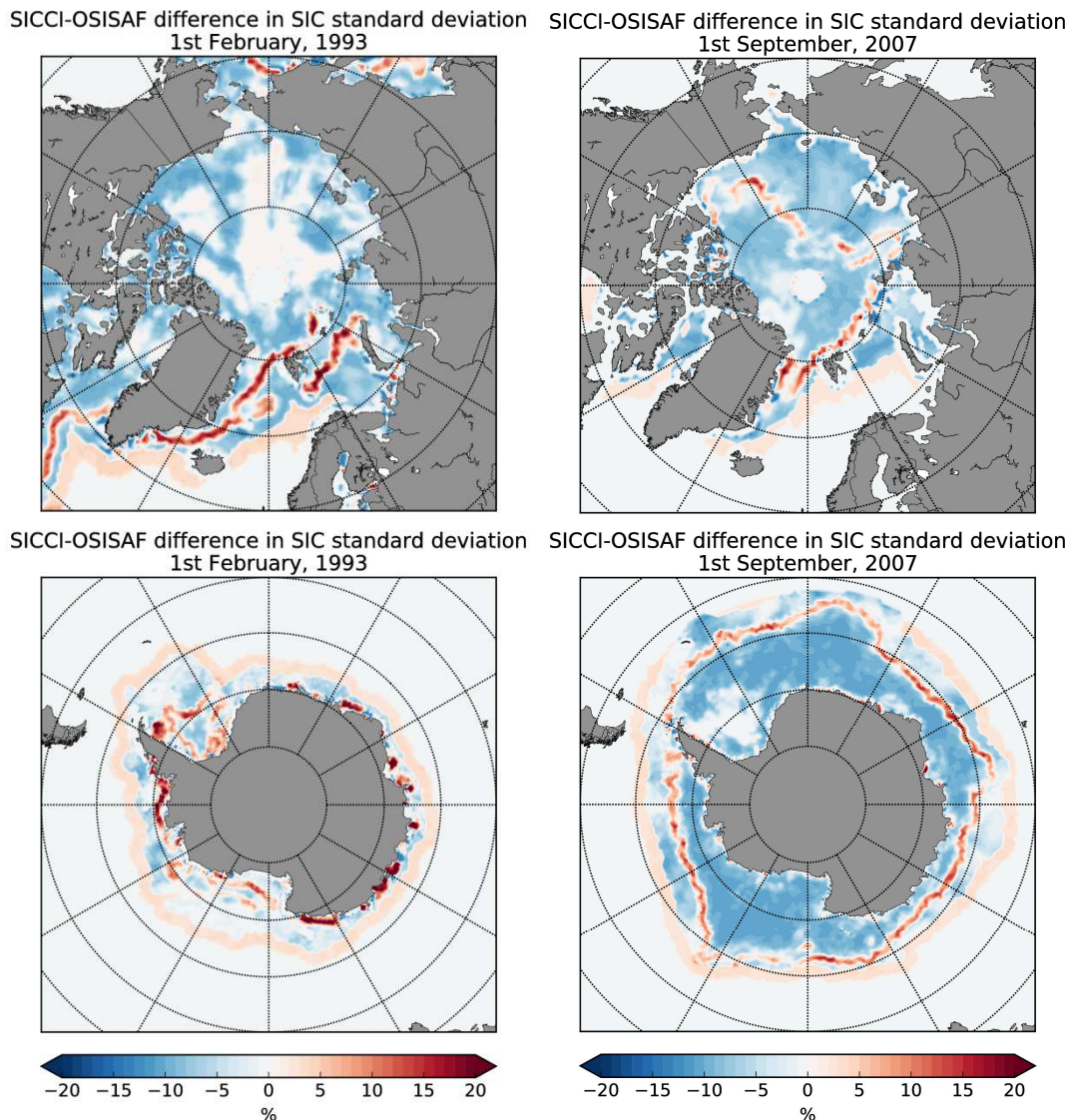


Figure 46: Difference (SICCI minus OSISAF) in sea ice concentration uncertainty (measured as standard deviation) for two dates: 1st February 1993 (left column) and 1st of September 2007 (right) for the Arctic (upper row) and the Antarctic (lower row).

Impact of observational uncertainty on assimilated sea ice concentration

The ensemble spread in the model SIC is shown in Figure 47 (upper left panel) for one particular date (1st of February 1993) for the Southern Hemisphere. The reason for picking the Southern Hemisphere is that the most interesting behavior of the data assimilation is seen at that time of the year (February corresponds to austral summer, and thus to a greater variability in SIC as well as larger errors). The innovations, defined as the misfit of the mean of model forecasts to the observations, show hardly any difference when the OSISAF is used instead of the SICCI product (center and right upper panels of Figure 47). This follows from the fact that the estimated SIC in these two products are very close to each other (not shown here). However, as pointed out in

CMUG Phase 2 Deliverable

Reference: D3.1: Quality Assessment Report

Due date: June 2016

Submission date: July 2016

Version: 2.0c



Figure 46, the *uncertainty* provided by these products vary, with the SICCI being in general more certain. The bottom row of Figure 47 shows the updates (difference between the model state after assimilation and the forecast) resulting from the assimilation of SIC from the SICCI product (lower left panel) and the OSISAF product (lower center panel). To quantify the magnitude of the correction that these two products allow in the model, we finally display the difference of absolute updates in the lower right panel. Although regional variability is present, corrections are generally larger (regardless of their sign) for the SICCI product, which confirms the results of Figure 46.

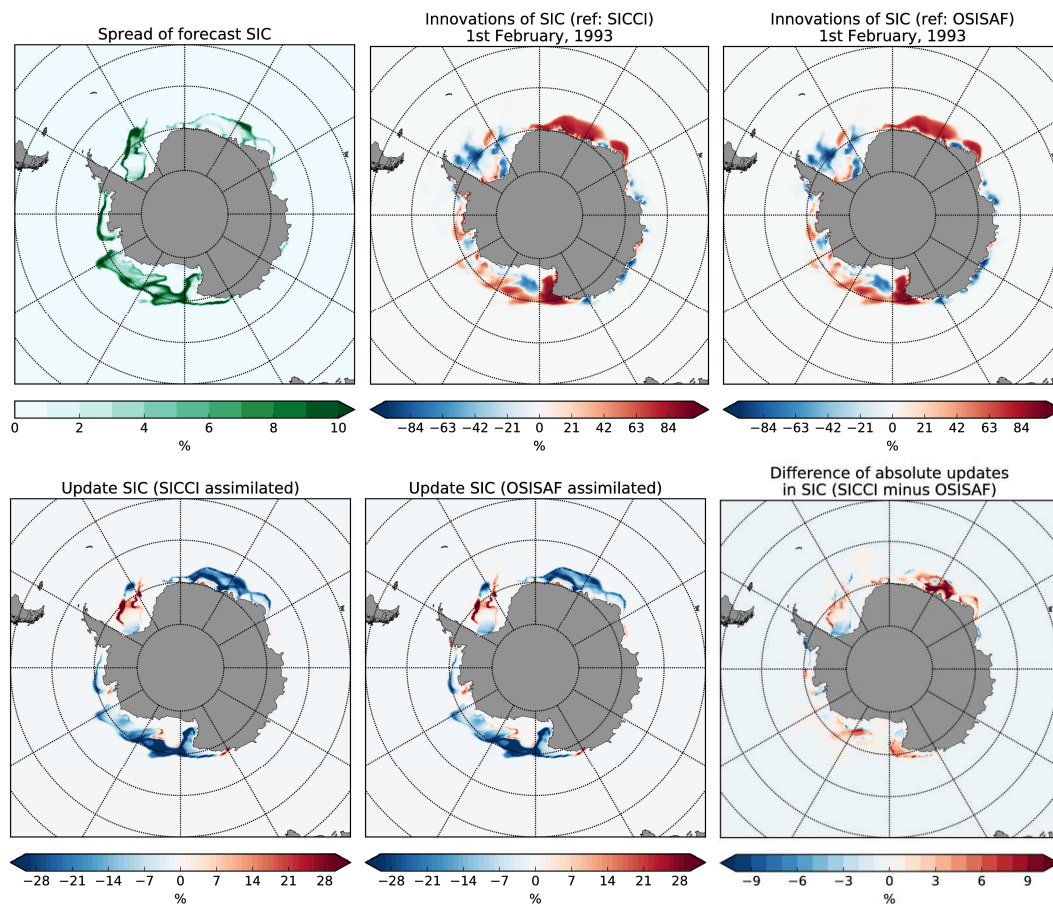


Figure 47: Spread of SIC in the forecasts, measured as the standard deviation of the 25-member ensemble (left) versus innovations of SIC (mean forecast minus observational reference) for the two products considered (center: SICCI and right: OSISAF). Second row: Updates in SIC (mean of analyses minus mean of forecasts) for the two products considered (left: SICCI and center: OSISAF) and the difference in absolute values of these updates (right). The situation refers to that of the 1st of February 1993.

CMUG Phase 2 Deliverable

Reference: D3.1: Quality Assessment Report
Due date: June 2016
Submission date: July 2016
Version: 2.0c



Conclusions and outlook

A prototype of assimilation of sea ice concentration (SIC) has been implemented and tested with two observational products: European Space Agency's SICCI and Norwegian Met Office's OSISAF products. The conclusions are as follows:

- The more recent product (SICCI) displays lower uncertainty except in the marginal ice zone. The reasons for these differences are yet to be identified. As discussed by Ivanova et al. (2016), the methodology for deriving SIC has benefited from accumulated knowledge about many other products, and there are therefore good reasons to believe that this product is intrinsically of higher quality.
- While estimated SICs are close to each other in these two observational references, information about uncertainty *has much importance*. This is verified in the data assimilation experiment proposed, that shows that more certain observations are prone to yield larger corrections to climate models. In view of the large biases of SIC, especially in the Southern Ocean, this represents an important aspect towards model improvement.

In spite of these efforts to report systematically observational uncertainties in SIC products, an essential aspect is still missing: a quantification of correlation of errors across space. This would not only allow for a more realistic constraint for the models; but it would also allow for a clean comparison of observational uncertainties (unlike what is presented in Figure 46, where this spatial correlation is assumed to be null) and a realistic way to propagate local errors to the basin-wide level. This would provide invaluable information for large-scale climate modelers, which focus frequently on integrated quantities (sea ice area/extent) for a first order evaluation of their models.

CMUG Phase 2 Deliverable

Reference: D3.1: Quality Assessment Report
Due date: June 2016
Submission date: July 2016
Version: 2.0c



3.14 *Assessment of Antarctic ice sheet ECVs for modelling [WP3.12]*

Will be reported on in version 3 of this report in 2017.

3.15 *Assessment of Greenland ice sheet ECVs for modelling [WP3.13]*

Will be reported on in version 3 of this report in 2017.



4. References

Adloff, F., G. Jordà, S. Somot, F. Sevault, T. Arsouze, B. Meyssignac, L. Li, and S. Planton, 2016: Improving sea level simulation in Mediterranean regional climate models. Submitted to Climate Dynamics.

Bakker, D. C. E., Pfeil, B., Smith, K., Hankin, S., Olsen, A., Alin, S. R., Cosca, C., Harasawa, S., Kozyr, A., Nojiri, Y., O'Brien, K. M., Schuster, U., Telszewski, M., Tilbrook, B., Wada, C., Akl, J., Barbero, L., Bates, N. R., Boutin, J., Bozec, Y., Cai, W.-J., Castle, R. D., Chavez, F. P., Chen, L., Chierici, M., Currie, K., De Baar, H. J. W., Evans, W., Feely, R. A., Fransson, A., Gao, Z., Hales, B., Hardman-Mountford, N. J., Hoppema, M., Huang, W.-J., Hunt, C. W., Huss, B., Ichikawa, T., Johannessen, T., Jones, E. M., Jones, S., Jutterstrøm, S., Kitidis, V., Körtzinger, A., Landschützer, P., Lauvset, S. K., Lefèvre, N., Manke, A. B., Mathis, J. T., Merlivat, L., Metzl, N., Murata, A., Newberger, T., Omar, A. M., Ono, T., Park, G.-H., Paterson, K., Pierrot, D., Ríos, A. F., Sabine, C. L., Saito, S., Salisbury, J., Sarma, V. V. S. S., Schlitzer, R., Sieger, R., Skjelvan, I., Steinhoff, T., Sullivan, K. F., Sun, H., Sutton, A. J., Suzuki, T., Sweeney, C., Takahashi, T., Tjiputra, J., Tsurushima, N., Van Heuven, S. M. A. C., Vandemark, D., Vlahos, P., Wallace, D. W. R., Wanninkhof, R. and Watson, A. J. 2014. An update to the Surface Ocean CO2 Atlas (SOCAT version 2). *Earth Syst. Sci. Data*, 6: 69-90.

Balmaseda, M. A., K. Mogensen, and A. T. Weaver, 2013: Evaluation of the ECMWF ocean reanalysis system ORA-S4. *Quarterly Journal of the Royal Meteorological Society*, 139 (674), 1132–1161.

Calbó, J., Badosa, J., González, J.-A., Dmitrieva, L., Khan, V., Enríquez-Alonso, A. and Sanchez-Lorenzo, A. (2016), Climatology and changes in cloud cover in the area of the Black, Caspian, and Aral seas (1991–2010): a comparison of surface observations with satellite and reanalysis products. *Int. J. Climatol.*, 36: 1428–1443

Cavalieri, D. J., P. Gloersen, and W. J. Campbell, 1984: Determination of sea ice parameters with the NIMBUS 7 SMMR. *Journal of Geophysical Research: Atmospheres* (1984–2012), 89 (D4), 5355–5369.

Cavalieri, D. C et al. (1996) Sea ice concentrations from Nimbus-7 SMMR and DMSP SSM/I passive microwave data. National Snow and Ice Data Center. Digital media, Boulder.

Comiso, J. C., 1995: SSM/I sea ice concentrations using the Bootstrap algorithm, Vol. 1380. National Aeronautics and Space Administration, Goddard Space Flight Center.

CMUG Phase 2 Deliverable

Reference: D3.1: Quality Assessment Report
Due date: June 2016
Submission date: July 2016
Version: 2.0c



-
- Cox, P. M., Pearson, D., Booth, B. B., Friedlingstein, P., Huntingford, C., Jones, C. D. and Luke, C. M. (2013). Sensitivity of tropical carbon to climate change constrained by carbon dioxide variability. *Nature*, 494(7437), 341-344.
- Dee, D., et al., 2011: The ERA-Interim reanalysis: Configuration and performance of the data assimilation system. *Quarterly Journal of the Royal Meteorological Society*, 137 (656), 553–597.
- Desroziers, G., Berre, L., Chapnik, B. and Poli, P. (2005), Diagnosis of observation, background and analysis-error statistics in observation space. *Q.J.R. Meteorol. Soc.*, **131**: 3385–3396. doi: 10.1256/qj.05.108.
- Dorigo, W. A., Gruber, A., De Jeu, R. A. M., Wagner, W., Stacke, T., Loew, A., and Kidd, R. (2015). Evaluation of the ESA CCI soil moisture product using ground-based observations. *Remote Sensing of Environment*, 162, 380-395.
- Dragani, R.: A comparative analysis of UV nadir-backscatter and infrared limb-emission ozone data assimilation, *Atmos. Chem. Phys. Discuss.*, doi:10.5194/acp-2016-96, 2016.
- Dussin, R and Barnier, The making of the Drakkar Forcing Set 5, <http://www.drakkar-ocean.eu/forcing-the-ocean/the-making-of-the-drakkar-forcing-set-dfs5> (2015).
- Eastwood S. et al., 2014: Global sea ice concentration reprocessing: Product user manual, http://osisaf.met.no/docs/osisaf_cdop2_ss2_pum_sea-ice-conc-reproc_v2p2.pdf
- Evensen, G., 2003: The ensemble Kalman filter: Theoretical formulation and practical implementation, *Ocean Dyn*, 53, 343–367 (2003).
- Evensen, G., 2007: *Data Assimilation—The Ensemble Kalman Filter*, Springer, N. Y. (2007).
- Ferry, N, L. Parent, G. Garric, B. Barnier, N. Jourdain, and the Mercator Ocean team, 2010: Mercator global eddy permitting ocean reanalysis gloryslv1: Description and results. Tech. rep., *Mercator Ocean Q. Newsl.*, 36, 15–28.
- Ford, D. A., Edwards, K. P., Lea, D., Barciela, R. M., Martin, M. J., and Demaria, J. 2012. Assimilating GlobColour ocean colour data into a pre-operational physical-biogeochemical model, *Ocean Sci.*, 8: 751-771.
- Gehlen, M., Barciela, R., Bertino, L., Brasseur, P., Butenschön, M., Chai, F., Crise, A., Drillet, Y., Ford, D., Lavoie, D. and Lehodey, P., 2015. Building the capacity for forecasting marine biogeochemistry and ecosystems: recent advances and future developments. *Journal of Operational Oceanography*, 8(sup1), pp.s168-s187.

CMUG Phase 2 Deliverable

Reference: D3.1: Quality Assessment Report
Due date: June 2016
Submission date: July 2016
Version: 2.0c



Giglio, L.; Randerson, J. T.; Werf, G. R.; Kasibhatla, P. S.; Collatz, G. J.; Morton, D. C.; DeFries, R. S. Assessing variability and long-term trends in burned area by merging multiple satellite fire products. *Biogeosciences* 2010, 7, 1171–1186.

Giglio, L., van der Werf, G. R., Randerson, J. T., Collatz, G. J., and Kasibhatla, P.; Global estimation of burned area using MODIS active fire observations, *Atmos. Chem. Phys.*, 6, 957–974, (2006).

Guemas, V. et al., A review on Arctic sea-ice predictability and prediction on seasonal to decadal time-scales, *Q. J. R. Meteorol. Soc.* DOI:10.1002/qj.2401 (2014).

Harris, I., Jones, P.D., Osborn, T.J. and Lister, D.H., 2014: Updated high-resolution grids of monthly climatic observations – the CRU TS3.10 Dataset. *Int. J. Climatol.*, 34, 623–642

Haylock, M. R., N. Hofstra, A. M. G. Klein Tank, E. J. Klok, P. D. Jones, and M. New, 2008: A European daily high-resolution gridded data set of surface temperature and precipitation for, *J. Geophys. Res.*, 113, 1950–2006.

Hazeleger, W. et al., 2010: *EC-Earth: A Seamless Earth System Prediction Approach in Action*. *BAMS*, 91, 1357-1363.

Heidinger AK, Foster MJ, Walther A, Zhao X. 2014. The pathfinder atmospheres extended AVHRR climate dataset. *Am. Meteorol. Soc.* 95: 909–922

Hemmings, J. C. P., Barciela, R. M., and Bell, M. J. 2008. Ocean color data assimilation with material conservation for improving model estimates of air-sea CO₂ flux. *J. Mar. Res.*, 66: 87-126.

Ivanova, N. et al., Inter-comparison and evaluation of sea ice algorithms: towards further identification of challenges and optimal approach using passive microwave observations, *The Cryosph.* 9 1797-1817 (2016).

Kaspar, F., Hollmann, R., Lockhoff, M., Karlsson, K.-G., Dybbroe, A., Fuchs, P., Selbach, N., Stein, D., and Schulz, J., 2009: Operational generation of AVHRR-based cloud products for Europe and the Arctic at EUMETSAT's Satellite Application Facility on Climate Monitoring (CM-SAF), *Adv. Sci. Res.*, 3, 45-51, doi: 10.5194/asr-3-45-2009

Lasslop, G., K. Thonicke, and S. Kloster, SPITFIRE within the MPI Earth system model: Model development and evaluation, *J. Adv. Model. Earth Syst.*, **2014**, 6, 740–755, doi:10.1002/2013MS000284.

CMUG Phase 2 Deliverable

Reference: D3.1: Quality Assessment Report
Due date: June 2016
Submission date: July 2016
Version: 2.0c



Lebeaupin-Brossier, C. P., Drobinski, K. Béranger, S. Bastin, and F. Orain, 2013: Ocean memory effect on the dynamics of coastal heavy precipitation preceded by a mistral event in the northwestern Mediterranean. *Quarterly Journal of the Royal Meteorological Society* 139(3-4), 1583–1597, Doi: 10.1007/s00382-014-2252-z.

L'Hévéder, B, L. Li, F. Sevault, and S. Somot, 2013: Interannual variability of deep convection in the Northwestern Mediterranean simulated with a coupled AORCM. *Climate Dynamics* 41(3-4), 937–960, Doi: 10.1007/s00382-012-1527-5.

Lindstedt, D., Lind, P., Jones, C., Kjellström, E., 2015. A new regional climate model operating at the meso-gamma scale; performance over Europe. *Tellus A* 67, 24138, doi: 10.3402/tellusa.v67.24138.

Loew, A., Stacke, T., Dorigo, W., Jeu, R. D., Hagemann, S. (2013). Potential and limitations of multidecadal satellite soil moisture observations for selected climate model evaluation studies. *Hydrology and Earth System Sciences*, 17(9), 3523-3542.

Madec, G., and the NEMO team: "NEMO ocean engine". Note du Pôle de modélisation, Institut Pierre-Simon Laplace (IPSL), France, No 27 ISSN No 1288-1619 (2016)

Massonnet, F., et al., Prospects for improved seasonal Arctic sea ice predictions from multivariate data assimilation, *Oc. Modell.*, <http://dx.doi.org/10.1016/j.ocemod.2014.12.013> (2015)

Rayner, N. A., D. E. Parker, E. B. Horton, C. K. Folland, L. V. Alexander, D. P. Rowell, E. C. Kent, and A. Kaplan (2003), Global analyses of sea surface temperature, sea ice, and night marine air temperature since the late nineteenth century, *J. Geophys. Res.*, 108, 4407

Reichle, R. H., Koster, R. D., Dong, J. and Berg, A. A. (2004). Global soil moisture from satellite observations, land surface models, and ground data: Implications for data assimilation. *Journal of Hydrometeorology*, 5(3), 430-442.

Samuelsson, P., Gollvik, S., Jansson, C., Kupiainen, M., Kourzeneva, E., van de Berg, W., 2014. The surface processes of the Rossby Centre regional atmospheric climate model (RCA4). Report in *Meteorology* 157, SMHI, SE-601 76 Norrköping, Sweden.

Sevault F., S. Somot, A. Alias, C. Dubois, C. Lebeaupin-Brossier, P. Nabat, F. Adloff, M. Déqué, and B. Decharme, 2014: A fully coupled Mediterranean regional climate system model: design and evaluation of the ocean component for the 1980-2012 period. *Tellus A*, 66, 23967, <http://dx.doi.org/10.3402/tellusa.v66.23967>.

CMUG Phase 2 Deliverable

Reference: D3.1: Quality Assessment Report
Due date: June 2016
Submission date: July 2016
Version: 2.0c



Stengel, M., Mieruch, S., Jerg, M., Karlsson, K.-G., Scheirer, R., Maddux, B., Meirink, J.F., Poulsen, C., Siddans, R., Walther, A., Hollmann, R. 2013: The Clouds Climate Change Initiative: Assessment of state-of-the-art cloud property retrieval schemes applied to AVHRR heritage measurements, 2015: *Remote Sens. Environ.*, 162, 363–379

Stevens, B., et al., 2013: Atmospheric component of the MPI-M Earth System Model: ECHAM6. *Journal of Advances in Modeling Earth Systems*, 5 (2), 146–172.

Storkey, D., Blockley, E. W., Furner, R., Guiavarc'h, C., Lea, D., Martin, M. J., Barciela, R. M., Hines, A., Hyder, P., and Siddorn, J. R. 2010. Forecasting the ocean state using NEMO: The new FOAM system. *Journal of Operational Oceanography*, 3: 3-15.

Strandberg, G., Barring, L., Hansson, U., Jansson, C., Jones, C., Kjellstrom, E., Kolax, M., Kupiainen, M., Nikulin, G., Samuelsson, P., Ullerstig, A., Wang, S., 2014. CORDEX scenarios for Europe from the Rossby Centre regional climate model RCA4. Reports Meteorology and Climatology 116, SMHI, SE-601 76 Norrkoping, Sweden.

Palmer, J. R., and Totterdell, I. J. 2001. Production and export in a global ocean ecosystem model, *p-Sea Res. Pt. I*, 48: 1169-1198.

Tietsche, S., Balmaseda, M. a., Zuo, H., Mogensen, K. (2015). Arctic sea ice in the global eddy-permitting ocean reanalysis ORAP5. *Climate Dynamics*. <http://doi.org/10.1007/s00382-015-2673-3>

Tietsche, S., Notz, D., Jungclaus, J. H., and Marotzke, J., 2013. Assimilation of sea-ice concentration in a global climate model – physical and statistical aspects. *Ocean science*, 9, 19-36.

Vancoppenolle, M. et al. Simulating the mass balance and salinity of Arctic and Antarctic sea ice. 1. Model description and validation. *Ocean Modelling*, 27(1), 33-53 (2009).

Wagner, W., Dorigo, W., de Jeu, R., Fernandez, D., Benveniste, J., Haas, E., Ertl, M., 25 August-1 September 2012. Fusion of active and passive microwave observations to create an essential climate variable data record on soil moisture. In: XXII ISPRS Congress, Volume I-7. ISPRS Annals of the Photogrammetry, Remote Sensing and Spatial Information Sciences (ISPRS Annals), Melbourne, Australia, pp. 315–321.

Wenzel, S., Cox, P. M., Eyring, V. and Friedlingstein, P. (2014) Emergent constraints on climate-carbon cycle feedbacks in the CMIP5 Earth system models. *Journal of Geophysical Research: Biogeosciences*, 119(5),794-807.

CMUG Phase 2 Deliverable

Reference: D3.1: Quality Assessment Report
Due date: June 2016
Submission date: July 2016
Version: 2.0c



Zuo, H., Balmaseda, M. A., and Mogensen, K. (2015). The new eddy-permitting ORAP5 ocean reanalysis: description, evaluation and uncertainties in climate signals. *Climate Dynamics*.

<http://doi.org/10.1007/s00382-015-2675-1>